

**SATELLITE BASED
EVAPOTRANSPIRATION ESTIMATION
AND RUNOFF SIMULATION:
A TOPMODEL APPLICATION TO THE
GILGEL ABAY CATCHMENT, ETHIOPIA**

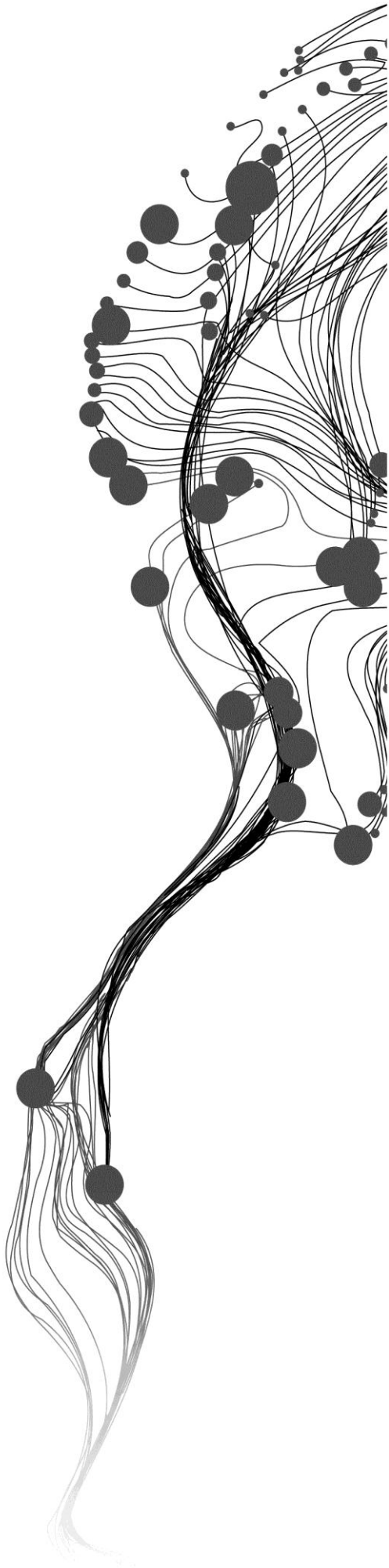
AHMED HAMID MUHAMMED

February, 2012

SUPERVISORS:

Dr. Ing. T.H.M. Rientjes

Dr. Ir. C. van der Tol



SATELLITE BASED EVAPOTRANSPIRATION ESTIMATION AND RUNOFF SIMULATION: A TOPMODEL APPLICATION TO THE GILGEL ABAY CATCHMENT, ETHIOPIA

AHMED HAMID MUHAMMED

Enschede, The Netherlands, February, 2012

Thesis submitted to the Faculty of Geo-Information Science and Earth Observation of the University of Twente in partial fulfilment of the requirements for the degree of Master of Science in Geo-information Science and Earth Observation.

Specialization: Water Resources and Environmental Management

SUPERVISORS:

Dr. Ing. T.H.M. Rientjes

Dr. Ir. C. van der Tol

THESIS ASSESSMENT BOARD:

Dr. Ir. C.M.M Mannaerts (Chair)

Dr. M.J. Waterloo (External Examiner, Universiteit Amsterdam)

DEDICATED TO:
MY MOTHER ZEINEB MUHABIE
AND
MY WIFE SADIYA ENDRIS

DISCLAIMER

This document describes work undertaken as part of a programme of study at the Faculty of Geo-Information Science and Earth Observation of the University of Twente. All views and opinions expressed therein remain the sole responsibility of the author, and do not necessarily represent those of the Faculty

ABSTRACT

The semi-distributed rainfall-runoff model (TOPMODEL) has been applied to the Upper Gilgel Abay catchment; one of the largest catchment which contributes inflow to the Lake Tana. Application of remote sensing for estimation of spatially heterogeneous variables and surface parameters was found important for the data poor catchment like the Upper Gilgel Abay Basin.

In the study remote sensing was applied to estimate spatially distributed actual evapotranspiration (ET_a) through the application of surface energy balance system (SEBS) approach. For SEBS MODIS satellite remote sensing products and meteorological station data were used. Daily average ET_a from each land cover class as well as for the whole catchment has been estimated for a full season as required by the TOPMODEL. The ET_a from SEBS has shown to be realistic when related to seasonal condition of the study area. Highest (5.3 mm/day) and the lowest (0.78 mm/day) ET_a was recorded in September 22 and March 19 respectively of the year 2004.

An SRTM 90m DEM was used to compute the topographic index, the basement and basic input for the TOPMODEL to simulate the streamflow of the basin. TOPMODEL calculates the actual evapotranspiration from the potential evapotranspiration, the root zone storage deficit and maximum root zone storage deficit for its water balance calculation. The model was calibrated for the year 1996 to 2003 dataset by using ET_p from Penman-Monteith with Nash-Sutcliffe model efficiency (NS) of 0.773 and the Relative Volume Error (RV_E) of -6.3%. A sensitivity analysis of the model indicated significant changes in the simulation result for the three parameters that are the exponential transmissivity function (m), the soil transmissivity at saturation (T_o) and the root zone available water capacity (SR_{max}). Validation was also done for the 2004 dataset and has shown good model performance results with (NS=0.80, RV_E=9.98%). By the main objective of this study, TOPMODEL was applied to simulate the streamflow hydrograph by using the remote sensing based ET_a from SEBS algorithm compared to the simulation results from potential evapotranspiration. Satisfactory results on both the Nash-Sutcliffe efficiency (NS=0.78) and Relative Volume Error (RV_E=0.59%) were found. The capability and possibility of the TOPMODEL to use ET_a estimated directly from satellite remote sensing data was found very important to represent spatial variation of ET_a in the streamflow simulation. In this study it has shown that ET_a calculated in TOPMODEL from ET_p was only after a rainfall event and sometime became zero for no rainfall days. This suggests the inaccurate estimation and representation of ET_a in TOPMODEL.

Intercepted rainfall amount was also determined using MODIS LAI products for different land cover classes. The model also has been used to simulate streamflow hydrograph from different land cover classes by treating each land cover as a sub-catchment. For each land cover class, the topographic index distribution and area distance distribution values were calculated and then the model runs using average ET_a value of each land cover class. The result has shown that 60% of the annual discharged by volume was contributed from agricultural area and the rest 19%, 12%, 8% from forest, shrubs and grassland respectively. Less than 1% volume of water is contributed from both wetland and marshy area. Finally the effect of changes in ET_a on the streamflow simulation of the model has been done for the whole catchment by only changing the average ET_a value from each land cover class. The simulation results from ET_a value of each land cover were tried to compare and good model performance were observed when ET_a was used from Agricultural and wetland with NS= 0.769 and 0.773 and RV_E =-1.75% and -2.42% respectively .while the lowest model efficiency was when ET_a used from the forest The NS=0.685 and RV_E=21%. This indicates how the TOPMODEL is sensitive to the changes in ET_a.

Key words: Gilgel Abay, MODIS, SEBS, TOPMODEL, SRTM, Nash-Sutcliffe, Streamflow

ACKNOWLEDGEMENTS

First of all I would like to thank the Netherlands fellowship programme (NFP) for giving the opportunity in financial support to continue my MSc study at ITC.

I would like to forward my sincere gratitude to my first supervisor Dr. Ing T.H.M. Rientjes, for his day to day support and valuable suggestions and guidance he has provided me throughout my research. His unforgettable effort on the modification of TOPMODEL code and his critical comments and continuous discussion we made throughout the research period helped me a lot. I learnt a lot from you.

I would also like to give my great appreciation to Dr.Ir.C. van der. Tol my second supervisor, for his great support comments and valuable suggestion and assistance spatially on the Surface Energy balance system (SEBS).

My special thanks goes to Webster Gumindoga former ITC MSc student from Zimbabwe for his support in giving the TOPMODEL IDL code and his valuable suggestion and his sooner response to my questions.

I would like to express my gratefulness to Dr. B.H.P. Maathuis for his special support in the DEM extraction in Hydro-processing part.

I would like to extent my gratitude to Dr. J. (Joris) Timmermans for his valuable support in programing the Mat lab code for conversion and reprojection of the NetCdf to Geotiff. His help is unforgettable.

I would like to express my thankfulness to Mohammad Abouali for his support and advice in the reprojecting and resampling of the MODIS images using MRT.

I would to express my appreciation to all WREM department staffs the ITC community and Ethio-Eritrea community. I thank you so much for your special treatments and kindness and the fellowship we shared together.

I would also like to forward my gratitude to all my family, my father, my mother, my sisters and brothers (especially M brothers and sisters) for their moral support and Motivation during my study. I would like to extend my Spectral thankfulness to my beloved wife Sadiya Endris for her encouragement and support in moral and praying.

All Praised be to the Almighty (Allah), the most Gracious and the most Merciful and Beneficent for its willing to my wonderful and success study time.

TABLE OF CONTENTS

| | |
|--|-----|
| Abstract | i |
| Acknowledgements | ii |
| Table of contents | iii |
| List of figures | v |
| List of tables | vii |
| | |
| 1. Introduction..... | 1 |
| 1.1. Background..... | 1 |
| 1.2. Problem statement | 2 |
| 1.3. Research objectives | 2 |
| 1.4. Research questions and hypothesis | 3 |
| 1.5. Thesis outline | 3 |
| | |
| 2. Study area and data availability | 5 |
| 2.1. Study area..... | 5 |
| 2.1.1. Geographical location and topography..... | 5 |
| 2.1.2. Climate..... | 5 |
| 2.1.3. Land cover and soil..... | 6 |
| 2.2. Data availability..... | 6 |
| 2.2.1. In situ data | 6 |
| 2.2.2. MODIS satellite data..... | 8 |
| 2.2.3. SRTM 90m Digital Elevation Model..... | 10 |
| 2.2.4. Landsat satellite data | 10 |
| | |
| 3. Literature review and model descriptions..... | 13 |
| 3.1. Runoff modelling by TOPMODEL..... | 13 |
| 3.1.1. Runoff processes | 13 |
| 3.1.2. The topographic index..... | 14 |
| 3.1.3. TOPMODEL approach..... | 15 |
| 3.1.4. Subsurface flow..... | 15 |
| 3.1.5. Unsaturated zone and root zone..... | 17 |
| 3.1.6. Streamflow..... | 17 |
| 3.2. Actual evapotranspiration estimation | 18 |
| 3.2.1. Surface energy balance system (SEBS)..... | 18 |
| 3.2.2. Net radiation..... | 18 |
| 3.2.3. Soil heat flux..... | 19 |
| 3.2.4. Sensible heat flux | 19 |
| 3.2.5. Evaporative fraction..... | 19 |
| | |
| 4. Methods and materials..... | 21 |
| 4.1. Methodological approach..... | 21 |
| 4.2. TOPMODEL approach..... | 23 |
| 4.2.1. Spatial interpolation of rainfall | 23 |
| 4.2.2. Potential evapotranspiration | 24 |
| 4.2.3. Interception module..... | 24 |

| | | |
|--------|--|----|
| 4.2.4. | TOPMODEL inputs and parameters | 25 |
| 4.2.5. | TOPMODEL modification..... | 26 |
| 4.2.6. | Sensitivity analysis, model calibration and validation | 27 |
| 4.3. | Energy balance modelling..... | 28 |
| 4.3.1. | Meteorological data processing for SEBS | 28 |
| 4.3.2. | MODIS satellite data preparation..... | 31 |
| 4.3.3. | Reprojection of MODIS products. | 34 |
| 4.3.4. | Shortwave solar radiation downward..... | 36 |
| 4.3.5. | SEBS time series completion..... | 37 |
| 4.4. | DEM hydro-processing..... | 38 |
| 5. | Results and Discussion..... | 43 |
| 5.1. | Intercepted rainfall | 43 |
| 5.2. | Actual Evapotranspiration time series from SEBS | 44 |
| 5.3. | Streamflow simulation using potential evapotranspiration..... | 47 |
| 5.3.1. | Sensitivity analysis | 48 |
| 5.3.2. | Model calibration and validation..... | 51 |
| 5.4. | Streamflow simulation using ETa from SEBS..... | 53 |
| 5.4.1. | ETa simulation by SEBS and TOPMODEL..... | 55 |
| 5.4.2. | Streamflow Simulation for specific land covers using ETa from SEBS | 56 |
| 6. | Conclusion and recommendation..... | 57 |
| 6.1. | Conclusion | 57 |
| 6.2. | Recommendation | 58 |
| | List of References..... | 61 |
| | Appendices..... | 63 |

LIST OF FIGURES

| | |
|--|----|
| Figure 2-1: Location of the Upper Gil gel Abay basin: Ethiopia..... | 5 |
| Figure 2-2: Meteorological and hydrological stations used for this study | 7 |
| Figure 2-3: Annual rainfall of the meteorological stations for the period 1996-2005 | 7 |
| Figure 2-4: Daily time series discharge of the Gilgel Abay river at Wetet Abay station (1996-2005)..... | 8 |
| Figure 2-5: The tile where the study area is located in the MODIS image product (Source: http://modis-land.gsfc.nasa.gov/MODLAND_grid.html) | 9 |
| Figure 2-6: Land cover of Upper Gilgel Abay (source: Kebede(2009)) | 11 |
| Figure 3-1: Runoff processes at the hill slope (After Rientjes (2010)) | 13 |
| Figure 3-2: Expansion of the saturation overland flow areas during a storm event (After Rientjes (2010)) | 14 |
| Figure 3-3: The relation between topography, topographic index and soil moisture deficit (Quinn and Beven, 1993) | 15 |
| Figure 3-4: A linear storage reservoir and lateral saturated subsurface flow through a soil column (After Rientjes (2010)) | 16 |
| Figure 4-1: Flow chart showing the whole process and Methodology | 22 |
| Figure 4-2: Thiessen polygon map for Gilgel Abay catchment..... | 23 |
| Figure 4-3: Sample windspeed map prepared after interpolation by moving average..... | 28 |
| Figure 4-4: Estimated surface pressure map from digital elevation map | 30 |
| Figure 4-5: MODIS average leaf area index of Gilge Abay for dry and wet months..... | 33 |
| Figure 4-6: Annual maximum and minimum crop height map based on the land used classification | 34 |
| Figure 4-7: MODIS re-projection Tool | 35 |
| Figure 4-8: Surface downward solar radiation from ECMWF..... | 36 |
| Figure 4-9: Daily average ETa for original and interpolated days for Gilgel Abay catchment | 37 |
| Figure 4-10: Time series ETa from SEBS after applying interpolation for missing day..... | 38 |
| Figure 4-11: Original DEM, filled DEM and sink map of Upper Gilgel Abay..... | 39 |
| Figure 4-12: Flow direction, flow accumulation, slope and Tan β maps..... | 40 |
| Figure 4-13: Topographic index map (left) and topographic index value distribution histogram (right) ... | 41 |
| Figure 4-14: Distance area map for channel routing | 41 |
| Figure 5-1: LAI distribution of different land cover classes for Gilgel Abay catchment..... | 43 |
| Figure 5-2: Daily Intercepted Rainfall of different land cover classes for 2004..... | 44 |
| Figure 5-3: Daily average actual evapotranspiration for 152 days for different land cover classes..... | 44 |
| Figure 5-4: Average daily ETa by SEBS for each land cover class contributed to the whole catchment before interpolation of missed days..... | 45 |
| Figure 5-5: Daily average ETa from each land cover class estimated using SEBS (2004)..... | 46 |
| Figure 5-6: The monthly average actual evapotranspiration (2004) | 47 |
| Figure 5-7: Simulation results for the Upper Gilgel Abay catchment for the period of 1996 – 2003 | 47 |
| Figure 5-8: Sensitivity of the model changes in m parameter (1996-2003) | 48 |
| Figure 5-9: Sensitivity of the model to the changes in m parameter (2000-2001) | 49 |
| Figure 5-10: Sensitivity of the model to the T _o parameter (1996-2003)..... | 50 |
| Figure 5-11: Sensitivity of the model to the T _o parameter (2000-2001) | 50 |
| Figure 5-12: Sensitivity of the model to the changes in SRmax parameter..... | 51 |
| Figure 5-13: Sensitivity of the model to the changes in SRmax parameter (2000-2001) | 51 |
| Figure 5-14: Calibration results for the catchment (1996 – 2003) | 52 |
| Figure 5-15: Calibrated result of the catchment (2000-2001) | 52 |
| Figure 5-16: Validation result (2004) | 53 |

| | |
|--|----|
| Figure 5-17: Simulated hydrograph using ETa from SEBS..... | 53 |
| Figure 5-18: Simulated hydrograph when using ETa and ETp | 54 |
| Figure 5-19: Cumulative discharge using ETa from SEBS and ETp in TOPMODEL simulation..... | 54 |
| Figure 5-20: Daily evapotranspiration from SEBS and TOPMODEL and Rainfall distribution for 2004.. | 55 |
| Figure 5-21: Cumulative ETa from TOPMODEL and SEBS..... | 56 |
| Figure 5-22: Simulated hydrograph from each land cover class using average daily ETa from SEBS..... | 56 |
| Figure 5-23: Simulated hydrograph applying ETa from land cover classes treating as the whole catchment. | 57 |

LIST OF TABLES

| | |
|---|----|
| Table 2-1: Meteorological stations and variables collected..... | 6 |
| Table 2-2: MODIS products..... | 10 |
| Table 4-1: Thiessen weight values for the stations..... | 23 |
| Table 4-2: Different parameters for the TOPMODEL..... | 26 |
| Table 4-3: Stations and some values used for correlation air temperature with elevation..... | 29 |
| Table 4-4: The distribution of MODIS products in each month of 2004 used for SEBS algorithm..... | 31 |
| Table 4-5: Attribute of annual minimum and maximum crop height for different land cover classes | 34 |
| Table 4-6: MODIS re-projection settings for this study | 35 |
| Table 4-7: MODIS conversion factors from the HDF viewer | 36 |
| Table 5-1: Parameter values used for TOPMODEL simulation (Gumindoga, 2010)..... | 48 |
| Table 5-2: Effects of the m parameter on TOPMODEL efficiency..... | 48 |
| Table 5-3: Effects of the To parameter on TOPMODEL efficiency..... | 49 |
| Table 5-4: Effects of the SRmax parameter on TOPMODEL efficiency | 50 |
| Table 5-5: Optimum parameter values and model efficiencies after calibration..... | 52 |
| Table 5-6: Model efficiencies when applied to ETa from different land cover classes | 57 |

1. INTRODUCTION

1.1. Background

Hydrological assessments on streamflow in many catchments in Ethiopia are limited although emphasis must be given to support water resource management. The Ethiopian Highland is a major water contributor to the Blue Nile River Basin and reliable runoff information from this region is of great importance for the sustainable management of water resources. Gilgel Abay catchment is one of the largest catchments in the Blue Nile basin that drains to Lake Tana which is the origin of the Blue Nile River.

Human activities and natural phenomena have significance influence on the hydrological water balance of a catchment. For the Upper Gilgel Abay catchment an increase in population caused changes in the land cover (Kebede, 2009) and various hydrological processes like evapotranspiration, interception, and infiltration are affected. A semi-distributed hydrological model, TOPMODEL that is used to simulate the rainfall runoff relations of the catchment is applied. The model was first described by Beven and Kirkby (1979) and aims to evaluate the effect of catchment heterogeneity and, particularly, topography on the dynamics of hydrological response (Quinn and Beven, 1993). The model uses Inputs of land surface parameters, topographic index, discharge, rainfall and evapotranspiration. Over the last decade the use of satellite remote sensing is advocated to represent catchment characteristics and processes. Much research has been done on using satellite remote sensing examples are for retrieving rainfall (Iguchi et al., 2000), evapotranspiration (Glenn et al., 2007; Yanbo et al., 2005), spatial and temporal variation of soil moisture (Houser et al., 1998). Various remote sensing and GIS techniques are applied to identify the physical factors that control the process of rainfall into runoff and other components. Nowadays the role of remote sensing to support water resources assessments and modelling is improving, but still limited due to the complex nature and phenomena of the real world.

Evapotranspiration (ET) is the second largest term in the terrestrial water budget after precipitation. Accurate estimates of ET are needed for numerous management activities at local to regional scales. Nowadays remote sensing is probably the only feasible means for projecting ET over large-scale area. Satellite sensors with different spatial and temporal resolution for the observation of atmospheric and hydrologic variables are available and are used for the estimation of ETa. Estimation of evapotranspiration by using satellite remote sensing technique has become popular and is applied to various places. Evapotranspiration is also an important component in the surface energy balance, which has significant effects on the water balance of a catchment. Potential evapotranspiration is one of the inputs of the TOPMODEL to estimate the discharge of a catchment. In the past decades various algorithms and models are developed to estimate ET over larger scales combining remote sensing data and meteorological data

In previous study of TOPMODEL in the Gilgel Abay catchment (Deginet, 2008; Gumindoga, 2010) satellite remote sensing data of ETa were ignored for assessing the effect the spatial variability of the surface parameters for the simulation of the water balance and streamflow hydrograph of the catchment. As stated, the spatial and temporal variations in hydro-meteorological and environmental components affect the energy fluxes of the lower layer atmosphere. It is expected that improved estimation of these fluxes at the landscape can improve the modeling of surface hydrological processes. In previous runoff modeling studies in the Gilgel Abay catchment, evapotranspiration was estimated from point

meteorological data by applying the Penman-Monteith equation. Modeling of the spatial variability and heterogeneity of the catchment to calculate actual evapotranspiration (ET_a) for the large area has to be considered because such variability largely affects ET_a, stream flow responses and the general water balance of the catchment.

1.2. Problem statement

The simulation and quantification of hydrological processes is far from trivial by issues that relate to temporal and spatial variability of real world properties. In modelling, such properties are represented by model parameters and variables which also require estimation. In this study catchment runoff behaviour and related streamflow hydrographs are simulated by use of the TOPMODEL see (Beven and Kirkby, 1979a; Beven and Wood, 1983; K. Beven et al., 1995). The model has many applications and a wide range of articles are available on model performance issues that relate to the representation of model parameters and meteorological forcing terms (i.e. rainfall and ET_p). For simulation of ET_a, TOPMODEL relies on estimation of ET_p and the estimation of soil moisture in the so called root zone store. An important constraint and problem to this approach is that meteorological data only is available at weather stations that, commonly, only are sparse, uneven distributed and are few in number for the area of interest. Also simulation of ET_a relies on uncertain estimates of available soil moisture storage in the root zone store the distribution of soil moisture is largely affected by different surface and atmospheric conditions such as the rainfall amount and distribution, the land cover, physical and chemical property of soil layer, and the topographic nature etc. of the study area and as such estimation of ET_a is largely constraint. In this study TOPMODEL is tested for input of satellite based ET_a that is estimated by the SEBS approach that solves the energy balance at the land surface. The use of satellite based ET_a estimates is argued for since the estimates directly affect the water balance of the TOPMODEL and since ET_a representation has spatial and temporal coverage by use of a time series of satellite images that overlay the area of study (i.e. Gilgel Abay catchment, Ethiopia). To what extend the performance of the TOPMODEL will be affected by use of satellite based ET_a as compared to use of weather station based ET_p is uncertain. It appears to be trivial that the water balance of the model will be affected but, presumably, such will be different for the different time period of the year with clear wet seasons and dry seasons. While water storage in the model is affected it is uncertain how peak flows, base flows and runoff volumes are affected.

1.3. Research objectives

- The main objective of this study is to estimate actual evapotranspiration by the satellite based SEBS approach and to assess effects to hydrological modelling by the TOPMODEL approach.

Specific objectives are:

- To estimate ET_a using the satellite based energy balance approach (SEBS) for the day and wet seasonal coverage.
- To simulate the streamflow of the catchment using SEBS based ET_a estimates as an input to the TOPMODEL.
- To identify optimum parameter values of the TOPMODEL that allow for the estimation of hydrological stream flow response of the catchment.
- To evaluate the change in the stream flow response by using SEBS based ET_a as compared to the traditional Penman-Monteith approach.
- To analyse the effect of the changes of ET_a estimation on stream flow such as total, high and low flow of the catchment.

1.4. Research questions and hypothesis

Research questions:

- How can actual evapotranspiration be estimated using remote sensing?
- How well does TOPMODEL simulate stream flow response when satellite based actual evapotranspiration is used?
- How will the change in ET_a estimation affect the TOPMODEL peak flow and the baseflow simulation results?
- What calibration procedure to select to improve the simulating results of the streamflow?

Research hypothesis:

- Actual evapotranspiration can be estimated for the Gilgel Abay catchment using SEBS and can represent the catchment very well.
- Actual evapotranspiration estimated from satellite remote sensing with better spatial coverage accounts the variability in the catchment so that the TOPMODEL simulation result can represent better than when potential evapotranspiration is used.
- Actual evapotranspiration will have effect on the TOPMODEL simulation results of the peak flow, baseflow and total volume so that it improves the efficiency of model performance.

1.5. Thesis outline

This thesis consists of six chapters. The first chapter starts with a brief background to the study and review of various hydrological processes and components that could be handled with the application of GIS and remote sensing. The advance of remote sensing application for the estimation of important surface and atmospheric parameters are also reviewed. The problem statement, research objectives, research question and hypothesis of the study area are also addressed in this chapter.

The second chapter starts with the description of the study area location, topography, climate land cover. In this chapter the data collection during the field campaign (in situ) and remote sensing data used for the study are described. The third chapter describes some literature reviews on the basic approaches and assumption on the TOPMODEL and surface energy balance system (SEBS).

In the fourth chapter, the methodological approach in a conceptual framework and data preparation of different input variables and parameters for both TOPMODEL and SEBS are discussed.

The fifth chapter describes about the results and discussion of both SEBS ET_a and TOPMODEL simulation. In this chapter the TOPMODEL simulation results using both potential and actual evapotranspiration and comparison of ET_a from SEBS and TOPMODEL is addressed.

The last (sixth) chapter contains conclusions and recommendations for further study to be emphasis on this type of research by describing its limitation ate this moment.

2. STUDY AREA AND DATA AVAILABILITY

2.1. Study area

2.1.1. Geographical location and topography

The Northern and northwestern part of Ethiopia is characterized by rugged and mountainous topography. The study area is located in northwestern Ethiopia with geographical coordinates of 10°56' to 11°51'N latitude and 36°44' to 37°23' E longitudes. The Gilgel Abay catchment has elevation variation from 1787 to 3518m a.m.s.l with highest elevation ranges located in the Southeast of the catchment. From the total area of catchment (around 70%) falls in the slope range of 0-8% and 25% of the area falls in the slope range of 8-30% and the rest 5% of the area has a slope of greater than 30% (Shaka, 2008).

The Gilgel Abay River originates from a place where a small spring near Gish Abay at elevation of about 2900 m a.m.s.l It drains the Southern part of Lake Tana and it contributes the most inflow to Lake Tana with 30% of the total area contribution to the Upper Blue Nile basin (Abdo et al., 2009). The catchment area of Gilgel Abay up to Wetet Abay gauging station is around 1661km² while at the outlet to Lake Tana is around 5000km² (Deginet, 2008).

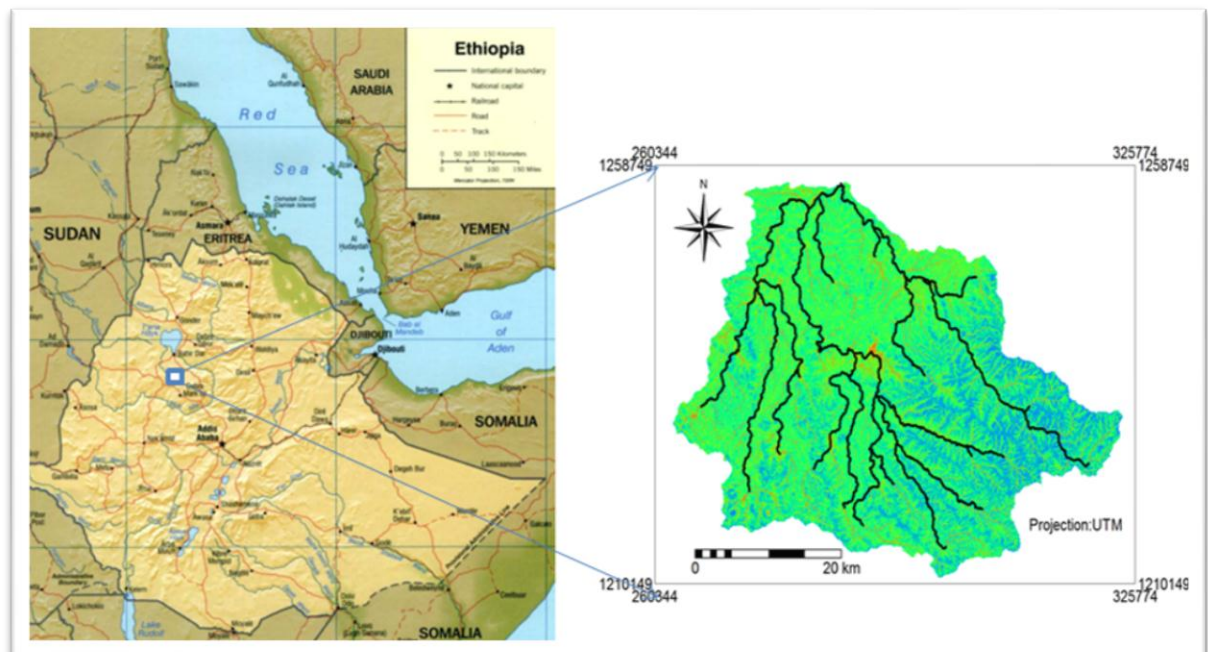


Figure 2-1: Location of the Upper Gil gel Abay basin: Ethiopia.

2.1.2. Climate

The climate of Ethiopia is mainly controlled by seasonal movement of the Intertropical Convergence Zone (ITCZ) and its atmospheric circulation (Shaka, 2008), and topography. As the Gilgel Abay catchment is located in the high land part of Ethiopia its climate is also affected by topography. The mean annual temperature of cool semi-humid zone is 17 – 20 °C while that of the cool -humid zones is 11.5 – 17 °C. The dry and the wet season occur between October and May and between June and September

respectively. Generally the rainy season of the catchment is from June to September with its contribution of 70–90% of the annual rainfall (Abdo, et al., 2009). The area has a mean annual rainfall of 1900mm in the Southern and 1200mm in Northern part (Kebede, 2009).

2.1.3. Land cover and soil

The Gilgel Abay catchment can be partitioned in cropland with little and discontinuous woodlands and forested uplands. The land cover is dominated by agricultural land with almost 62% of the area, 17% forest land ,9% shrubs land, 9% grass land and the rest 3% land covered by water and marshy (Kebede, 2009). Most of the downstream part of the Gilgel Abay basin is characterized by soils of alluvial sediments (SMEC, 2007) by long time erosion from upstream area.

2.2. Data availability

2.2.1. In situ data

During the field campaign, meteorological data were collected from the national Meteorological Agency of Ethiopia (NMA) Addis Ababa, and from Regional Meteorological Branch Office, in Bahir Dar for the stations inside and around the study area. According to NMA, the meteorological station are in four categorical classes. Class I (principal) stations estimates a range of meteorological variables and have observation frequency of every three hours. Adet, Dangila and Bahir Dar meteorological stations principal stations. Kidamaja and Wotet Abay stations are class III with three meteorological variables (rainfall, maximum and minimum temperature) and the remaining two stations Sekela and Enjibara are class IV and only collect rainfall. Table 2-1 shows the stations and meteorological variables collected for this study. These data were collected for the period of 1996 to 2005. Figure 2-2 shows the locations of meteorological and hydrological stations in the study area.

Table 2-1: Meteorological stations and variables collected

| Station Name | Coordinates of station | | | Type of meteorological data collected in the stations | | | | | |
|--------------|------------------------|-----------|----------|---|------|------|----|----|----|
| | X | Y | Altitude | RF | Tmax | Tmin | RH | WS | SS |
| Adet | 332663.3 | 1245939.5 | 2180 | X | X | X | X | X | X |
| Danila | 262994.7 | 1244290.6 | 2119 | X | X | X | X | X | X |
| Enjibara | 270514 | 1213131 | 2540 | X | | | | | |
| Sekela | 304679.7 | 1214109.7 | 2690 | X | | | | | |
| Wetet Abay | 287108.5 | 1257029.5 | 1920 | X | X | X | | | |
| Kidamaja | 259513 | 1216653 | 1913 | X | X | X | | | |
| Bahir Dar | 324455 | 1281713 | 1797 | X | X | X | X | X | X |

Where RF- Rainfall, Tmax –Daily maximum Temperature, Tmin – daily minimum temperature, RH – Relative humidity ,WS – Wind speed and SS – Sunshine hours

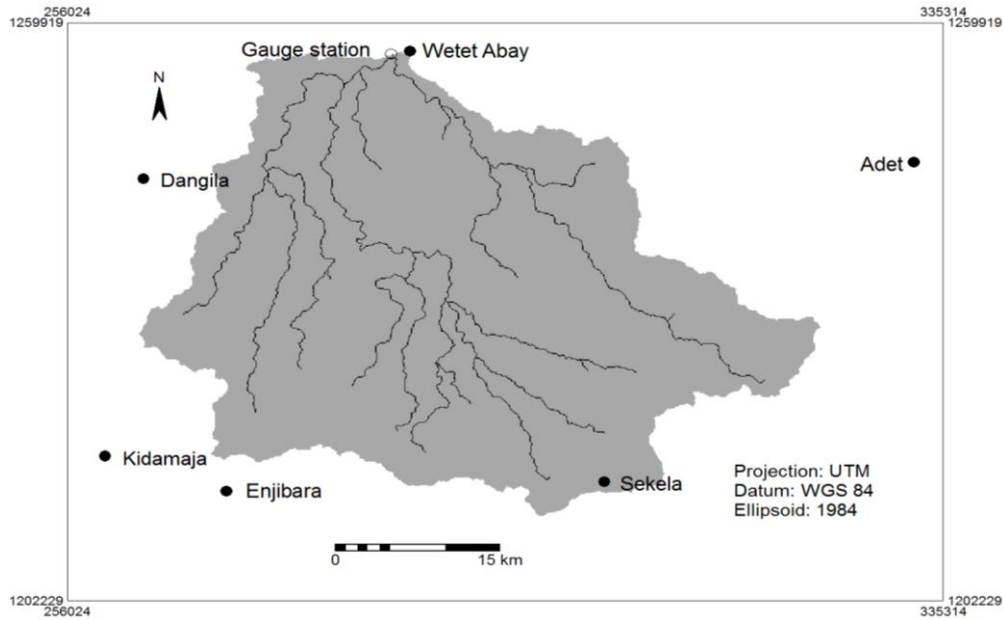


Figure 2-2: Meteorological and hydrological stations used for this study

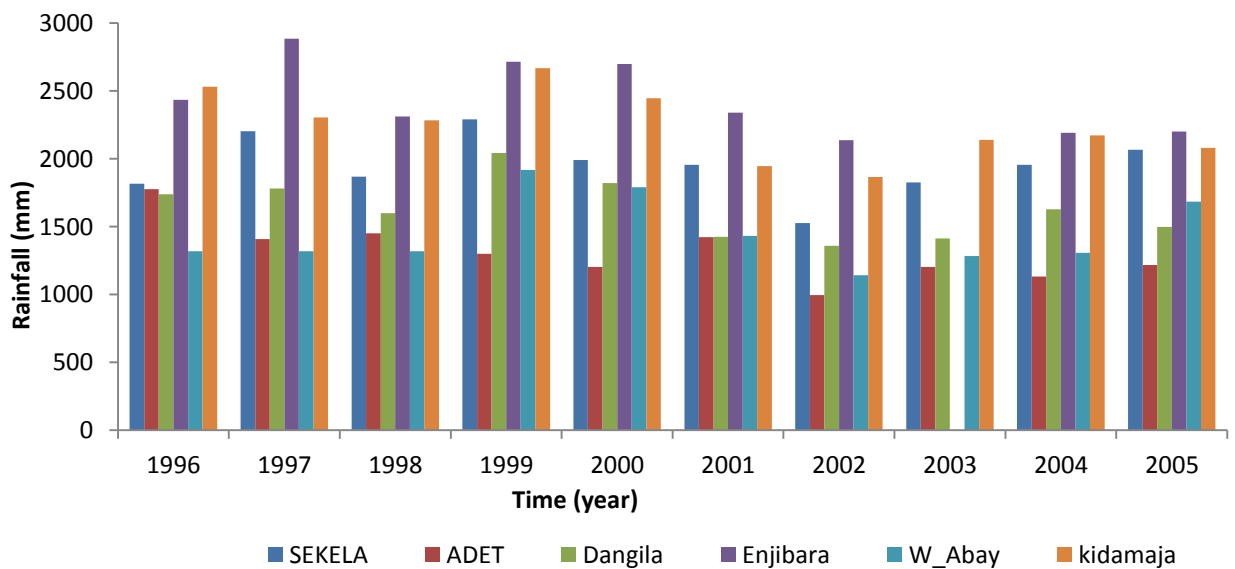


Figure 2-3: Annual rainfall of the meteorological stations for the period 1996-2005

Hydrological data

The hydrological data for the study area were collected from the Ministry of Water Resources of Ethiopia (MoWR) Addis Ababa. The discharge data is measured at Wetet Abay Gauge station with gauged area of 1656.2 Km². The historical discharge data were collected for the period of 1994 to 2005. However, the data used for the study were only from 1996 - 2005.

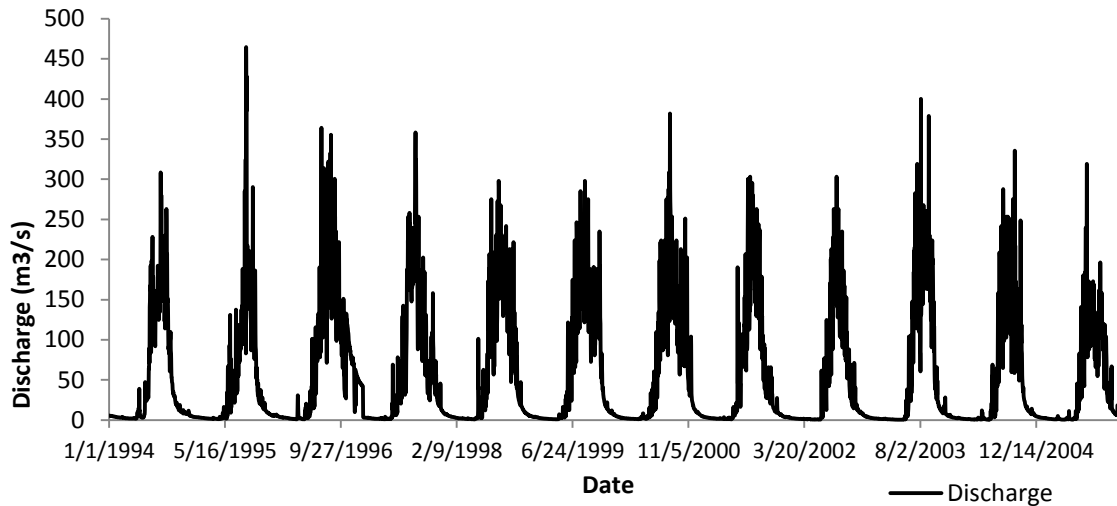


Figure 2-4: Daily time series discharge of the Gilgel Abay river at Wetet Abay station (1996-2005)

2.2.2. MODIS satellite data

MODIS (Moderate Resolution Imaging Spectroradiometer) a key instrument operating on aboard of the Terra (EOS AM) launched in December 1999 and Aqua (EOS PM) launched in May 2000. Terra's orbit around the Earth is timed so that it passes from north to south across the equator in the morning, while Aqua passes south to north over the equator in the afternoon.

MODIS is playing a vital role in the development of validated, global, interactive Earth system models to predict global change to assist policy makers in making decisions concerning the protection of our environment (<https://lpdaac.usgs.gov/>). The MODIS land products are produced and distributed by the Land processe Distributed Active Archive Center (LP DAAC) which process , archives and distributes land data and products derived from the EOS sensors. The technical sepecification of MODIS satellite is shown in Appendix A.

The MODIS HDF products are tiled in grids of 10^0 by 10^0 . Each tile is assigned by horizontal (h) and vertical (v) contains 0 to 35 to horizontally and 0 to 17 vertically with its upper left corner assigned by (0,0) coordinate and its bottom is (35,17). The Gilgel Abay catchment lies in the horizontal and vertical cordinates of (21,7) so that all the MODIS products under this tile are downloaded for further processing. These tiled products are archived with sinusoidal projection. Figure 2-2 shows the location of the study area in MODIS tile product.

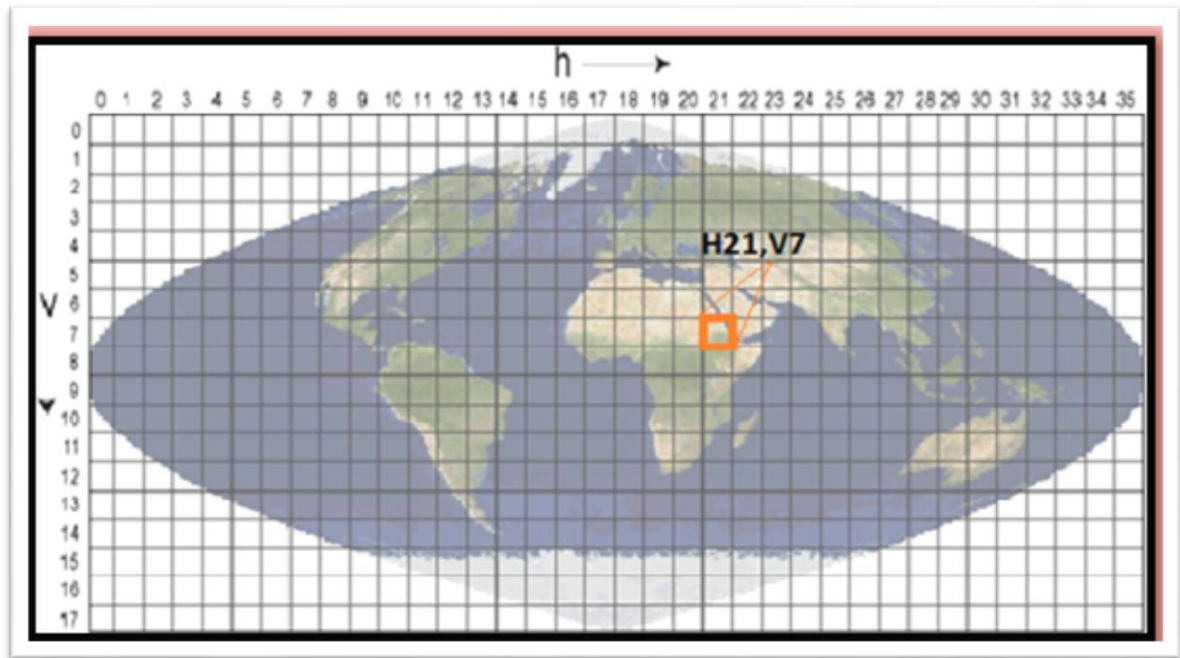


Figure 2-5: The tile where the study area is located in the MODIS image product (Source: http://modis-land.gsfc.nasa.gov/MODLAND_grid.html)

In this study, MODIS Terra, preprocessed products are used for the estimation of actual evapotranspiration (ET_a). The MODIS products are collected from the MODIS ftp site <ftp://e4ftl01.cr.usgs.gov/MOLT>. Table 4-2 shows MODIS satellite Data downloaded from NASA ftp server.

The preprocessed MODIS satellite data for the study area have been downloaded from the NASA website (<http://modis-land.gsfc.nasa.gov/>) and the cloud free images for 2004 years were selected for the SEBS algorithm (see Section 3.2). SEBS uses inputs data from remote sensing such as land surface temperature, Emissivity, albedo, NDVI, Vegetation proportion (fc), Sun Zenith angle and Digital Elevation Model (DEM) map. SEBS for ILWIS Open provides a set of routines for bio-geophysical parameter such as maps of net radiation (R_n), latent heat flux (LE), sensible heat flux (H), soil heat flux (G), Hwet limit, Hdry limit, evaporative fraction (EF), actual evapotranspiration (ET_a) instantaneous and daily, and complementary files as standard outputs.

Some MODIS products were also found together with other products. For example, MIR (mid infrared reflectance) was found with Vegetation index (VI) product. This product is used for the estimation of total emissivity of the area.

Table 2-2: MODIS products

| Short Name | Product type & name | Spatial resolution (m) | Temporal resolution |
|------------|---|------------------------|---------------------|
| MOD11A1 | Land Surface Temperature & Emissivity | 1000 | Daily |
| MCD43A3 | Surface Reflectance BRDF/Albedo Parameter | 500 | 8 days |
| MOD13A1 | Gridded Vegetation index(NDVI) | 250 | 16 days |
| MOD15A2 | Leaf Area Index & FPAR | 1000 | 8 days |

2.2.3. SRTM 90m Digital Elevation Model

The NASA Shuttle Radar Topographic Mission (SRTM) has provided digital elevation data (DEMs) for over 80% of the globe. These data are currently distributed free of charge by USGS and is available for download from the National Map Seamless Data Distribution System, or the USGS ftp site. The SRTM data is available as 3 arc second (approx. 90m resolution) DEM.

For this study SRTM 90 resolution DEM is selected because the vertical error is reported to be less than 16m. The Upgraded new version 4 SRTM data is available from the website and has been used. This latest version represents the significant improvement from previous versions using new interpolation algorithm and better auxiliary DEM. This data is available in both Arc-Info ASCII and GeoTiff format to facilitate their ease of use in a variety of image processing and GIS applications and were downloaded from the website (<http://srtm.csi.cgiar.org/>).

2.2.4. Landsat satellite data

The land use/cover map used for this study was from the work of Kebede (2009) who performed a supervised land cover classification with the use of Landsat ETM images. He used a confusion matrix to validate the accuracy of land classification of the area. This land cover map was further used by Gumindoga (2010) by performing the confusion matrix to cross validate the land cover classification map. The land cover map of the upper Gilgel Abay catchment and the percentage of each land cover class are shown in the figure 2-1 below.

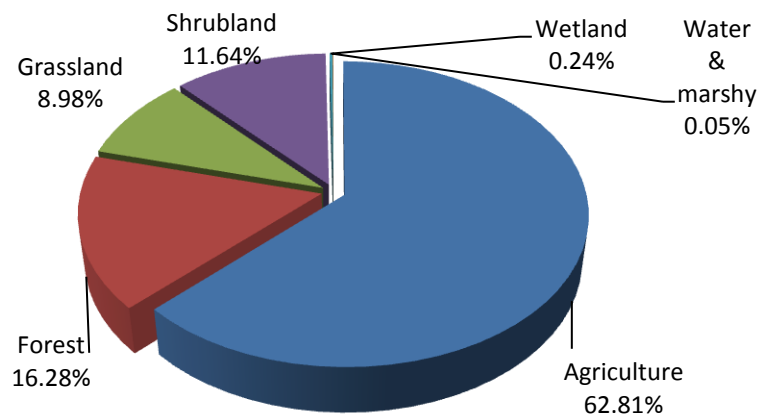
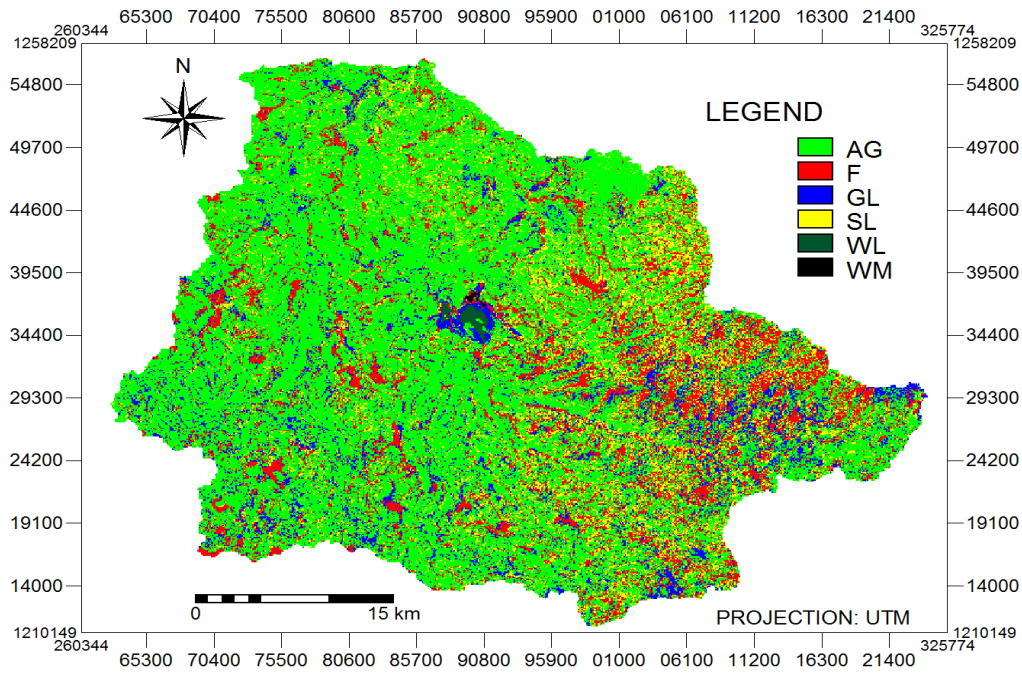


Figure 2-6: Land cover of Upper Gilgel Abay (source: Kebede(2009))

3. LITERATURE REVIEW AND MODEL DESCRIPTIONS

3.1. Runoff modelling by TOPMODEL

The TOPMODEL is a semi-distributed rainfall-runoff model which is based on a simple theory of hydrological similarity of points in the catchment and was described by Beven and Kirkby (1979). As stated by Kirkby (1997) the model makes use of topographic data so that it is easy to obtain evidences that give strengths and limitations from the original and theoretical concepts. There is a strong interdependency between topographic index and the soil moisture status of the area. When the area that contributes to the runoff increases, the soil moisture (wetness index) also increases and leads to the sub-surface water table rise up to the surface.

Over the past decades, TOPMODEL has been applied to catchments of local (< 10 km²) and regional scales (< 1000 km²) to predict the hydrological stream flow. The model is often used by its relatively high capability to predict hydrological responses. For example the model was applied on Plynlimon, mid-Wales catchment to predict the soil moisture pattern and its influence on the spatial prediction of evapotranspiration (Quinn and Beven, 1993). Studies with the TOPMODEL approach are reported for many places in the world in many climatic zones as such it is relevant for this study as well.

TOPMODEL has many advantages to use. The model uses very few numbers of parameters so that calibration process can be handled easily. Since the model uses topographic index data from Digital Elevation Model of the catchment, many parameters can be theoretically measured in situ and serve to represent catchment variability. The model often is termed a conceptual model with runoff generation processes that rely on accurate representation of catchment topography and the soil transmissivity that diminishes with depth (modified after Rientjes(2010)).

3.1.1. Runoff processes

Streamflow at the outlet of a catchment results from various runoff processes. Figure 3-1 shows a schematic representation of hillside slope flow processes which contribute to the catchment runoff.

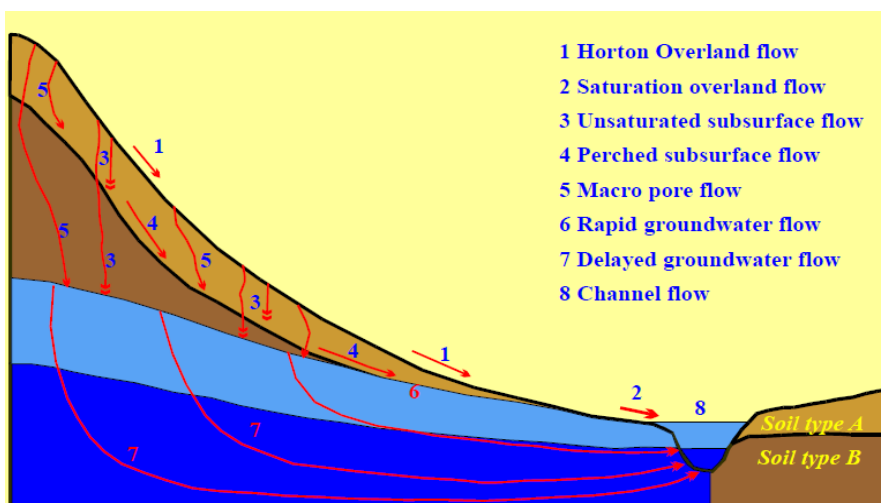


Figure 3-1: Runoff processes at the hill slope (After Rientjes (2010))

Many catchment scales, in theory all the processes described in the above diagram can be present. The infiltration excess overland flow (Horton overland flow) is produced when the rainfall intensity exceeds the infiltration capacity and when the rainfall duration is longer than the ponding time of small depressions at the land surface. Whereas saturation excess overland flow occurs when the subsurface is completely saturated by the rising of ground water table that is mostly resulted from percolated water from upslope areas. The size of the saturated areas changes during rainfall events(After Rientjes(2010))

On top of these saturated zones, overland flow can be generated by exfiltration of subsurface water and by rainfall. Saturated zones are termed ‘saturation overland flow source areas’. An increasing of the source areas causes higher peak flow that in extreme cases causes flooding. Figure 3-2 shows the expansion of saturation overland flow over space and time (After Rientjes (2010))

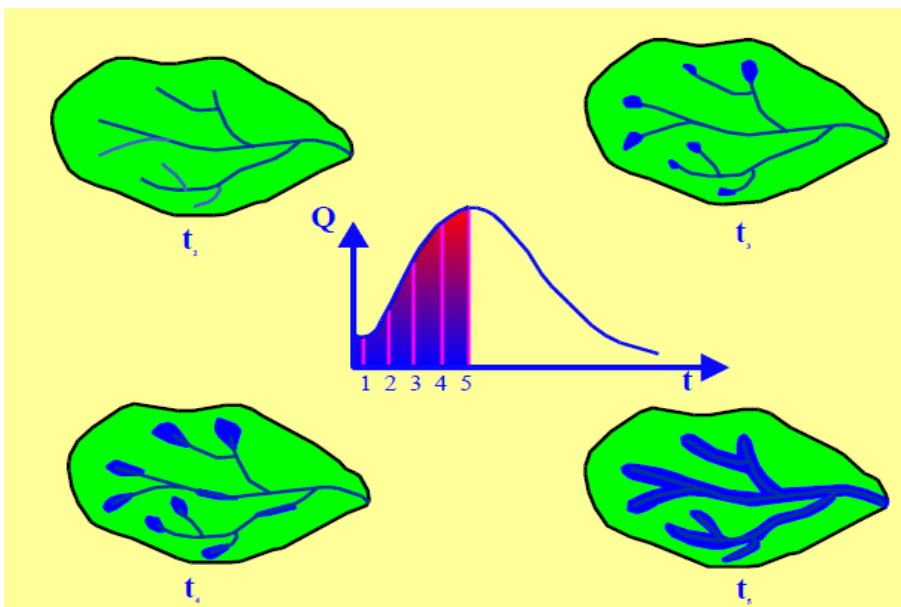


Figure 3-2: Expansion of the saturation overland flow areas during a storm event (After Rientjes (2010))

3.1.2. The topographic index

The topographic index is given by the formula $\ln(a/\tan\beta)$ where a is upslope contributing area per unit contour; $\tan\beta$ is local slope angle. The index serves to approximate the distribution of the variables source areas within a catchment. As stated by Quinn and Beven (1993) topographic index has direct relation with soil moisture status so that a higher topographic index relate to a lower soil moisture deficit and this can be shown in Figure 3-3. This topographic index is a fixed property that measures the hydrological similarity of any point in the catchment by assuming that equal values of the topographic index behave in a hydrological similar manner (Rientjes, 2010)

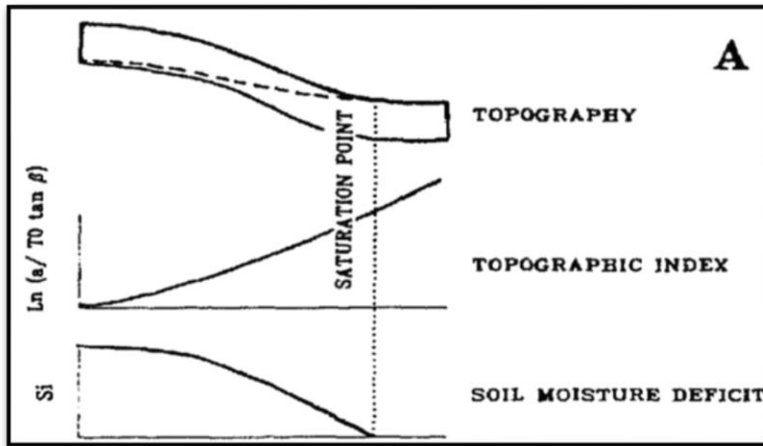


Figure 3-3: The relation between topography, topographic index and soil moisture deficit (Quinn and Beven, 1993)

3.1.3. TOPMODEL approach

In the TOPMODEL approach, topography of a catchment is analysed using Digital Elevation Model (DEM), which represent the topographic, or elevation distribution of the catchment. Surface saturation and soil moisture deficits across the subsurface model domain are directly related to the three topographic characteristics slope, specific catchment area and topographic convergence (Rientjes, 2010).

According to Beven et al (1995) TOPMODEL is “a set of concepts that can be used to reproduce the hydrological behaviour of catchments in a distributed or semi-distributed way and has four basic simplifications and assumptions that are to be considered when using this model.”

TOPMODEL assumptions are:

- “1 The dynamics of the saturated zone can be approximated by successive steady state representations;
2. The hydraulic gradient of the saturated zone can be approximated by the local surface topographic slope, $\tan\beta$.
3. The distribution of downslope transmissivity (depth X hydraulic conductivity) with depth is an exponential function of storage deficit or depth to the water table.
4. Saturation of a soil column occurs from the below and as such runoff is generated by the saturation excess overland flow mechanism.”

3.1.4. Subsurface flow

TOPMODEL is based on the storage principle of Darcy type flow equation, which allows water transport between subsurface storages. One of the parameters in the Darcy is the transmissivity, which is equal to the depth of the flow domain as multiplied by the hydraulic conductivity. Since the groundwater flow is only possible in the saturated zone, transmissivity should be calculated from the part of the subsurface that is fully saturated.

In general, the distribution of transmissivity in the downslope direction can be simulated by an exponential function of the local storage deficit.

$$T = T_0 e^{-S_i/m} \tag{3.1}$$

Where

T_0 = lateral transmissivity [L²/T]

S_i = local storage deficit [L]

m = a scaling parameter [L]

The maximum discharge of the subsurface is observed when the entire soil profile becomes saturated and is given by

$$q_{\max} = TS \tag{3.2}$$

Where

S = storage deficit

The actual groundwater discharge is also a function of the upstream area ‘a’ multiplied by the recharge rate ‘R’ and is given by the equation:

$$q_{\text{act}} = Ra \tag{3.3}$$

The relative wetness at a point and depth to water table can be determined by the comparing

q_{act} and q_{\max}

$$W = \frac{q_{\text{act}}}{q_{\max}} = \frac{Ra}{T \tan\beta} \tag{3.4}$$

Where

- q_{act} = actual lateral discharge [L²/T]
- q_{\max} = maximum discharge [L²/T]
- R = recharge rate [LT⁻¹]
- a = specific catchment area [L]

the inflow and outflow discharge into and from any catchment can be shown by means of simple linear reservoir approach in which the subsurface elements can be interpreted as reservoir and are combined to represent a hill slope as shown in Figure 3-3.

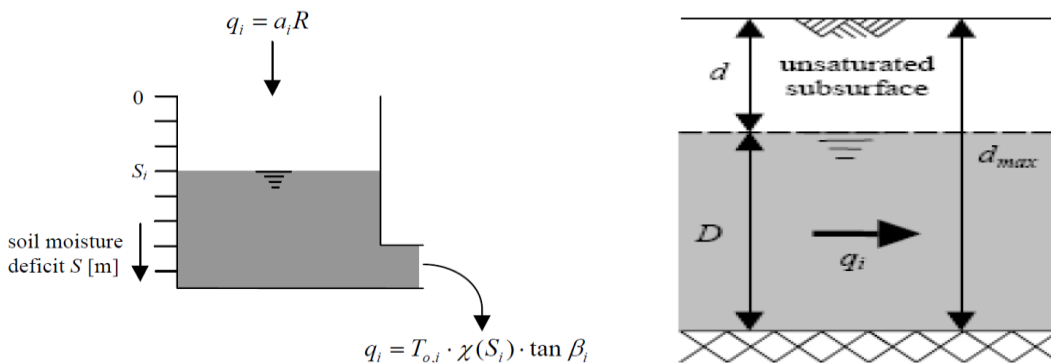


Figure 3-4: A linear storage reservoir and lateral saturated subsurface flow through a soil column (After Rientjes (2010))

Since in any simulation, the recharge rate is assumed constant throughout the catchment for calculation the actual groundwater discharge which also implies that the local moisture deficit is a function of catchment average wetness:

$$W = \frac{Ra}{T \tan\beta} = \bar{W} = \frac{a/\tan\beta}{\frac{1}{A} \int (a/\tan\beta) da} \tag{3.5}$$

Following the reasoning of above equation, the local soil moisture deficit can be expressed by

$$Z_i = -\frac{1}{f} \ln \left(\frac{Ra}{T \tan \beta} \right) = \bar{Z} - \frac{1}{f} \left(\ln \frac{a}{\tan \beta} - \lambda \right) \quad (3.6)$$

Detail equations and descriptions TOPMODEL can be found in (Beven and Kirkby, 1979a; Gumindoga, 2010; Rientjes, 2010) see also appendix C.

3.1.5. Unsaturated zone and root zone

The initial saturation deficit approach was found to be a convenient way to allow the effect of the unsaturated zone. Assuming that the delay in the unsaturated-zone is directly proportional to deficit at a point, the input from unsaturated zone for saturated zone was suggested and is given by the following equation (Beven and Wood, 1983):

$$q_v = \frac{S_{uz}}{S_i t_d} \quad (3.7)$$

Where

| | | |
|----------|---|----------------------|
| q_v | = the vertical (gravity) drainage from the unsaturated zone | [L T ⁻¹] |
| S_{uz} | = the unsaturated zone storage | [L] |
| S_i | = local saturated zone deficit | [L] |
| t_d | = time delay constant of the unsaturated zone | [T] |

In the root zone, some of the precipitation can be lost by evapotranspiration. The actual evapotranspiration is calculated as a function of potential evapotranspiration and maximum root zone moisture storage deficit. A reduction from the potential evapotranspiration value occurs depending on the moisture status of the root zone.

$$ET_a = ET_p \left(1 - \frac{SR_z}{SR_{max}} \right) \quad (3.8)$$

Where

| | | |
|------------|-------------------------------------|-----|
| ET_a | = actual evapotranspiration | [L] |
| ET_p | = potential evapotranspiration | [L] |
| SR_z | = the root zone storage deficit | [L] |
| SR_{max} | = maximum root zone storage deficit | [L] |

Any remaining water based on the relative values of the unsaturated zone storage and local storage deficit is allowed to evaporate with the maximum limit of SR_{max} . SR_{max} represents the maximum amount of water matrix that can be held against gravity.

However, in this study, the ET_a estimate (eq. 3.8) was replaced by the remote sensing base actual evapotranspiration estimated from surface energy balance system (SEBS) approach. This part of equation in the IDL code of the TOPMODEL has been modified to directly use the ET_a from SEBS.

3.1.6. Streamflow

To simulate the travel time, TOPMODEL uses a delay approach by using fractional area and its distance from the outlet as well as a fixed channel velocity across the catchment. The time span for each water particle to travel from each fractional area to the outlet is computed. Then contributions from each area are defined and accumulated for the calculation time steps (K. J. Beven and Kirkby, 1979b). The time taken to reach the catchment outlet (td_j) from any point can be given by

$$td_j = \sum_{i=1}^N \frac{x_i}{CHV \tan \beta_i} \quad (3.9)$$

Where

x_i = the length of the i^{th} flow path

$\tan\beta_i$ = the slope of the i^{th} segment of a flow-path comprising N segments between point j and the catchment outlet.

CHV = velocity parameter (main channel routing velocity)

3.2. Actual evapotranspiration estimation

3.2.1. Surface energy balance system (SEBS)

The satellite remote sensing approach for the estimation of ETa is an alternative and the only feasible means for projecting ETa over large-scale area and is important to account for the spatial variability and heterogeneity in the area. The surface energy balance system (SEBS) is one of the recently applied methods used to estimate the energy fluxes using remote sensing data. Evapotranspiration (ET) is the sum of evaporation of water from different bodies of the earth surface and transpiration from various types of plants. Evapotranspiration needs a heat energy source to convert water from liquid to vapour phase. Surface Energy Balance System (SEBS) proposed by Su (2002) is used to estimate the atmospheric turbulent fluxes and evaporative fraction by using satellite earth observation and meteorological information data for both local and regional scale.

Different satellite sensor products with different spatial, temporal and spectral resolution can be used with the integration of meteorological data to estimate the actual evapotranspiration. The application of remote sensing data on SEBS to estimate ETa has great improvement on its spatial coverage and considers the heterogeneity of the land surface on a larger scale. SEBS pre-processing in ILWIS has also many advantages because of its capability in the determination of the land surface physical parameters such as albedo, emissivity, and fraction of vegetation cover and NDVI from spectral reflectance and radiance signatures after (Su, 2002)

SEBS requires a set of inputs to estimate the energy fluxes. The two main sources are from satellite remote sensing and from meteorological stations. From remote sensing land surface albedo, land surface temperature, emissivity, fraction of vegetation cover (fc), leaf area index (LAI), normalized difference vegetation index (NDVI) can be obtained. From meteorological station data such as wind speed, air temperature, pressure at reference height, humidity and sunshine hours are also available. The incoming shortwave solar radiation is also important input for the SEBS and can be from different sources.

The simplified form of energy balance equation is given by

$$\lambda ET = R_n - G - H \quad (3.10)$$

Where λ = latent heat of evaporation of water, R_n = net radiation flux, G = soil heat flux and H = sensible heat flux (unit is w/m^2 or wm^{-2}).

3.2.2. Net radiation

$$R_n = (1 - a)(R_{S,\text{sun}} + R_{S,\text{sky}}) + R_{L,\text{sky}} - R_{L,\text{out}} \quad (3.11)$$

Where; R_s = incoming and outgoing short wave radiation

R_L = incoming and outgoing long wave radiation

a = albedo

3.2.3. Soil heat flux

The soil heat flux (G) is the component of the energy flux in the energy balance equation, which goes down into the soil during the day time and comes from the soil during the night time. Mostly, it can be considered as zero over the duration of 24 hours (daily base). The equation to calculate soil heat flux is given by

$$G = R_n(\Gamma_c + (1 - f_c)(\Gamma_s - \Gamma_c)) \quad (3.12)$$

Where it is assumed that the ratio of soil heat flux to net radiation $\Gamma_c = 0.05$ for full vegetation canopy (Monteith (1973) cited in Su (2002)) and $\Gamma_c = 0.315$ for bare soil (Kustas and Daughtry, 1989). Here interpolation is performed between these limiting cases using the fractional canopy coverage, f_c from remote sensing data modified after (Su, 2002).

3.2.4. Sensible heat flux

The sensible heat flux, which is difficult to measure directly, can be calculated through iteration due to the interdependency between sensible heat flux and aerodynamic resistance in theory of similarity.

$$H = \frac{\rho C_p (T_s - T_a)}{r_{ah}} \quad (3.13)$$

Where ρ - is the air density [kg m^{-3}], C_p - The heat capacity of dry air [$\text{J kg}^{-1} \text{K}^{-1}$], T_s = the surface temperature [K], T_a = air temperature at reference height [K], and r_{ah} = is aerodynamic resistance [s m^{-1}] which depends on the wind speed and surface roughness.

In SEBS it is possible to estimate the friction velocity, the sensible heat flux and the Obukhov stability length by solving a system of non-linear equations using an iteration procedure in all ranges of possible atmospheric stabilities. This procedure only needs inputs of wind speed and temperature at the reference height, as well as the surface temperature and is independent of other surface energy balance terms (Su, 2002).

3.2.5. Evaporative fraction

The evaporative fraction in SEBS is determined by considering the two limiting conditions known as the dry-limit and the wet-limit. In dry-limit, soil moisture is limited and the sensible heat flux is at its maximum value so that evaporation becomes zero after (Su, 2002) and is given by:

$$\Lambda = \frac{\lambda E}{R_n - G} = \frac{\Lambda_r \lambda E_{wet}}{R_n - G} \quad (3.14)$$

Considering the evaporative fraction as constant throughout the day, daily actual evapotranspiration can be estimated as:

$$E_{daily} = 8.64 \cdot 10^7 \cdot \Lambda_0^{24} \cdot \frac{R_n - G}{\lambda \rho_w} \quad (3.15)$$

Where E_{daily} is the daily actual evapotranspiration [mm/day] Λ_0^{24} is the daily evaporative fraction, ρ_w density of water [kg/m^3] and λ is latent heat of vaporization which can be calculated as $\lambda = (2.501 - 0.00237 * T_{air}) \times 10^6$

4. METHODS AND MATERIALS

4.1. Methodological approach

The TOPMODEL simulation results have been performed based on the parameters and available data sets. The data sets were obtained using satellite remote sensing and field observation. During the field work activities meteorological and hydrological data were collected from the respective offices. Some ground control points data at field level using GPS at different land cover classes were also collected for geo-referencing purpose. The meteorological data collected are listed in Section 2-3 of table 2-1.

Different satellite data that are used for the process of modelling were downloaded from the websites. Various MODIS pre-processed data for the SEBS algorithm were downloaded from the NASA ftp server. Resampling, re-projection and converting the MODIS HDF file format to Geotiff was done as a result of this study. The SRTM 90 m resolution DEM were also downloaded for the DEM-Hydro processing for the calculation of topographic index

The IDL code for the TOPMODEL has been modified and some adjustment to the set of parameters and variables were done. The workability of the code for the model simulation was checked. The general conceptual framework of the whole pre-processing and process is summarized in Figure 4-1

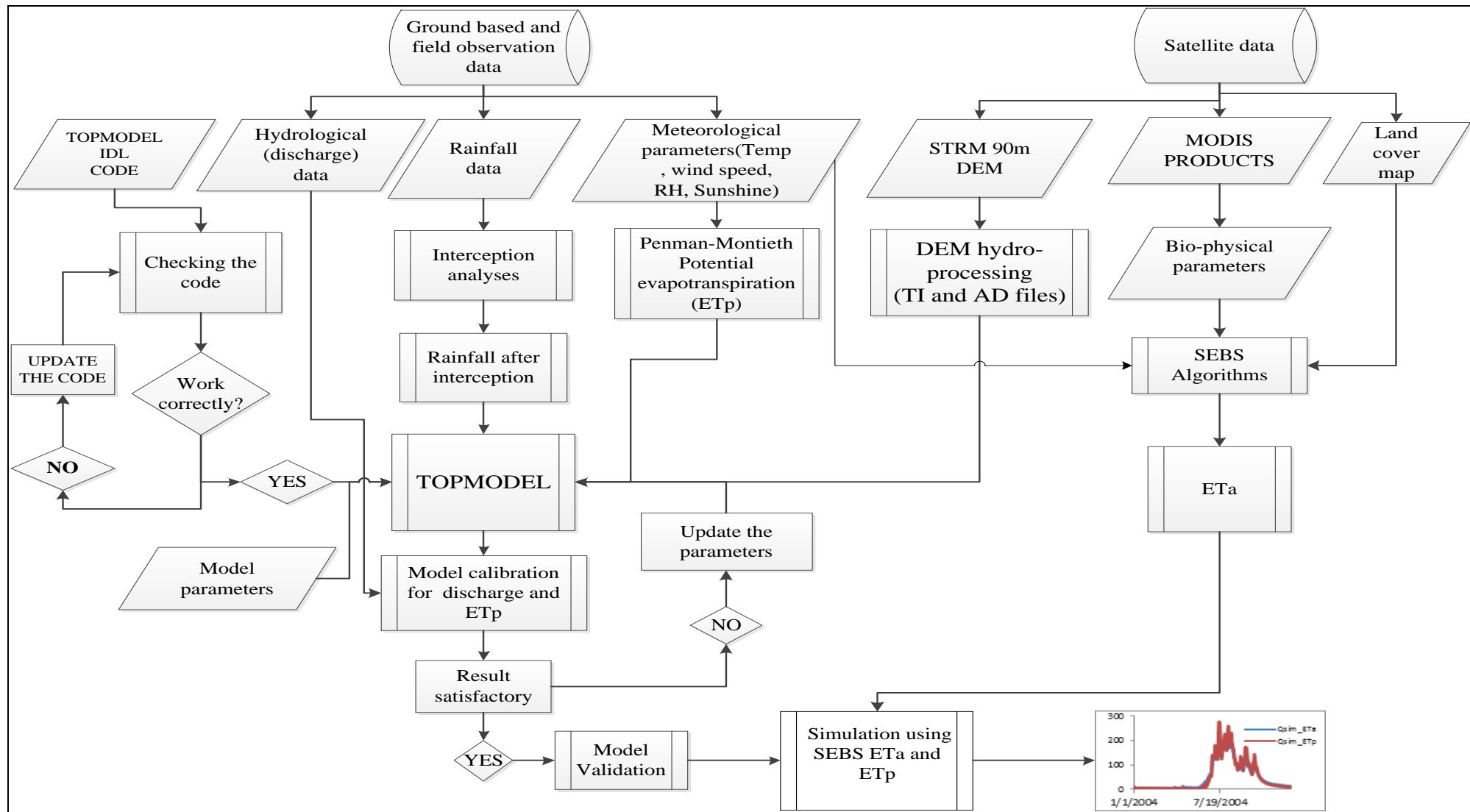


Figure 4-1: Flow chart showing the whole process and Methodology

4.2. **TOPMODEL approach**

4.2.1. **Spatial interpolation of rainfall**

The rainfall data for the study area were interpolated using the Thiessen polygon method which was named after Thiessen (1911) who used to estimate the regional average of rainfall. Based on the distribution of rainfall in the weather station, the Thiessen polygon is applied to calculate the average rainfall by connecting the neighbouring station to form polygons by forming the vertical bisector of each sides of the lines. The spatial average precipitation is then calculated by weighting the individual stations with their representative area and is given by

$$P = \frac{1}{A} \sum_{i=1}^n A_i P_i \tag{4.1}$$

Where

n is the number of rain gauge stations and A is the total surface area [m²] of the catchment which is the sum of sub-areas.

Using the point station data, the daily rainfall for the study area is interpolated using the Thiessen polygon in ILWIS Software to get the areal distribution pattern of rainfall.

Table 4-1: Thiessen weight values for the stations

| Station | Elevation [m] | Thiessen weight | Pann(2004) [mm] |
|------------|---------------|-----------------|-----------------|
| ADET | 2180 | 0.009691 | 1132 |
| DANGILA | 2119 | 0.135208 | 1627 |
| ENJIBARA | 2540 | 0.159391 | 2191 |
| KIDAMAJA | 1913 | 0.013183 | 2171 |
| SEKELA | 2690 | 0.385199 | 1959 |
| WETET_ABAY | 1913 | 0.297328 | 1308 |

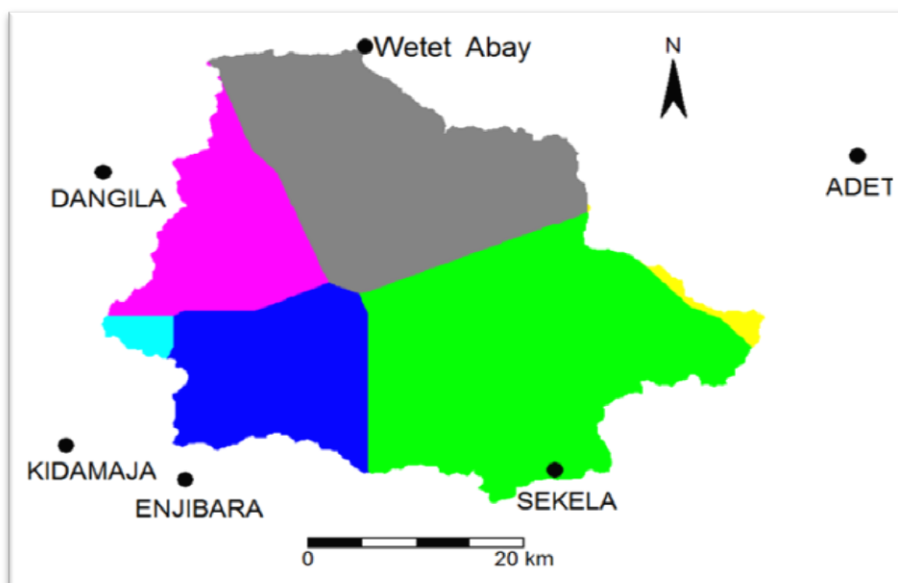


Figure 4-2: Thiessen polygon map for Gilgel Abay catchment

4.2.2. Potential evapotranspiration

Daily evapotranspiration is estimated by using FAO Penman-Monteith method of reference evapotranspiration. For calculation of potential evapotranspiration, data from stations Dangila, Adet and Bahir Dar were used. Evapotranspiration is calculated using FAO Penman-Monteith equation.

$$ET_o = \frac{0.408\Delta(R_n - G) + \gamma \frac{900}{T + 273} U_2 (e_s - e_a)}{\Delta + \gamma(1 + 0.34U_2)} \quad (4.2)$$

Where:

| | | |
|-------------|--------------------------------------|---|
| ET_o | = reference evapotranspiration | [mm day ⁻¹] |
| R_n | = Net radiation at the crop surface | [MJ m ⁻² day ⁻¹] |
| G | = Soil heat flux density | [MJ m ⁻² day ⁻¹] |
| T | = air temperature at 2 meter height | [°C] |
| U_2 | = Wind speed at 2 meter height | [m s ⁻¹] |
| e_s | = Saturation vapour pressure | [KPa] |
| e_a | = actual vapour pressure | [KPa] |
| $e_s - e_a$ | = saturation vapour pressure deficit | [KPa] |
| Δ | = slope of vapour pressure curve | [KPa °C ⁻¹] |
| γ | = psychometric constant | [KPa °C ⁻¹] |

4.2.3. Interception module

An Intercepted rainfall amount was estimated based on the method described on the work of Gumendoga (2010) using rainfall method. The rainfall method which was described in agro hydrological model Soil-Water-Atmosphere and Plant (SWAP) was used to estimate this intercepted rainfall amount by different vegetation type such as crop, grass and forest.

For the crops and grasslands, the intercepted precipitation based on Van Dam (2000) was estimated using the following equation

$$P_i = aLAI \left[1 - \frac{1}{1 + \frac{bP_{gross}}{aLAI}} \right] \quad (4.3)$$

Where

| | | |
|-------------|--------------------------------------|-----------------------------------|
| P_i | = intercepted precipitation | [cm] |
| LAI | = Leaf area index | [m ² m ⁻²] |
| P_{gross} | = gross precipitation | [cm] |
| a | = empirical coefficient | [cm] |
| b | = the soil cover fraction (=LAI/3.0) | [-] |

This method is an assumption that the amount of interception storage asymptotically reaches a maximum value that is factored in the a LAI part of equation. The aLAI is called the saturation amount. The value of a here is taken from literatures though the actual value should be determined experimentally. The value of a for crops is a= 0.25 was assumed based on Van Dam(2000).

In the case of forest, Equation (4.3) has limitations to consider the effects of rainfall and evaporation during the rain events which is not taken into account at this form. Hence, interception by forest trees and the effect of evaporation during rainfall event should be considered. For forest interception, The storm-based analytical model described by Gash (1979) demonstrate that the evaporation of rainfall intercepted by forest canopies can be estimated from the forest structure, the mean evaporation and rainfall rates, and

the rainfall pattern. This model has been used with some success over various different forests. The model considers three discrete rainfall phases, wetting period, saturation and drying period after rainfall stop. Here the canopy is assumed to have sufficient time to dry out between storms events. During the wetting period, an increase intercepted amount is described (Gash, 1979; Gash et al., 1995) given by:

$$\frac{\Delta P_i}{\Delta t} = (1 - p - p_t)P_{\text{mean}} - \frac{P_i}{S} E_{\text{mean}} \quad (4.4)$$

Where

- p = a free throughfall coefficient [-]
 p_t = the portion of the rainfall diverted to stemflow [-]
 P_{mean} = the mean rainfall rate [mmh⁻¹]
 E_{mean} = the mean evaporation rate of intercepted water when the canopy is saturated [mmh⁻¹]
 S = the maximum storage of intercepted water in the canopy [mm]

The integration of equation [4.4] yields the amount of rainfall, P_s [mm] that saturates the canopy:

$$P_s = \frac{P_{\text{mean}}}{E_{\text{mean}}} S \ln \left(1 - \frac{E_{\text{mean}}}{P_{\text{mean}}(1-P-p_t)} \right) \quad \text{with} \quad 1 - \frac{E_{\text{mean}}}{P_{\text{mean}}(1-P-p_t)} \geq 0 \quad (4.5)$$

For small storms ($P_{\text{gross}} < P_s$) the intercepted rain amount can be calculated from:

$$P_i = (1 - p - p_t)P_{\text{gross}} \quad (4.6)$$

For large storms ($P_{\text{gross}} > P_s$) the interception is given by:

$$P_i = (1 - p - p_t)P_s + \frac{E_{\text{mean}}}{P_{\text{mean}}} (P_{\text{gross}} - P_s) \quad (4.7)$$

The Gash's analytical model of rainfall interception describe above is reformulated by Gash et al (1995), with improving the boundary conditions for a better description of the evaporation from sparse forest.

4.2.4. TOPMODEL inputs and parameters

1. The hydro meteorological file: This file is a text file format containing three column in the following order;
 - A. Daily average Rainfall data for the whole catchment estimated using Thiessen polygon method from meteorological stations.
 - B. Evapotranspiration (ET) data: This input data were estimated using two methods. The first one was from SEBS by using MODIS data. The second one is using the Penman-Monteith equation by applying the meteorological stations data.
 - C. The daily historical discharge data is used to estimate the two parameters m and T_0 . The base flow recession that is not affected largely by evapotranspiration and rainfall has been calculated and transferred in to simple time function.
2. The topographic index data has been prepared using the SRTM 90 m resolution DEM using ILWIS Software. The file is in text format with two columns. The first is the percentage of the basin area with particular values in histogram bin and the second is the value of the topographic index in that histogram bin.
3. Area distance file this is also a text file which gives the cumulative of the area with distance from the catchment outlet for routing the streamflow and overland flow. Here the catchment is divided into sub catchments based on the distance interval from the outlet.

4. A parameter file which is also a text file that contains the values of different parameters and their values. Table 4-2 shows the parameters that are used in TOPMODEL and their definition and applications.

Table 4-2: Different parameters for the TOPMODEL

| Parameters | Descriptions | Used in |
|-----------------------|---|---|
| m [m] | The parameter of the exponential transmissivity function or recession curve that controls the rate of decline of T_o . Derived from analysis of catchment recession curves and its lower limit is 0.005 | The decline of local transmissivity equation showing decreasing storage in the soil profile. $T = T_o e^{-S_i/m}$ |
| To[m ² /h] | The natural logarithm of the effective transmissivity of the soil when just saturated A homogeneous soil throughout the catchment is assumed | Used in the same equation like above , $T = T_o e^{-S_i/m}$ |
| SRmax [m] | The soil profile storage available for transpiration, i.e. an available water capacity | $E_a = E_p(1 - \frac{SR_z}{SR_{max}})$ |
| SRinit [m] | The initial storage deficit in the root zone (an initialisation parameter) | |
| CHV[m/h] | Effective surface routing velocity for scaling the distance/area or network width function. Linear routing is assumed. | The velocity used in the channel routing. $td_j = \sum_{i=1}^N \frac{x_i}{CHV \tan \beta_i}$ |
| RV[m/h] | Channel routing velocity in the catchment | |
| Td [h] | Time delay constant for routing understand flow (>0.0). | Used in time delay per unit time of deficit equation $q_v = \frac{S_{uz}}{S_{itd}}$ |
| Q _o [m/h] | Initial stream discharge mostly set to the first observed discharge. This flow is assumed to represent only the subsurface flow contribution of the catchment. | |
| dθ DTH(dtheta) | Change in water content across the wetting front | |
| XKo | Surface hydraulic conductivity. Used in the unsaturated zone time delay function if td is negative. | |
| INFEX [-] | An infiltration flag set to 1 to include infiltration excess, otherwise 0. Infiltration excess runoff is calculated using Beven’s version of the Green-Ampt model. | Set to zero (0) for simplicity |
| | | |

4.2.5. TOPMODEL modification

For this study the model approach has been developed using Interactive Data Language Programming (IDL) using the equation and algorithm from (K. Beven, 1997) and (Beven, 2001). The TOPMODEL is primary concerned with a simplified model of the saturated zone and its control of surface and subsurface contributing area. However, for its complete simulation, other components like interception, infiltration, evapotranspiration, unsaturated zone and flow routing should be considered.

Modification of the TOPMODEL IDL code has been done to allow application of the TOPMODEL simulation using actual evapotranspiration estimated from SEBS. The model uses the potential evapotranspiration from Penman-Monteith to calculate actual ETa for modelling its water balance. For this the model uses the maximum root zone storage deficit (SRmax), actual root zone storage deficit (SR) and ETp to calculate ETa as described in equation (3.8) of section 3.1.8. In the application of ETa for the TOPMODEL simulation, this part of equation is changed and modified to use directly satellite based ETa estimated from SEBS.

4.2.6. Sensitivity analysis, model calibration and validation

The effects of change in parameters values on the output of TOPMODEL simulation can be done by sensitivity analysis. Parameters that are very sensitive and show significant change on simulation results are m , To and $SRmax$. These parameters were used to calibrate the model against the observed runoff. The sensitivity analysis for each parameter to the simulation result has been checked one-by-one keeping others constant.

The first simulation of the TOPMODEL is made for the period 1996- 2003 using parameter values obtained from the work of Gumindoga (2010). The model calibration for the TOPMODEL was done manually by trial and error changing the value of sensitive parameters until optimal model performance was gained. First the parameter values were changed to get better fits to baseflow and then the peak flow. Then the parameter values were adjusted until the recession tail and rising limbs show better fits. Model validation was performed using a 2004 dataset. The optimum parameter values obtained from calibration process were used for the validation of the TOPMODEL.

Two objective functions were applied to analyses the performance of TOPMODEL by comparing the simulated and observed streamflow. The performance measures used in this study are Nash-Sutcliffe Efficiency (NS) and Relative Volume Error (RVE).

Nash-Sutcliffe efficiency

The Nash-Sutcliffe efficiency measure is given by the formula

$$R^2 = 1 - \frac{\sum_{i=1}^N (Q_{obs} - Q_{sim})^2}{\sum_{i=1}^N (Q_{obs} - \bar{Q}_{obs})^2} \quad (4.8)$$

Where

| | | |
|-----------------|-----------------------------------|----------------|
| Q_{obs} | = the observed discharge | $[L^3 T^{-1}]$ |
| Q_{sim} | = predicted observed discharge | $[L^3 T^{-1}]$ |
| \bar{Q}_{obs} | = the observed mean discharge | $[L^3 T^{-1}]$ |
| N | = the total number of time steps. | $[-]$ |

The higher performance indicates when the R^2 value approach to 1 (Nash and Sutcliffe, 1970).

Relative Volume Error (RVE)

The other objective function used to measure the performance of the model is RVE. It uses to measure the volume error between the observed and simulated. It is given by:

$$RVE = \left[\frac{\sum (Q_{sim} - Q_{obs})}{Q_{obs}} \right] * 100 \quad (4.9)$$

When the relative volume error is 0 implies there is no difference between simulated and observed runoff volume and suggest that the model performs very well.

4.3. Energy balance modelling

For this study the surface energy balance system (SEBS) is applied in ILWIS software. SEBS uses Meteorological and Satellite data for its input to calculate ETa. In the following steps both meteorological data collected during field work and the MODIS satellite data pre-processing and preparation of all inputs for SEBS algorithm are discussed.

4.3.1. Meteorological data processing for SEBS

For the estimation ETa using SEBS algorithm meteorological data were collected from 7 stations of which three are principal stations with 6 parameters (rainfall, minimum and maximum temperature, wind speed, relative humidity and sunshine hours), two of stations are class-3 with only rainfall, maximum temperature and minimum temperature the remaining two are class-4 with only rainfall data.

Wind speed at 2 meter

The average daily wind speed data were collected from three weather station for analysis. From these stations point maps were created using ILWIS and applying the moving average interpolation technique, the areal map of wind speed was produce in daily based for the year 2004.

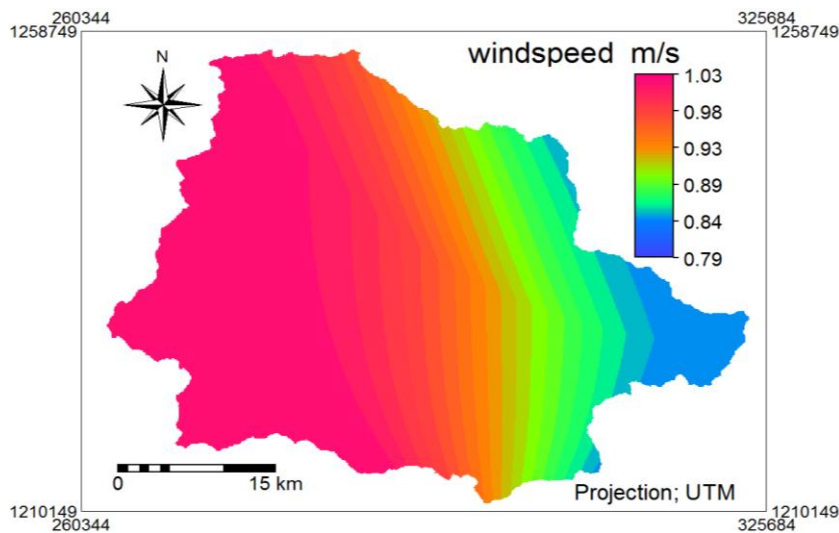


Figure 4-3: Sample windspeed map prepared after interpolation by moving average.

AIR Temperature at surface.

The air temperature of point observation data from four stations(Adet,Dangila,Bahir Dar and Kidamaja) were used for this study. The daily mean temperature of these stations were correlated with elevation of each station taking one station for example (Adet station) as fixed variable so that deviation from this station(daily temperature, and elevation) were calculated.The average correlation function of daily temperature with elevation was derived from this relation and found to be

$$T_s = \alpha(\text{Elev} - \text{Elev}_{\text{Adet}}) + \beta + T_{\text{Adet}} \quad (4.10)$$

Where T_s is air temperature at any point, Elev is Elevation map (SRTM DEM), and $\text{Elev}_{\text{Adet}}$ is elevation of Adet station, T_{Adet} is mean daily temperature of Adet setation, α and β are the slope and intercept of the correlation function. The value for slope and intercept are given in Table 4-3. The areal map of the air temperature for daily base was calculated using the SRTM DEM map the study area using ILWIS software.

Table 4-3: Stations and some values used for correlation air temperature with elevation

| Stations | Adet | Bahir Dar | Dangila | Kidamaja |
|--|--|-----------|---------|----------|
| Elevation | 2180 | 1797 | 2119 | 1913 |
| Difference in elevation with respect to Adet | 0 | 383 | 61 | 267 |
| Days | change in temperature with respect to Adet | | | |
| 1 | 0 | -1.3 | 1.1 | -0.6 |
| 2 | 0 | -0.6 | 0.85 | -0.73 |
| 3 | 0 | -0.8 | 3.5 | -0.38 |
| - | - | - | - | - |
| - | - | - | - | - |
| 366 | 0 | -2.2 | -0.7 | -2.2 |
| Average difference in temperature | 0 | -2.400 | 0.476 | 0.0281 |
| Average slope (α) | -0.005723 | | | |
| Average intercept (β) | 0.543730 | | | |

Reference and surface Pressure

The atmospheric pressures is an important parameter in SEBS for the estimation of surface turbulent heat flux at different location. In this study the SRTM (DEM) was used for the determination of air pressure at the surface and reference height from a simplified ideal gass law (Allen et al., 1998) is given below.

$$p = 101.3 * \left(\frac{293 - 0.0065 * Z}{293} \right)^{5.26} \quad (4.11)$$

Where P - is air pressure [KPa]

Z- the elevation above sea level [m] in this case DEM map of the study area.

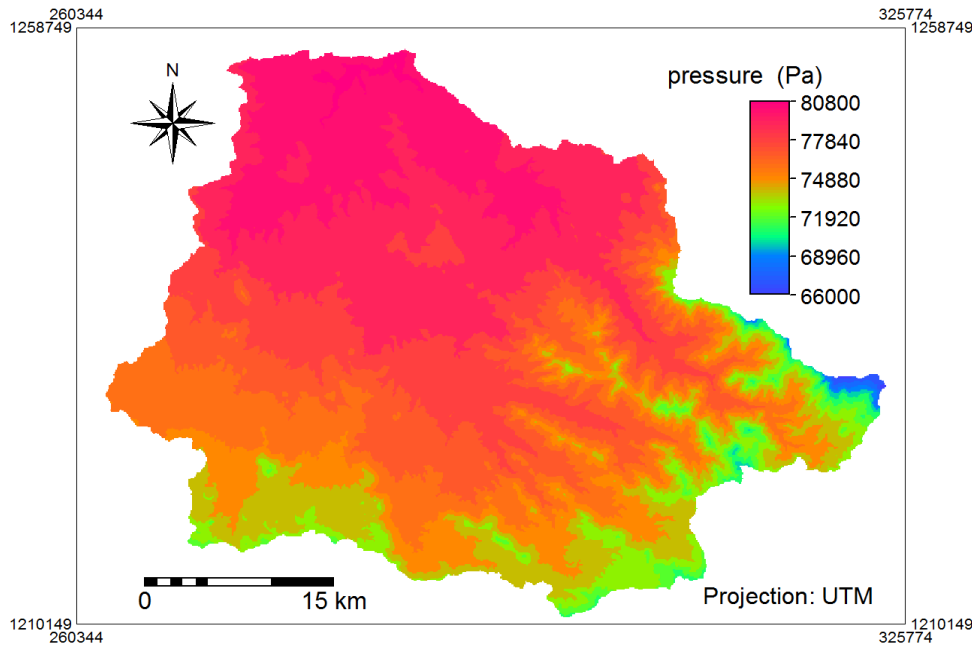


Figure 4-4: Estimated surface pressure map from digital elevation map

Sunshine hours.

Sunshine hours for this study were taken from 3 stations (Adet, Bahir Dar and Dangila). Average daily sunshine hours were calculated from this station.

Specific humidity

Specific humidity is defined by the mass of water vapour present in a unit mass of moist air (Brutsaert, 2005). SEBS required the value of the specific humidity at the meteorological stations. The specific humidity can be calculated as

$$q = \frac{5}{8} \cdot \frac{e_a}{p} \tag{4.12}$$

Where

e_a = the actual water vapor pressure

p = the surface pressure

Filling of missing data from stations

In some stations, missing data were observed during data collection. A simple statistical analysis was applied to fill the data gaps. Long time series data were used starting from 1996 to 2005. A simple averaging technique, which considers the same day of each year will have probability to have similar meteorological value so that the missing data will share this value too and will take the average value of the observed data of same day for all year. Using this method, the missing data of each station were first filled before further analysis is done. The data that have been filled by this method were, Temperature, wind speed, relative humidity and sunshine hours.

4.3.2. MODIS satellite data preparation

The MODIS Terra products were used for the estimation of surface energy fluxes of the Gilgel Abay catchment using SEBS algorithm. MODIS products acquired include the land surface temperature and Emissivity, Surface Reflectance Albedo, Normalized Difference Vegetation Index (NDVI), Leaf Area Index (LAI). Other products found jointly with other data are MIR (mid infrared reflectance and solar Zenith angle) with Vegetation index. Major MODIS products are collected from collection 5 and other inputs for the SEBS are calculated from these products such as fraction of vegetation cover (fc) from NDVI.

Land surface temperature (LST)

The MODIS/Terra Land Surface Temperature and Emissivity (LST/E) products provide per-pixel temperature and emissivity values in a sequence of swath-based to grid-based global products with sinusoidal projection and produced daily at 1 km spatial resolution.

Before re-projecting and resampling of the land surface temperature for the study area, the cloud free images were selected by help of BEAM software and by visualation over the area. 152 cloud free or very little cloud effect LST images were selected for further processing for the whole year of 2004. Those little cloud effect pixels were corrected and estimated through the correlation the LST images with DEM. Each LST map was crossed (overlaid) with the DEM map and using correlation function with polynomial of degree two in ILWIS and the relation function were derived. Based on their correlation function equation, only the cloud effect pixels were corrected by keeping the other pixels values untouched. The average relation function between DEM and LST is given by:

$$P = 316.389 - 0.008 * DEM \tag{4.13}$$

Where p= pixel with no value [k] , DEM= digital elevation map [m]

The distribution Land Surface Temperature and Emissivity and other MODIS products per month of the year is given in the Table 4-4.

Table 4-4: The distribution of MODIS products in each month of 2004 used for SEBS algorithm

| Months of the year | Product type & Name | | | | | | |
|--------------------------|---------------------|---------|---------|---------|----------|-----------------------|---------|
| | LST& Emissivity | Albedo | NDVI | LAI | MIR_refl | Solar Zenith Angle | FPAR |
| | MOD11A1 | MOD43A3 | MOD13Q1 | MOD15A2 | MOD13Q1 | MOD13Q1 | MOD15A2 |
| Jan | 19 | 4 | 2 | 4 | 2 | 2 | 4 |
| Feb | 15 | 4 | 2 | 4 | 2 | 2 | 4 |
| Mar | 17 | 4 | 2 | 4 | 2 | 2 | 4 |
| April | 5 | 4 | 2 | 4 | 2 | 2 | 4 |
| May | 13 | 3 | 2 | 3 | 2 | 2 | 3 |
| June | 4 | 3 | 2 | 3 | 2 | 2 | 3 |
| July | 7 | 4 | 2 | 4 | 2 | 2 | 4 |
| Aug | 4 | 4 | 2 | 4 | 2 | 2 | 4 |
| Sep | 14 | 4 | 2 | 4 | 2 | 2 | 4 |
| Oct | 16 | 4 | 2 | 4 | 2 | 2 | 4 |
| Nov | 16 | 3 | 2 | 3 | 2 | 2 | 3 |
| Dec | 22 | 4 | 2 | 4 | 2 | 2 | 4 |
| Total | 152 | 45 | 24 | 45 | 24 | 24 | 45 |

Albedo 16-Day L3 Global

Albedo is important parameter for the estimation of the energy flux in SEBS algorithm. The MODIS Albedo product (MCD43A3) provides 500-meter data describing both directional hemispherical reflectance (black-sky albedo) and bi-hemispherical reflectance (white-sky albedo) with 16 days temporal resolution level-3 gridded data set in Sinusoidal projection. The Total albedo under actual atmospheric conditions can be calculated by using the two black-sky (direct beam) albedo and white-sky (completely diffuse) albedo as a function of the fraction of diffuse skylight (DF) (Román et al., 2009) using the following formula

$$\alpha = (1 - DF) * (BSA_{sw}) + DF * WSA_{sw} \quad (4.14)$$

Where α - total albedo, BSA_{sw} and WSA_{sw} are Black-sky and white-sky albedo of MODIS products from shortwave bands

DF -fraction of diffuse skylight =0.75 ,This value is taken from Roman et al (2009)

Broadband surface Emissivity (ϵ_o)

From MODIS products emissivity was derived from the two thermal bands (band 31 and band 32) with wavelength of 10.5 μm and 11.5 μm respectively within the MOD11A1 products. The broadband emissivity was calculated using the formula stated by Jacob et al (2004).

By using thermal bands and midwave infrared band, $\rho_{2.13\mu m}$ broadband emissivity was calculated.

$$\epsilon_o = a + c\rho_{2.13\mu m} + b(\max(\text{band31}, \text{band32}) - \min(\text{band31}, \text{band32})) \quad (4.15)$$

Where ϵ_o - broadband emissivity, $\rho_{2.13\mu m}$ -midwave infrared band, Band31 and band32 thermal bands from MODIS. a,b and c are constants with values 0.986, 0.2662 and -0.0757 respectively.

Leaf area index (LAI)

The leaf area index (LAI) for this study was collected from MODIS products of MOD15A2 which is an eight-day composite product and is one of the biophysical data archived in the NASA HDF-EOS data format. These leaf area index images were reprojected resampled and converted to Geo-tiff format using modis reprojection tool and imported to ILWIS for further processing. The MODIS LAI products provide global LAI retrieved from atmospherically corrected bidirectional reflectance of (MOD09 surface reflectance product) by (Myneni et al., 2002). It has a spatial resolution of 1km and temporal resolution of 1 and 8 days.

on monthly basis the average leaf area index of the study area was calculated. The two extremes (the driest and the wettest) months were selected to see the change of LAI (Fig 4.5). The seasonal variation of LAI for different land cover class for 2004 is shown in Figure 5-1 in the result Section 5-1.

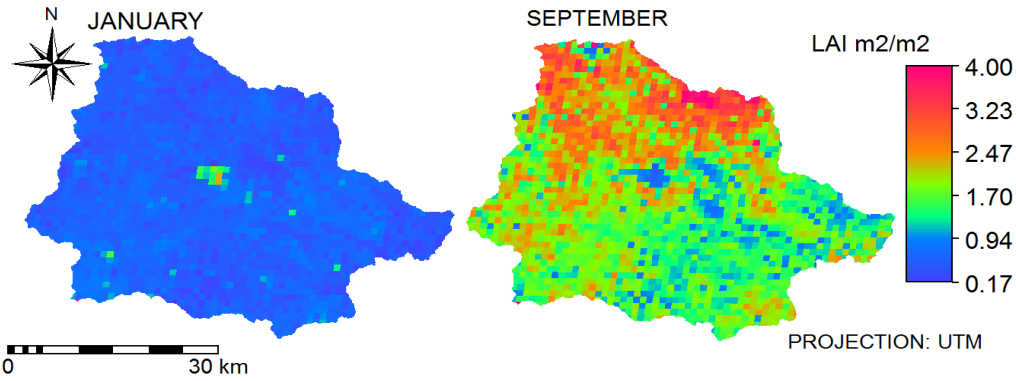


Figure 4-5: MODIS average leaf area index of Gilge Abay for dry and wet months.

Fraction of vegetation cover (FC)

The fraction of the vegetation cover is a compulsory input in SEBS since it will directly be used in the calculation Stanton number, KB^{-1} (a dimensionless heat transfer coefficient), the soil heat flux and other important variables. In this study, the fraction of vegetation cover was estimated based on the NDVI by using the following formula given below

$$fc = \left(\frac{NDVI - NDVI_{min}}{NDVI_{max} - NDVI_{min}} \right)^2 \quad (4.16)$$

Where $NDVI_{min}$ and $NDVI_{max}$ are the minimum and maximum NDVI during the study period. In this study area the maximum and minimum NDVI were 0.89 and 0.18 respectively.

Aerodynamic roughness height (Z_{om})

Aerodynamic roughness height (Z_{om}) is an important vegetation parameter which has influence on the transference of momentum in the surface energy balance system. It is the height above the displacement height (d) at which mean wind speed becomes zero (Brutsaert, 2005). In this study the Aerodynamic roughness height (Z_{om}) was calculated using the land cover map of the study area. The land cover map used was prepared by (Kebede, 2009) and further used by Gumindoga (2010).

Using this land cover map, two maps with maximum and minimum expected crop height during the whole season were prepared as shown in Figure 5-6. Using these two maps and NDVI, the crop height for every 16 days was prepared using the following.

$$h = h_{min} + \left(\frac{h_{max} - h_{min}}{NDVI_{max} - NDVI_{min}} \right) * (NDVI - NDVI_{min}) \quad (4.17)$$

where h - crop height , h_{min} -minimum crop height, h_{max} - maximum crop height, $NDVI_{max}$ & $NDVI_{min}$ maximum (fully vegetated) and minimum (bare soil) pixels NDVI value of the NDVI map. The unit is in meter (SEBS for ILWIS 3.4 open source).

Table 4-5 shows attribute tables used to create the maximum and minimum crop height map for different land cover classes. These crop height were decided from the experience for the study area. For instance during the dry season most agricultural lands have the minimum height and during the wet season experiences the maximum height. On the other hand forest do not have significant changes throughout the year.

Table 4-5: Attribute of annual minimum and maximum crop height for different land cover classes

| Land cover class | Minimum height [m] | Maximum height [m] |
|------------------|--------------------|--------------------|
| AG | 0.05 | 2.00 |
| F | 8.00 | 8.00 |
| GL | 0.10 | 0.50 |
| SL | 2.50 | 3.00 |
| WL | 0.20 | 1.00 |
| WM | 0.05 | 0.20 |

AG- agriculture, F- forest, GL- grassland, SL- shrubland WL -wetland and WM – water and marshy area

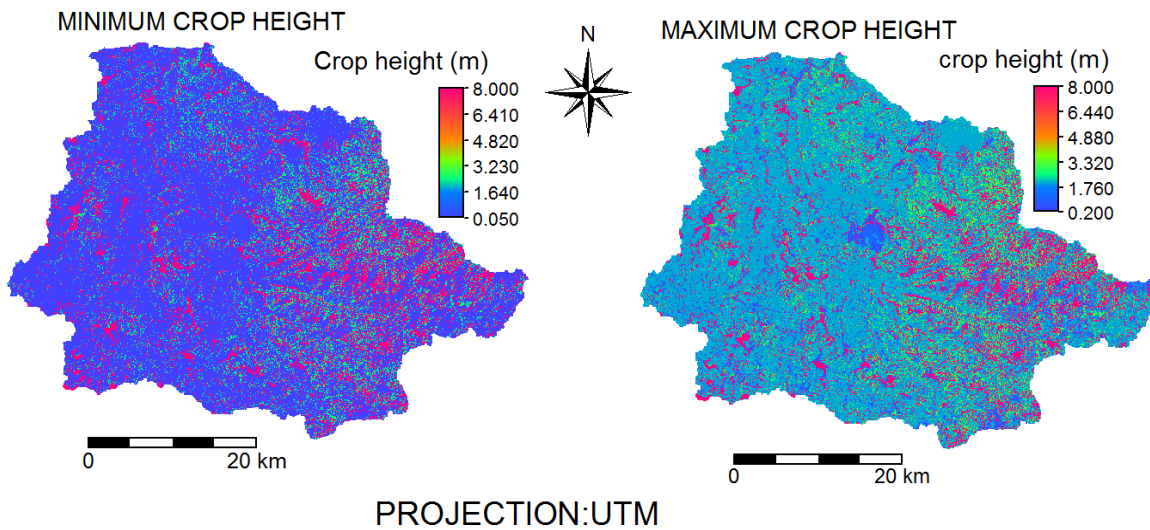


Figure 4-6: Annual maximum and minimum crop height map based on the land used classification

By using these crop height maps the Aerodynamic roughness height were calculated for every 16 days by the formula.

$$Z_{om} = 0.136 * h \tag{4.18}$$

Where h average crop height [m] calculated in equation 4-17 above and Z_{om} -Aerodynamic roughness height[m].

4.3.3. Reprojection of MODIS products.

MODIS Re-projection Tool is a software tool used for reading data files in HDF-EOS format, specify a geographic subset or band subset as input to processing, perform geographic transformation to a different coordinate system/cartographic projection and it also uses to write the output to file formats other than HDF-EOS. This software is downloaded free of charge after registration from the website

https://lpdaac.usgs.gov/tools/modis_reprojection_tool. Figure 4-7 shows an example of the MODIS Tool interface during reprojection and resampling process

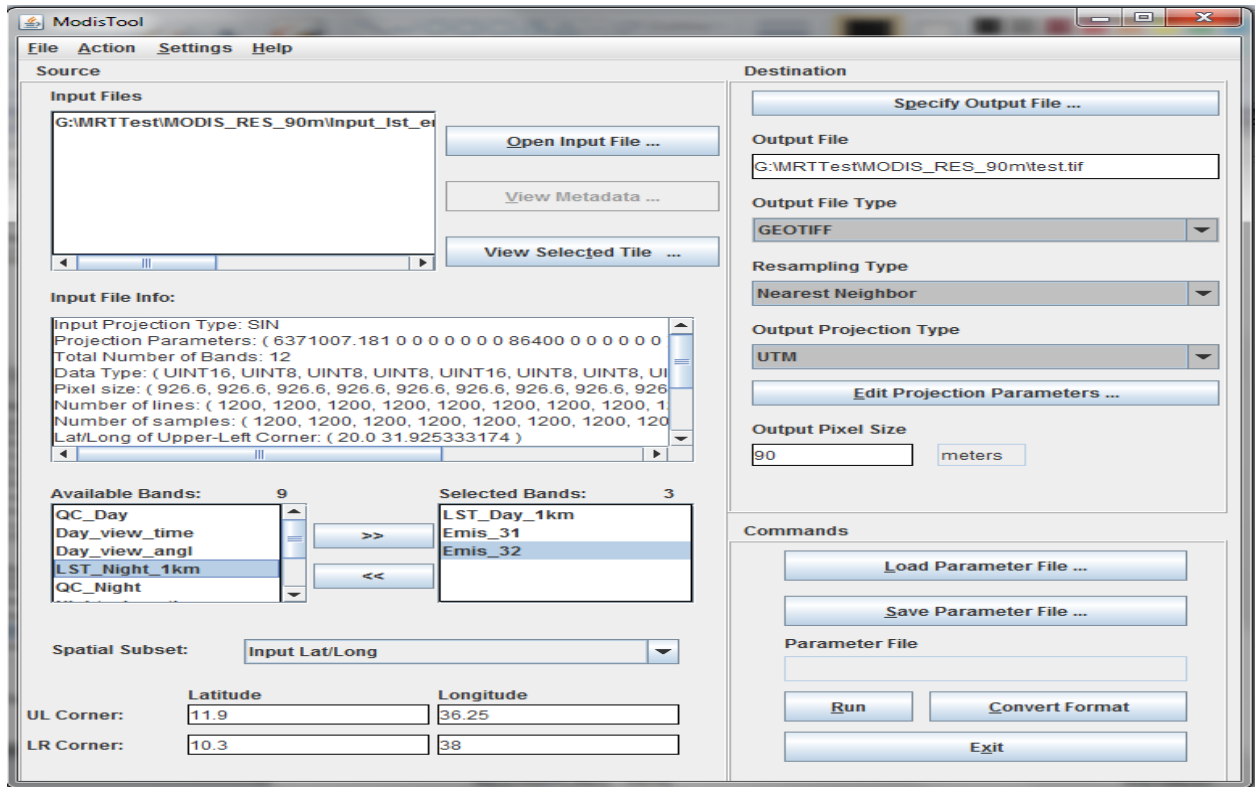


Figure 4-7: MODIS re-projection Tool

For the study area the MODIS product was reprojected, resampled and converted to Goetiff file format for further analysis by importing in ILWIS. Sample parameters for the re-projection and resampling of the MODIS product is given in the table 4-6.

Table 4-6: MODIS re-projection settings for this study

| sample re-projection setting | Parameters |
|----------------------------------|------------------|
| SPATIAL_SUBSET_UL_CORNER Lat/lon | 11.9 / 36.25 |
| SPATIAL_SUBSET_LR_CORNER lat/lon | 10.3 / 38.0 |
| RESAMPLING_TYPE | NEAREST_NEIGHBOR |
| OUTPUT_PROJECTION_TYPE | UTM |
| OUTPUT_PROJECTION_PARAMETERS | Geo-tiff |
| DATUM | WGS84 |
| UTM_ZONE | 37 |
| OUTPUT_PIXEL_SIZE | 90m |

The reprojected and resampled MODIS products were imported to ILWIS for further processes. All the HDF data format were converted to Geo-tiff data format using MODIS reprojection Tool. Correction of all the image to their actual value using scale factor and offsets have been done in ILWIS map calculation. The scale factor and offset were taken by opening the HDF data in the HDF viewer tool. Table 4-7 shows the MODIS products and the scale factor and offset used.

Table 4-7: MODIS conversion factors from the HDF viewer

| MODIS product | Unit | Scale factor | Offset |
|--------------------------|--------------------------------|------------------|--------|
| Land surface temperature | Kelvin | 0.002 | 0.0 |
| Emissivity | No unit | 0.002 | 0.49 |
| Albedo | No unit | 0.001 | 0.0 |
| Vegetation index (NDVI) | NDVI | 10 ⁻⁴ | 0.0 |
| leaf area index (LAI) | m ² /m ² | 0.10 | 0.0 |
| Solar zenith angle | Degree | 10 ⁻² | 0.0 |
| MIR (mid-wave infrared) | Reflectance | 10 ⁻⁴ | 0.0 |

4.3.4. Shortwave solar radiation downward

Incoming shortwave solar radiation for this study were taken from the website of ECMWF (the European Center for Medium-Range Weather Forecast). It is an intergovernmental Organization supported by 34 states and based in London, United Kingdom. ECMWF provides products of its operational forecasts to member states and co-operating states, WMO and public with various levels of access restriction.

The surface downward solar radiation was downloaded for the study area from the ECMWF website (http://data-portal.ecmwf.int/data/d/interim_daily/). The data have spatial resolution of 1.5 degree and 3 hours temporal resolution. The NetCDF file was converted into Geo-tiff file format by using Matlab programming for further processing. From all the 3 hourly data, 12:00 AM data were selected and imported in ILWIS software because this time is the nearest time to the satellite overpass time. The average three hourly shortwave radiations for the Gilgel Abay catchment are shown in the Figure 4-8.

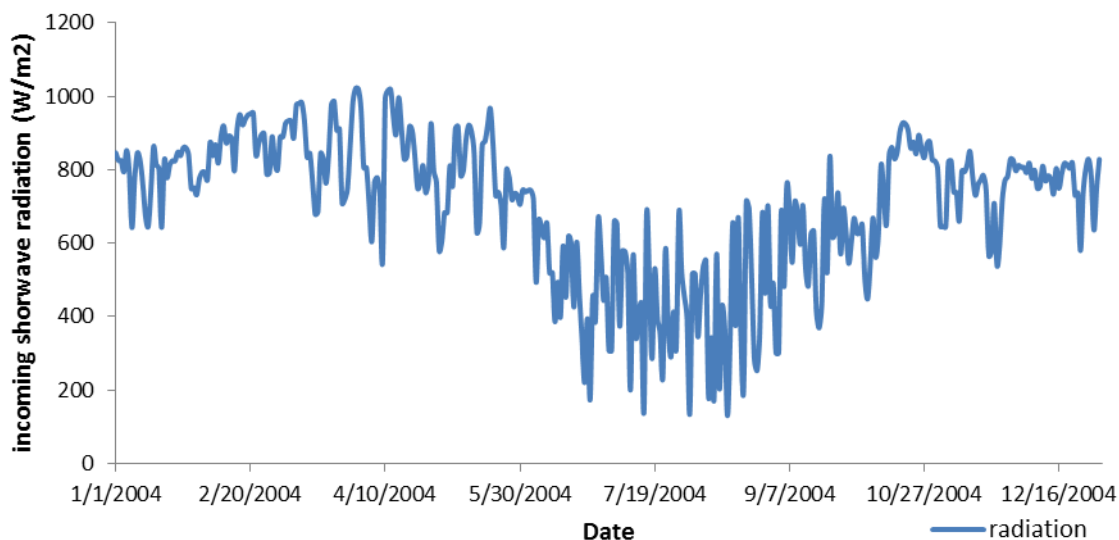


Figure 4-8: Surface downward solar radiation from ECMWF

From the graph the highest incoming short wave radiation is observed during the dry season (between November and April). This is because the incoming radiation can reach to the earth with less atmospheric effect like cloud. On the other hand the wet season (from June to September) the lowest value is recorded due to atmospheric and cloud effect.

4.3.5. SEBS time series completion

Due to some cloud effect specially on the land surface temperature of MODIS product , it was impossible to get full season daily remote sensing data. Only 152 days cloud free images were found with no cloud effect. Actual evapotranspiration was first estimated for those days. To fill this gap it was necessary to interpolate between consecutive ETa because TOPMODEL requires ETa value for daily base throughout the year. A simple linear interpolation technique was applied to estimate the ETa for cloudy days. An example of linear interpolation equation to calculate ETa is given below.

$$ET_2 = \left(\frac{ET_3 - ET_1}{X_3 - X_1} \right) (X_2 - X_1) + ET_1 \tag{4.19}$$

Where

ET_2 - the unknown ETa value, ET_3 and ET_1 are the ETa values or maps for day 3 and 1 respectively.

X_1, X_2 and X_3 are Julian days.

Based on the above linear interpolation technique the missing days ETa has been estimated and filled. The average daily ETa for the whole catchment and for each land cover classes for all julian days is shown in Figure 4-9 and 4-10 respectively.

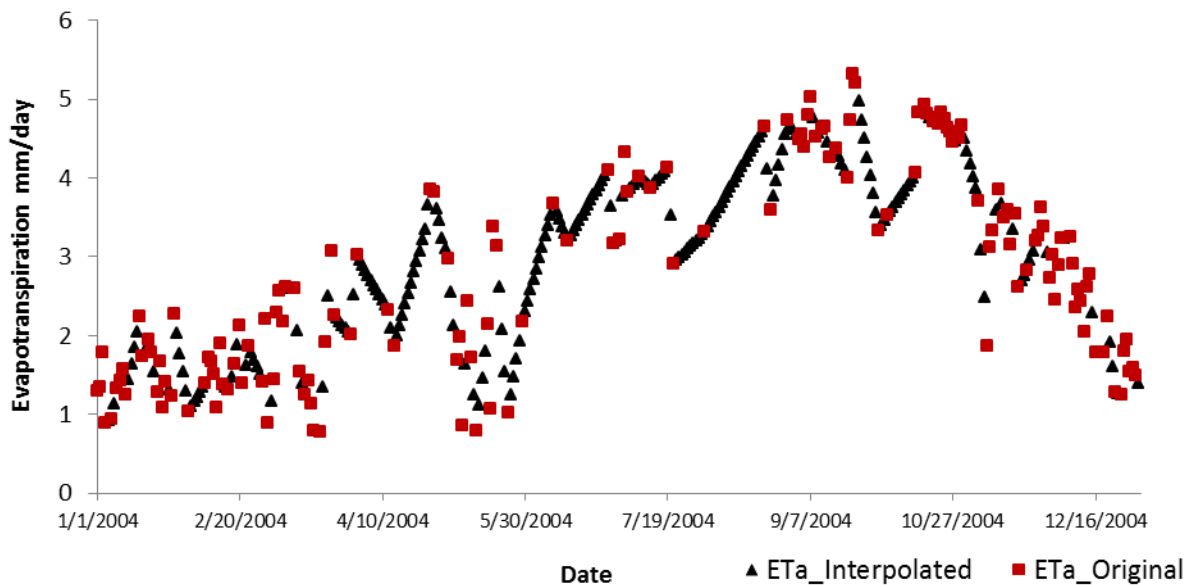


Figure 4-9: Daily average ETa for original and interpolated days for Gilgel Abay catchment

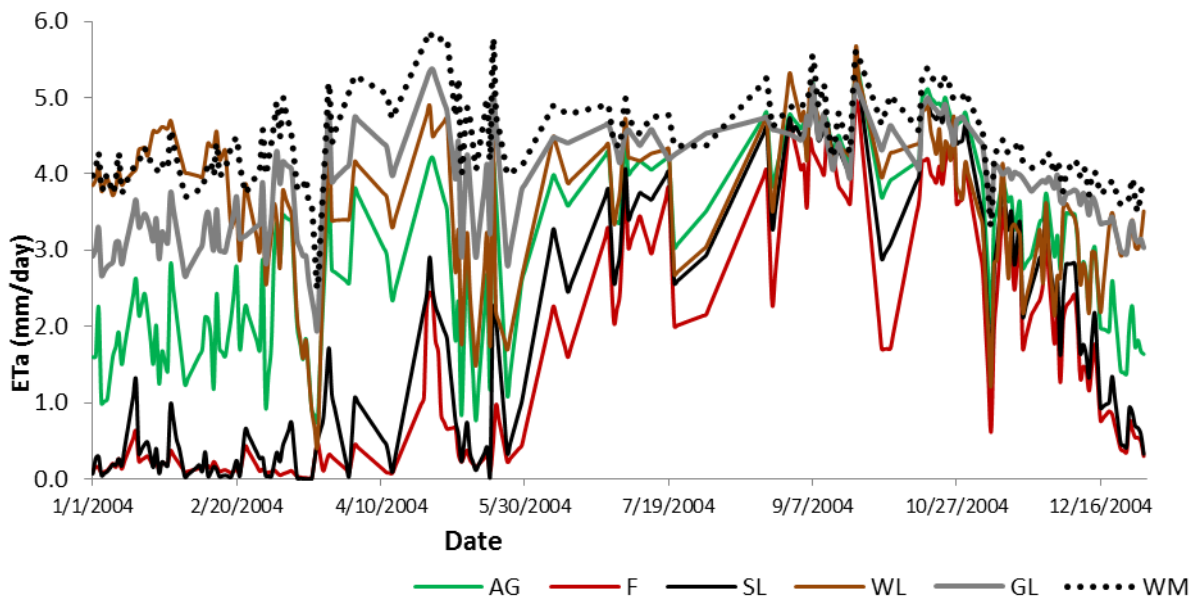


Figure 4-10: Time series ETa from SEBS after applying interpolation for missing day

4.4. DEM hydro-processing

The SRTM DEM 90m resolution has been selected for the study area because of its higher resolution and specially its relative vertical accuracy which is less than 10 meters. SRTM data cover nearly 80% of the Earth’s surface, home to 95 % of all humans (60 degree north to 56 degree South latitudes). The new version V4-1 with 5 by 5 degree tiles GeoTiff format file has been down loaded free of charge from the website¹. Figure 4-11 shows maps for the original DEM, filled and sink map.

Fill and sink

The fill and sinks operation in DEM hydro processing removes the local depressions. This operation is used to a Digital Elevation Model (DEM):

1. Depressions that consists of a single pixel: Any pixel with a smaller height value than all of its 8 neighbouring pixels will be removed by increasing to the smallest value of its 8 neighbour pixels.
2. Depressions that consists of multiple pixel: Any group of adjacent pixels where the pixels that have smaller height values than all pixels that surround such depression will be removed by increasing the smallest value of a pixels that is adjacent to the outlet (after Maathuis (2007))

¹ <http://www.cgiar-csi.org/data/elevation/item/45-srtm-90m-digital-elevation-database-v41>

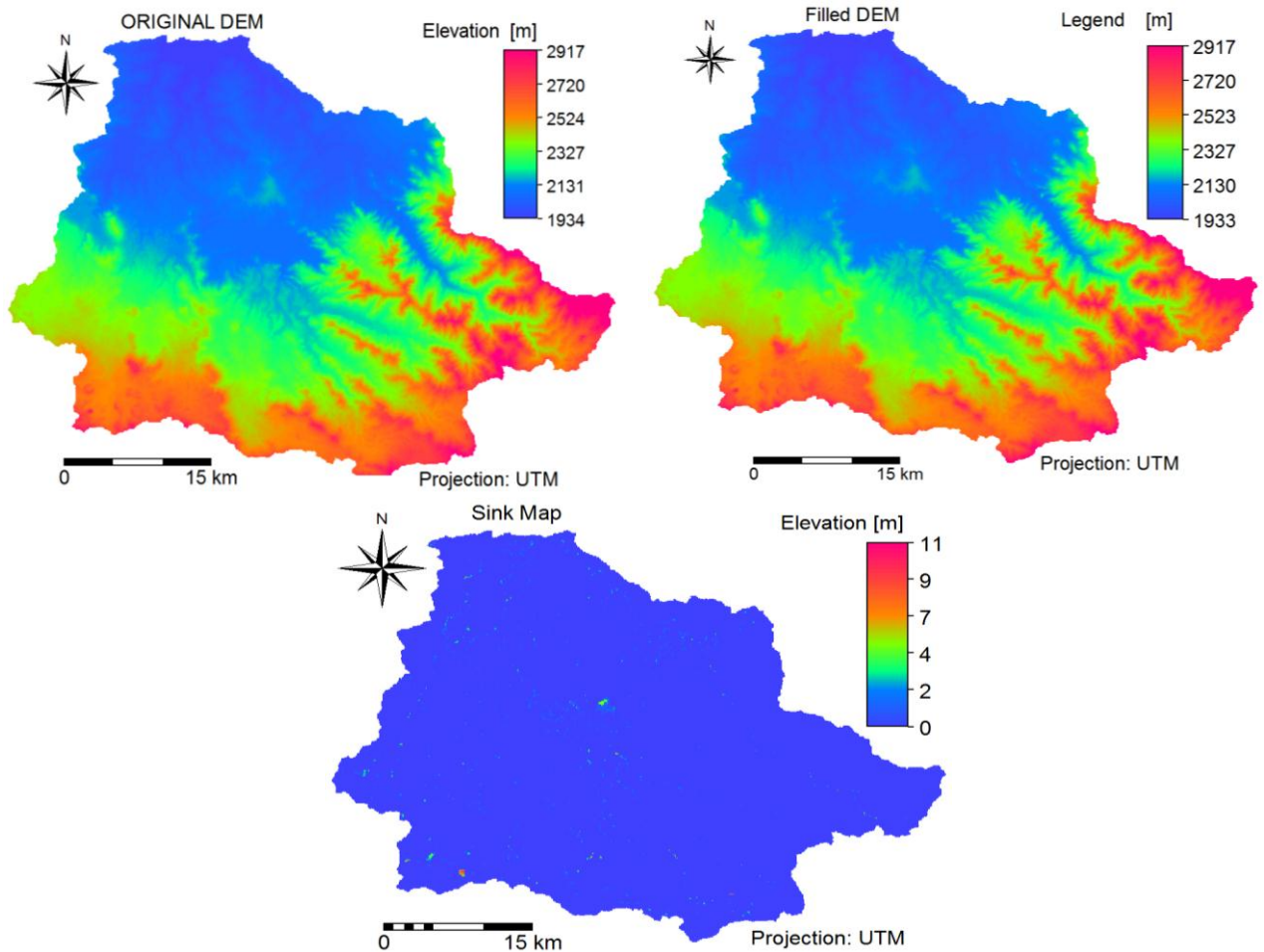


Figure 4-11: Original DEM, filled DEM and sink map of Upper Gilgel Abay

Flow Direction and accumulation determination

After fill-sink parts of Digital Elevation Model (DEM), the flow direction operation that determines the flow of water from neighbouring pixels towards the central pixel has been computed. Here the D-8 algorithm was applied to calculate the upslope contributing area using blocks of 3 by 3 pixels. Because it is more applicable to delineate the drainage network with well-developed channels (Garbrecht and Martz, 1999).

Flow accumulation operation is followed after the flow direction by using it as input. The flow accumulation operation is used to find the drainage pattern of a terrain and shows the number of upstream pixels that contribute any water to any outlet. The flow direction, flow accumulation, the slope and $\tan\beta$ maps of the Upper Gilgel Abay basin are shown in Figure 4-12.

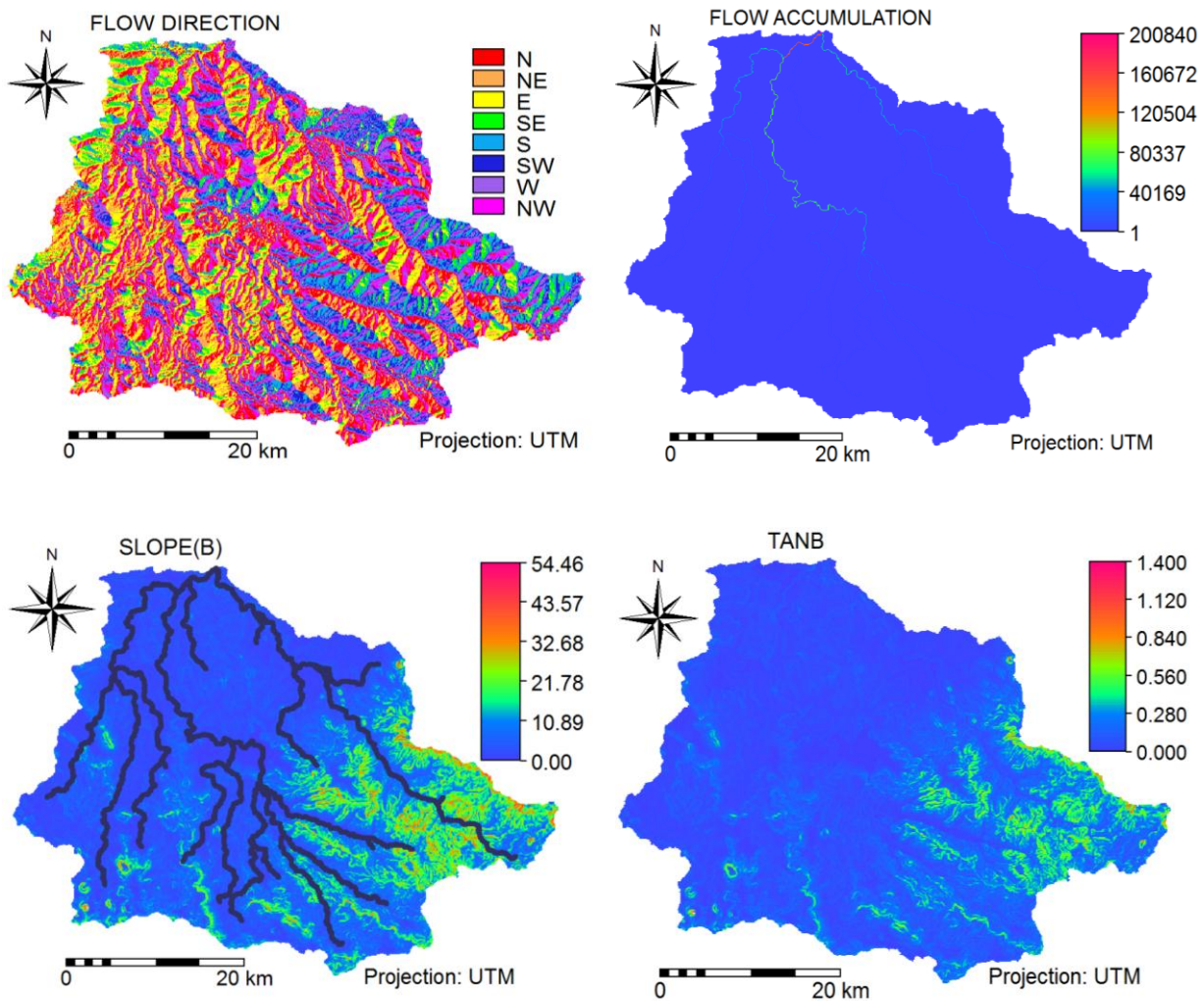


Figure 4-12: Flow direction, flow accumulation, slope and $Tan\beta$ maps

Topographic index (TI)

After these different DEM Hydro-processing procedures, the topographic index map for the study area was calculated as shown in Figure 4-13. This topographic index is one of the basic inputs for the TOPMODEL simulation where a higher topographic index value implies a higher wetness. From the result, a higher topographic index was found especially in the central and northern parts of the catchment. At the centre of the catchment, higher topographic index is observed due to the reason that the area was found to have lower slope and is the confluence point of two rivers. As shown in the histogram of topographic index map in Figure 4-12, most area has the TI value of 8, 9 and 7 with area contribution of 28 %, 22% and 19% respectively. The maximum TI is 25.

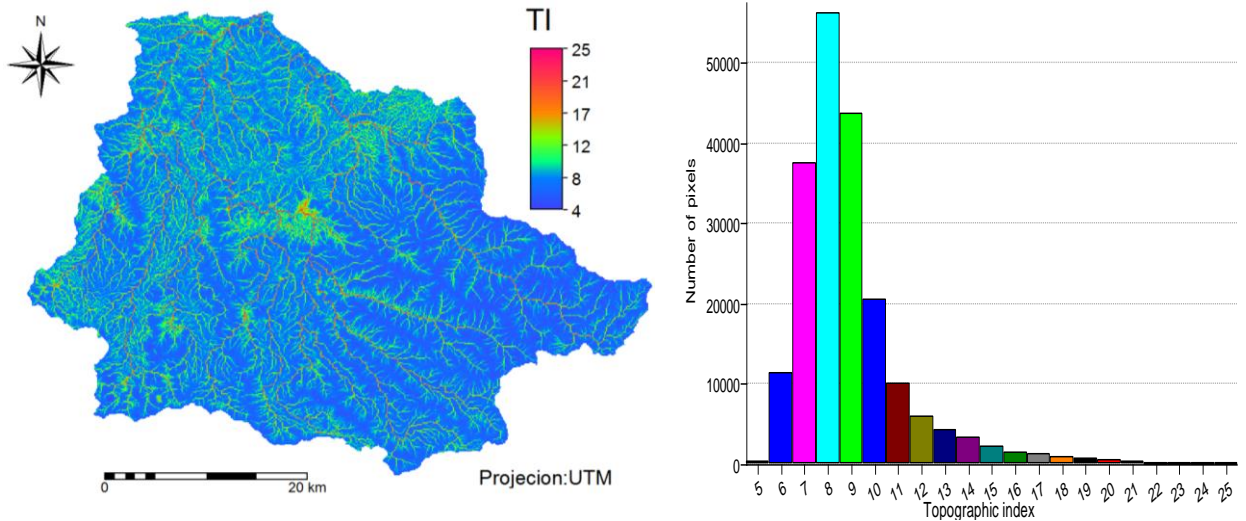


Figure 4-13: Topographic index map (left) and topographic index value distribution histogram (right)

Channel routing file

Figure 4-14 shows the area distance for channel routing for the upper Gilgel Abay catchment that is determined using slice operation from ILWIS software. The actual channel routing of the catchment could not be represented in this way. But for the sake of simplicity, the catchment was sliced into a distance interval from the outlet point so that any drop of water particle within the same sliced distance is assumed to reach to the outlet with equal interval of travel time. The outlet point map was used to produce the distance map of the routing of surface flows to the outlet. The ratio of each distance interval and cumulative area contribution is calculated and used for TOPMODEL simulation. (Gumindoga, 2010)

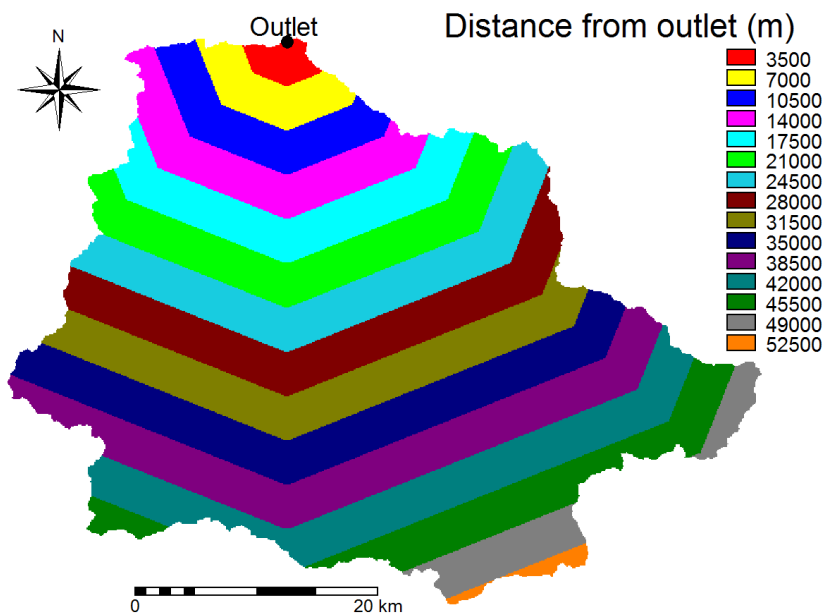


Figure 4-14: Distance area map for channel routing

5. RESULTS AND DISCUSSION

This chapter is divided into three main sections. The first section describes the results from the analytical interception model estimated from different land cover classes. The second main section deals with the surface energy balance system (SEBS) for the estimation of actual evapotranspiration from MODIS satellite Data. The last (third) section is the result from the TOPMODEL simulation using the potential evapotranspiration (ET_p) and actual evapotranspiration (ET_a).

5.1. Intercepted rainfall

The daily amount of intercepted rainfall was estimated. For the agricultural and grass lands the average monthly LAI values from MODIS were first calculated for different land covers. The distribution in the LAI for different land cover classes for 2004 is shown in Figure 5-1. For the forest lands the interception was estimated applying the Gash's analytical model. The total daily intercepted rainfall for 2004 and interception at each land cover classes is shown in Figure 5-2. The highest intercepted rainfall is observed during the rainy season (in August, 2.18mm/day). The total amount of interception for the 2004 is 136.5 mm which is only 7.8% of the total amount of rainfall recorded for the study area. This total amount of intercepted rainfall is deducted from the total rainfall recorded in stations at daily base to get the rainfall amount that reaches to the ground. The net rainfall after subtracting the interception amount was then used to the TOPMODEL simulation processes.

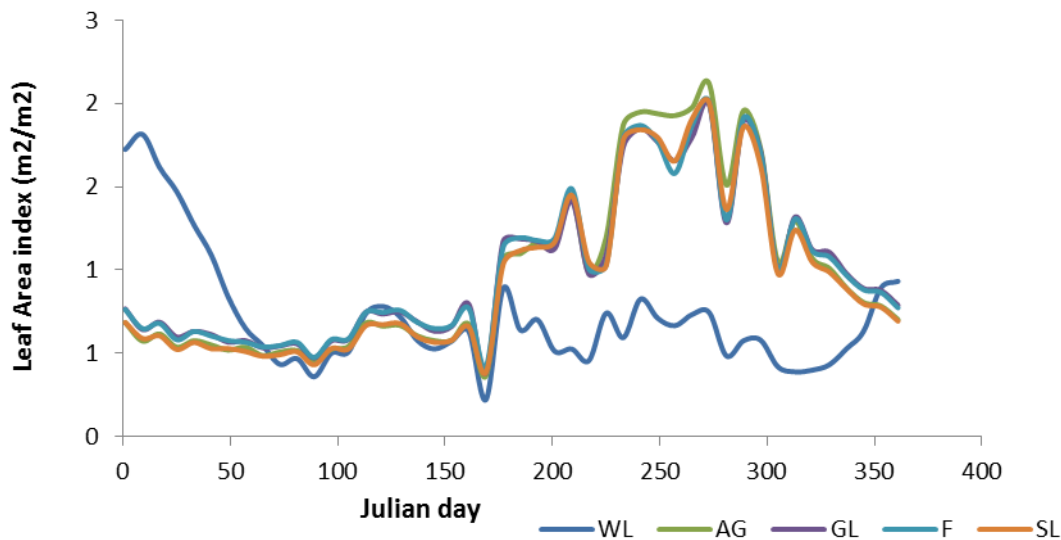


Figure 5-1: LAI distribution of different land cover classes for Gilgel Abay catchment

From the graph the highest LAI value is observed in the rainy season for the land cover agricultural, grass shrubs and forest lands. Whereas for the WL the highest LAI value is during the dry season. This is because in the WL area high irrigation activities are undertaken and land is covered by crops so that the LAI is higher during that time and is low during rainy season since the area will probably be covered by water and grass.

Figure 5-2 shows the daily intercepted rainfall for different land cover classes and the total sum for the year 2004.

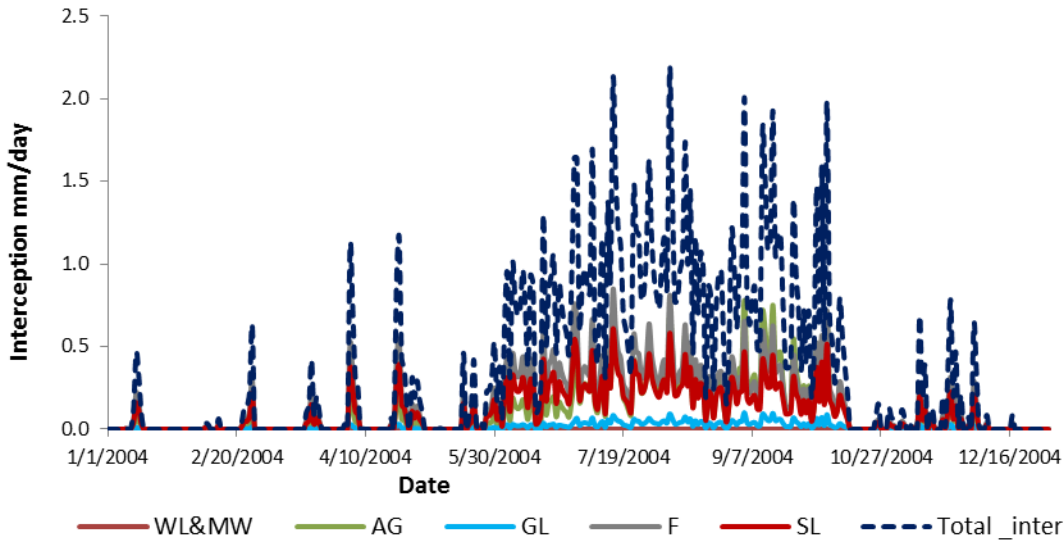
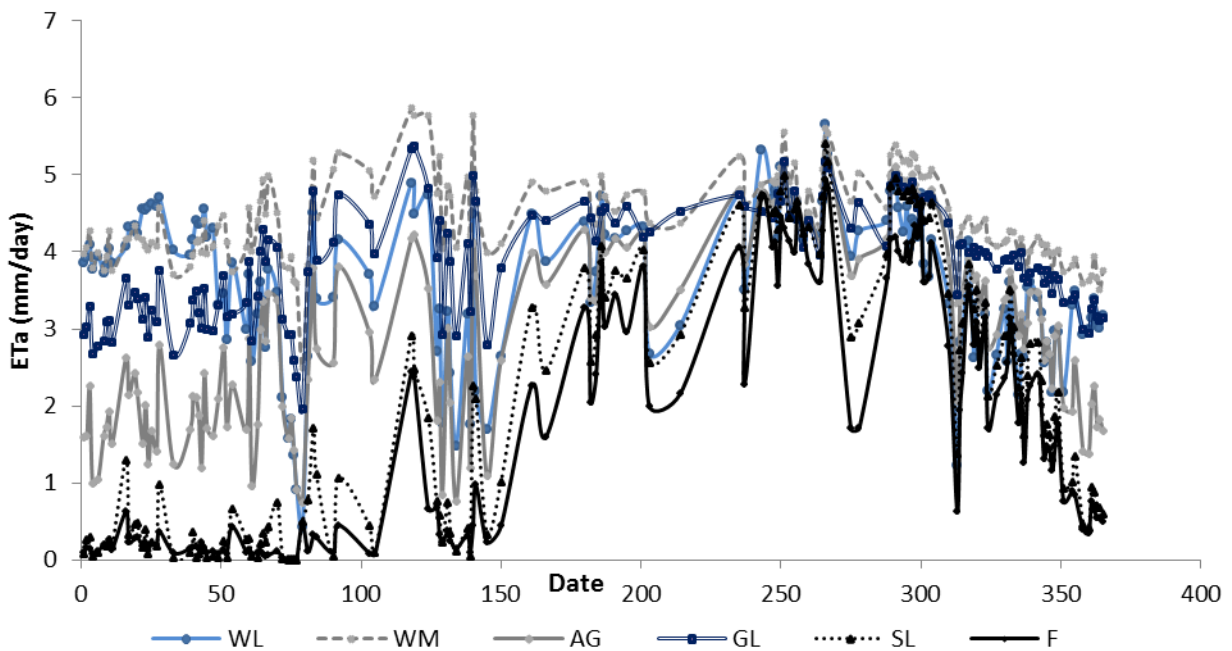


Figure 5-2: Daily Intercepted Rainfall of different land cover classes for 2004

5.2. Actual Evapotranspiration time series from SEBS

After all the input data has been prepared, actual evapotranspiration using the surface energy balance system was calculated using ILWIS software. At first SEBS was run for the available cloud free images (i.e 152) for the whole year. Daily average ETa is calculated for each land cover class of the catchment. Figure 5-3 shows the graph of daily average ETa from each land cover classes.



WL- wetland, WM-water and marshy area,AG-Agricultural land,GL-Grass land, SL- shrubs land, F-forest
Figure 5-3: Daily average actual evapotranspiration for 152 days for different land cover classes

From the graph, the highest actual evapotranspiration for each land cover class is observed at different seasons of the year. Wetland and marshy area have highest ETa during the dry season of the year as

compared to the other land cover classes. This is because during that time on those areas irrigation activities are practiced so that the land is covered by crops and the soil also has also high moisture content. At the beginning of the year which is the dry season for the study area ETa is comparatively lower and gradually increases for all land cover classes. This is presumably because in the julian day of around 90 to 150 (end of March to middle of May) for the area is the short rainy season so that there is some rain events which increases the moisture content of the area and have also effect land cover and land surface parameter which affect the ETa estimation in SEBS. During the dry season between 0 and 90 julian days (from January to end of March) , ETa from forest and shrubs lands has been underestimated. As stated by Badola (2009) variation in diurnal cycles of turbulent fluxes and instantaneous or daily average sensible and latent heat fluxes are difficult to obtain from remote sensing data and also difficult to represent the aerodynamic roughness length parameters (Z_{om} , d and h) accurately for the forest land cover using remote sensing based model.

In general, the highest ETa value for most land cover classes is observed in between 243 to 300 julian day of which the highest is at 266 julian day. During that time the area is expected to have a high potential soil moisture content in the soil surface and much of the agricultural area is covered by high growing crops so that actual evapotranspiration is expected to be high. The result from SEBS appears to be realistic when we see the highest and minimum estimated ETa and the general trend is comparable with the seasonal changes of the area. Based on the area coverage of each land cover class, average actual evapotranspiration from each land cover is also estimated. Figure 5-4 shows the average actual evapotranspiration for each land cover class.

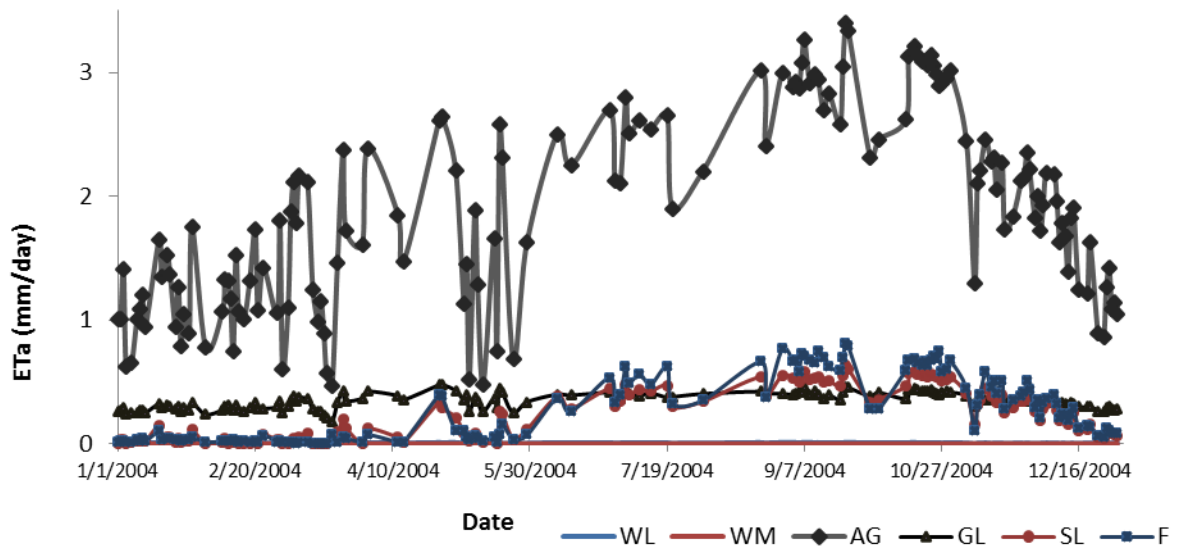


Figure 5-4: Average daily ETa by SEBS for each land cover class contributed to the whole catchment before interpolation of missed days

Calculating average daily ETa for the whole catchment

Using ILWIS software, map crossing (overlay) analysis has been done for land cover map and daily ETa maps. The average daily ETa for each land cover class has been calculated as stated above. After getting the average daily ETa of each land cover class and considering the area percentage contribution of each land cover classes to the whole catchment, the daily average ETa for the overall catchment was calculated from each land cover class. The graph in Figure 5-5 shows the daily ETa contribution from each land cover class.

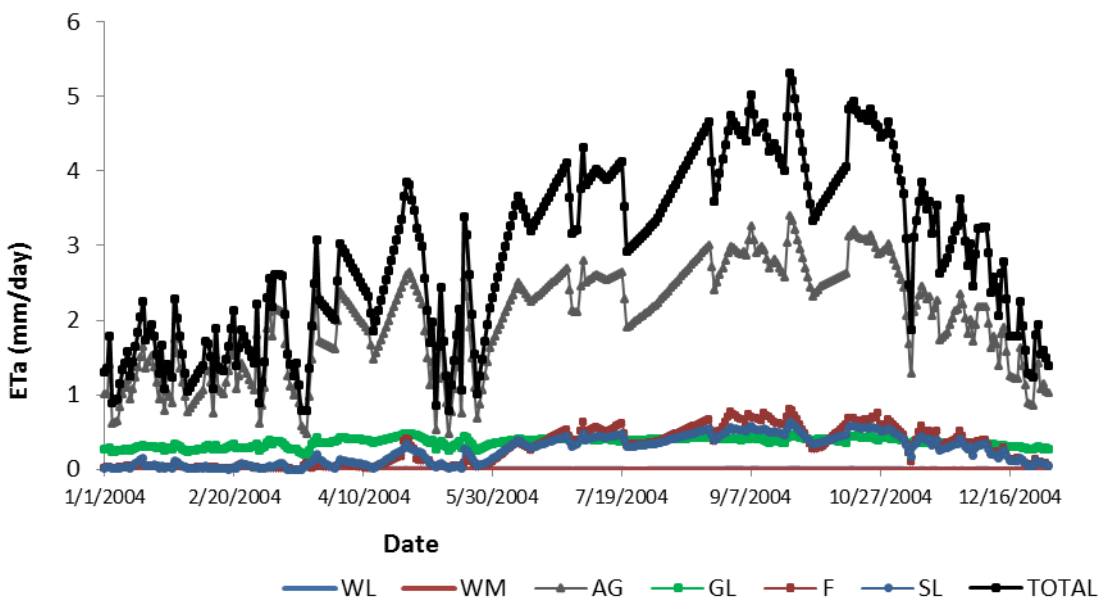


Figure 5-5: Daily average ETa from each land cover class estimated using SEBS (2004)

The average daily ETa value for the catchment as a whole is shown in the graph above and is used for the TOPMODEL simulation.

Figure 5-6 shows the Average monthly ETa map of the Gilgel Abay catchment. It is clearly shown that the highest actual evapotranspiration is observed in September. During this time most of the agricultural area are covered by different crops with their developing stage and the surface soil moisture content is also high in most of the area. Since the rainy season in the area starts in June and ends around October, the high soil moisture and high ground water label is also expected during this times so that the ETa get potential to be maximum.

Generally the ETa estimated from SEBS shows realistic and comparable results with seasonal variation of the study area. From field data (see the observed discharge hydrograph in Figure 2-4) the observed discharge is low in December to May. Since the season (with little rainfall in April) is dry and most of the agricultural fields are not covered by crops so that ETa is expected to be low in this time. When the rainy season starts on June, ETa gradually increases up to September and then start to decrease again .

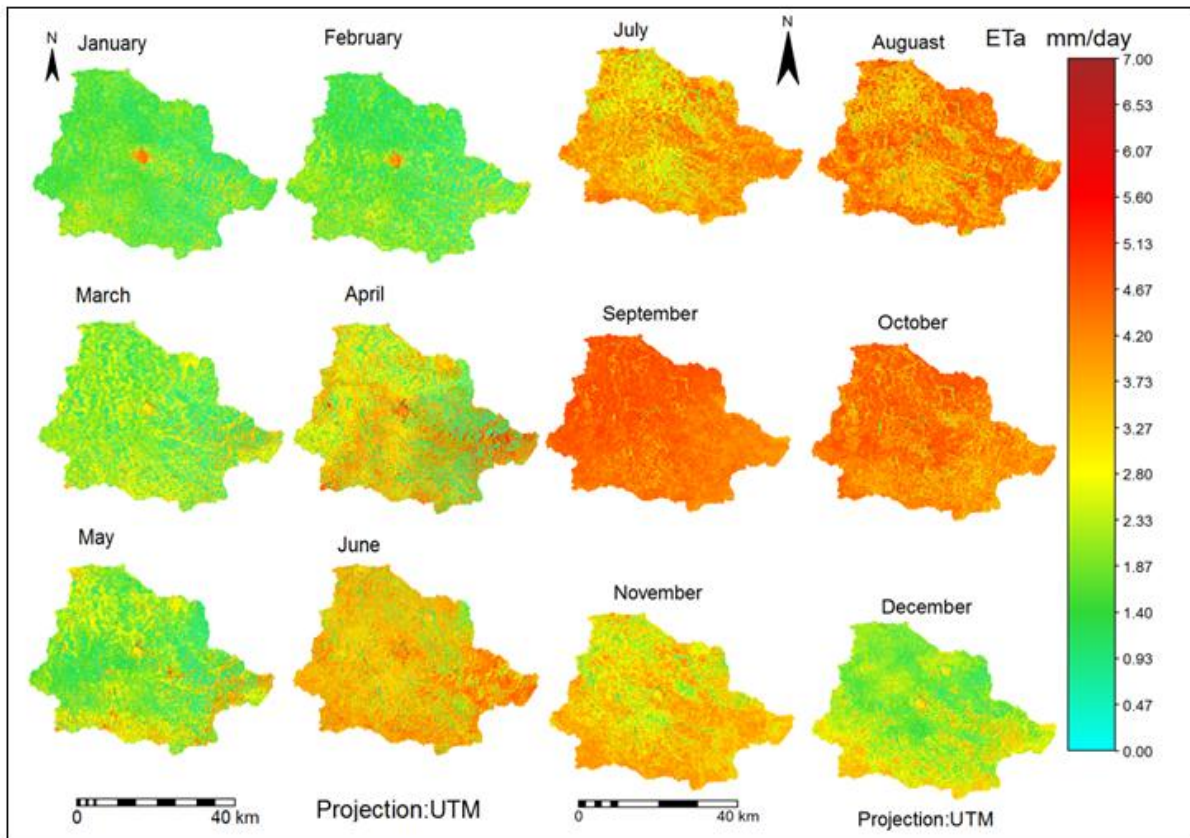


Figure 5-6: The monthly average actual evapotranspiration (2004)

5.3. Streamflow simulation using potential evapotranspiration

The streamflow simulation result for the period of 1996 to 2003 is shown in Figure 5-7. The TOPMODEL was able to simulate both the peaks and the baseflow satisfactorily except for the two years 1996 and 2003. For the 1996, the peaks and the falling limbs of the hydrograph did not match very well with the observed discharge hydrograph value. For the year 2003 the peaks do not match very well. However, for the simulation of all years (i.e. from 1996 to 2003), the Nash-Sutcliffe efficiency was 0.773 which indicates the ability of the model to simulate the streamflow in a satisfactory way. It was also found that the Relative Volume Error (RV_E) to be -7.45% that indicates fair performance of the model.

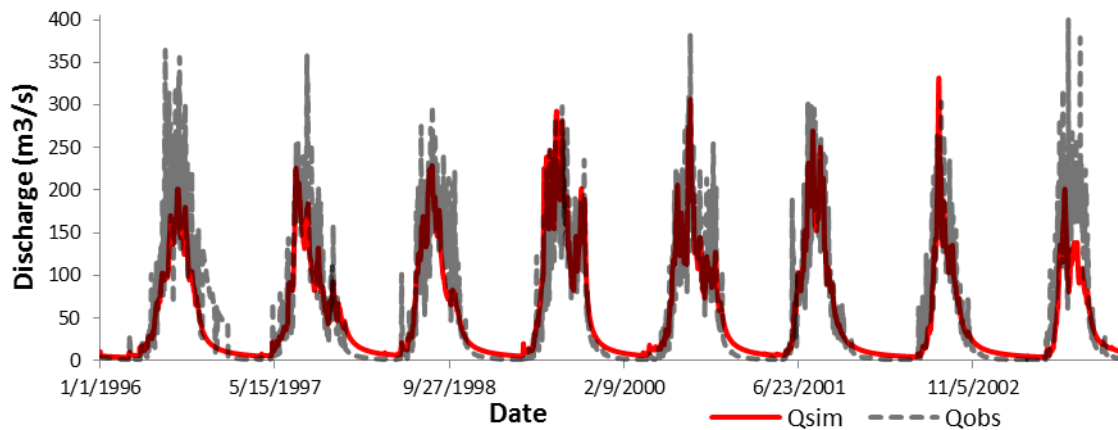


Figure 5-7: Simulation results for the Upper Gilgel Abay catchment for the period of 1996 – 2003

Table 5-1 shows the parameters and their values that are used to simulate the hydrograph in fig 5-7.

Table 5-1: Parameter values used for TOPMODEL simulation (Gumindoga, 2010)

| Parameter | m | InTo | TD | CHV | RV | SRmax | QO | SRO | INFEX | XKO | HF | DTH |
|-----------|-------|---------------------|-----|-------|-------|-------|----------|-------|-------|--------|-------|------|
| | [m] | [m ² /h] | [h] | [m/h] | [m/h] | [m/h] | [m/dt] | [m] | [-] | [m/hr] | [m] | [-] |
| Values | 0.055 | 5 | 22 | 3900 | 1900 | 0.009 | 0.000286 | 0.002 | 0 | 3 | 0.135 | 0.36 |

5.3.1. Sensitivity analysis

Sensitivity analysis on m parameter

The sensitivity analysis of TOPMODEL for the m parameter has been done for the value range 0.015 to 0.06. The values of the parameter were changed keeping the other parameter values fixed. For the lower value of m (i.e. 0.015, 0.02 and 0.02), the peak flow is much higher than for the higher value of m (i.e. 0.04, 0.055 and 0.06). For instance in June 1999 the peak flow is very high approximately 1350m³/s when m is 0.015 and 816m³/s when m is 0.02. However for the higher value of m parameter 0.055 and 0.06 the peak flow reduce to 332m³/s and 314m³/s respectively. For higher values of m, the peak flow is smaller than for the lower values of m, which shows that the portion of rainfall that reaches the outlet through surface flow is low. This also indicates that the effective soil depth that allows rainfall to infiltrate is larger. For the lower value of the m parameter, the subsurface flow decreased and the water flows faster and reaches the outlet with almost same time as surface flow. Table 5-2 shows The Nash-Sutcliffe model efficiency (NS) and the Relative Volume Error (RVE) for different values of the m parameter. Figure 5-8 and 5-9 clearly shows that except for the two year (1996 and 2003) the peak flow is higher for the lower value of m and gradually reduces when m increases

Table 5-2: Effects of the m parameter on TOPMODEL efficiency

| Run | m(m) | Nash Sutcliffe (NS) | Relative Volume Error RVE (%) |
|-----|-------|---------------------|-------------------------------|
| 1 | 0.015 | 0.528 | -6.600 |
| 2 | 0.02 | 0.663 | -6.620 |
| 3 | 0.03 | 0.736 | -6.721 |
| 4 | 0.04 | 0.762 | -6.859 |
| 5 | 0.055 | 0.773 | -7.094 |
| 6 | 0.06 | 0.772 | -7.183 |

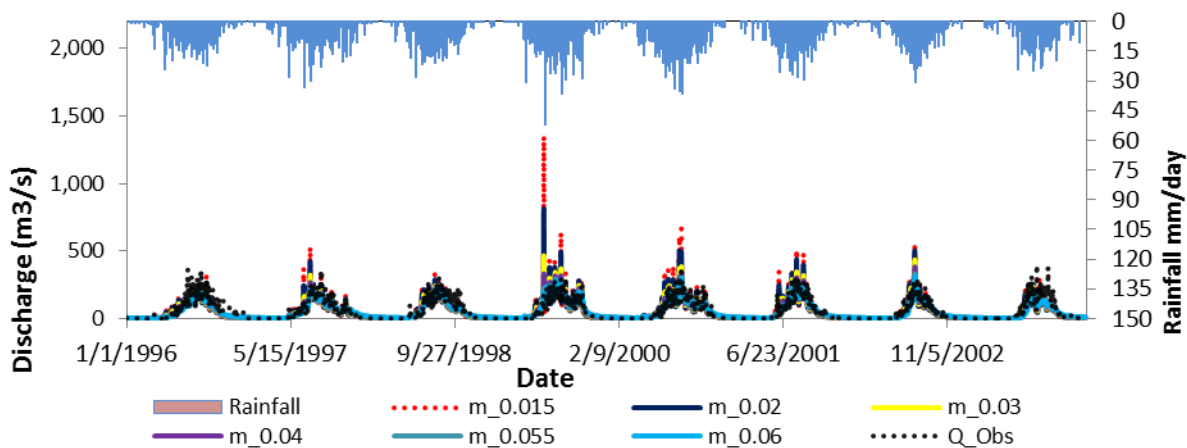


Figure 5-8: Sensitivity of the model changes in m parameter (1996-2003)

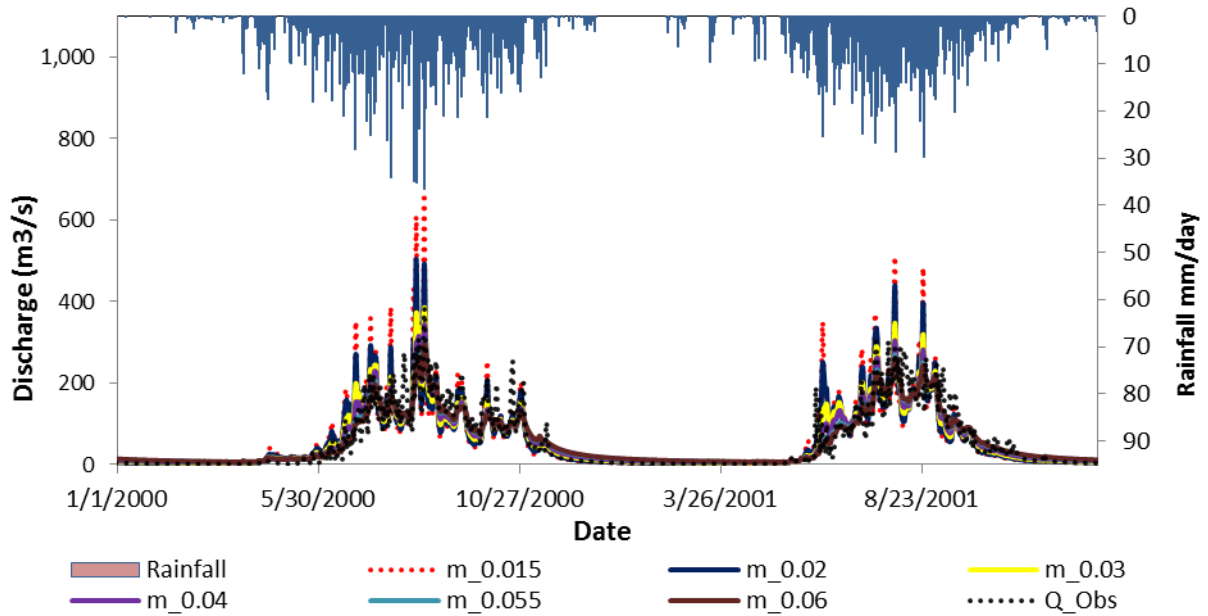


Figure 5-9: Sensitivity of the model to the changes in m parameter (2000-2001)

Sensitivity analysis on T0 parameter

Lateral transmissivity (T_0) is the value of lateral transmissivity when the water-table just cuts the surface (Quinn and Beven, 1993) and used to calculate the distribution of the transmissivity in downslope direction as exponential function of the local storage deficit (Rientjes, 2010). Sensitivity analysis was done fixing the other parameters in (Table 5-3).while the values of T_0 were changed from 1 - 30. Figure 5-10 and 5-11 show the effect of the parameter on the shape and on the peak flow of the hydrograph. The change in the peak flow from lower value (1 to 3) was significant but for the higher value, the observed change is very small. This parameter does not seem to significantly affect the recession tail of the hydrograph. However, the T_0 parameter has significant impacts on the surface runoff so that the peak flow seems to have large impact on the recession tail of the hydrograph or on the baseflow after the rainfall event. For lower value of T_0 the peak flow for most of the years is higher than the observed peak flow. The results from Figure 5-10 and Table 5-3 show the Nash-Sutcliffe efficiency and the Relative Volume Error as the T_0 parameter is changed. NS first increases from 0.708 to 0.773 and then decreases slightly to 0.763 with increasing T_0 Parameter value and the Relative Volume Error (RV_E) changes from -6.067% to -7.358 which only is a minor increase.

Table 5-3: Effects of the T_0 parameter on TOPMODEL efficiency

| Run | T_0 (m3/s) | Nash Sutcliffe (NS) | Relative Volume Error RV_E (%) |
|-----|--------------|---------------------|----------------------------------|
| 1 | 1 | 0.708 | -6.067 |
| 2 | 3 | 0.765 | -6.029 |
| 3 | 5 | 0.773 | -7.094 |
| 4 | 10 | 0.770 | -7.327 |
| 5 | 20 | 0.768 | -7.356 |
| 6 | 30 | 0.763 | -7.358 |

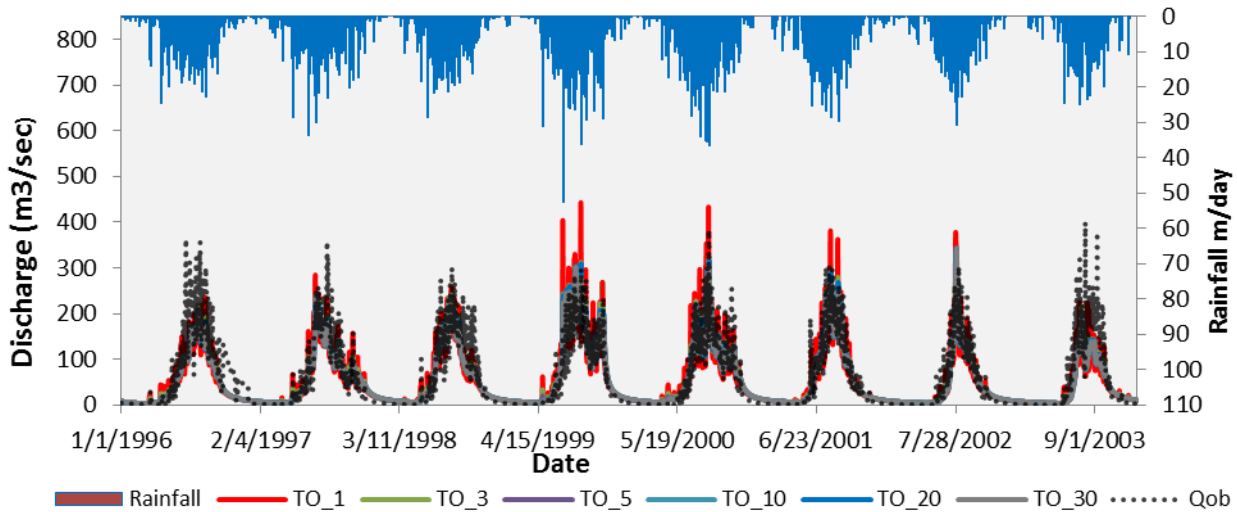


Figure 5-10: Sensitivity of the model to the T_o parameter (1996-2003)

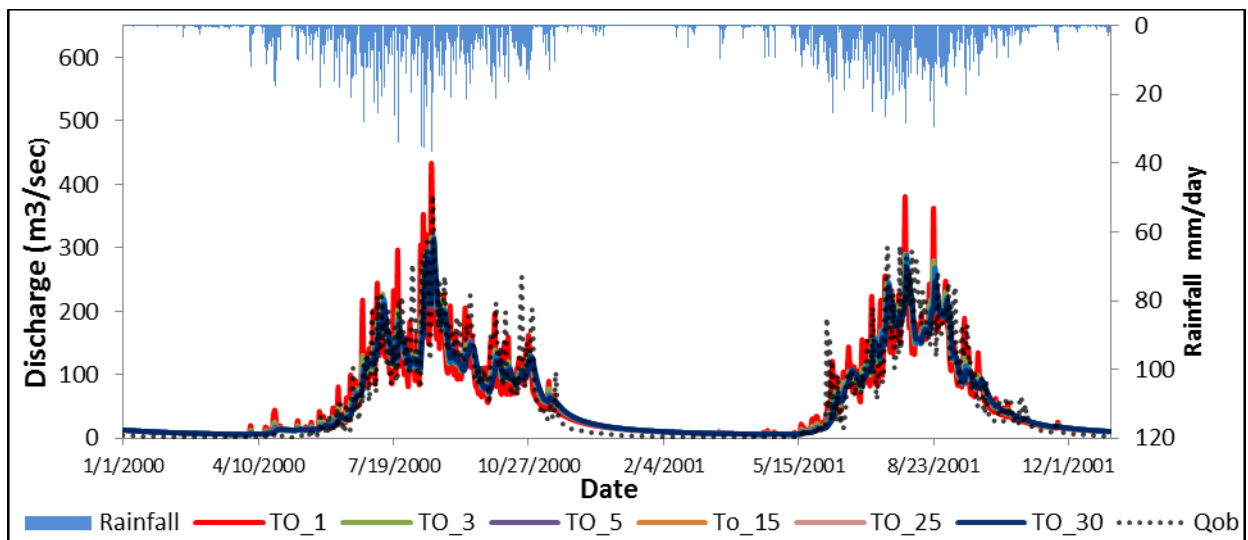


Figure 5-11: Sensitivity of the model to the T_o parameter (2000-2001)

Sensitivity analysis on SRmax parameter

Figure 5-12 and 5-13 show the effect of changes in SRmax Parameter on the stream flow hydrograph of the catchment. This parameter seems to impact on the overall pattern of the hydrograph. For smaller value of SRmax the simulation, result shows higher peaks and reduces as its value is increased. Table 5-4 shows the model efficiency as the changes on SRmax. For smaller value of SRmax 0.009, the NS is 0.773 and RV_E is -7.45%. The increase of the SRmax values causes deterioration of model performance. NS decreases and RV_E increases.

Table 5-4: Effects of the SRmax parameter on TOPMODEL efficiency

| Run | SRmax | Nash Sutcliffe (NS) | Relative Volume Error (RVE) (%) |
|-----|-------|---------------------|---------------------------------|
| 1 | 0.009 | 0.773 | -7.45 |
| 2 | 0.025 | 0.768 | -10.41 |
| 3 | 0.05 | 0.760 | -12.69 |
| 4 | 0.2 | 0.698 | -20.695 |
| 5 | 0.3 | 0.642 | -25.49 |

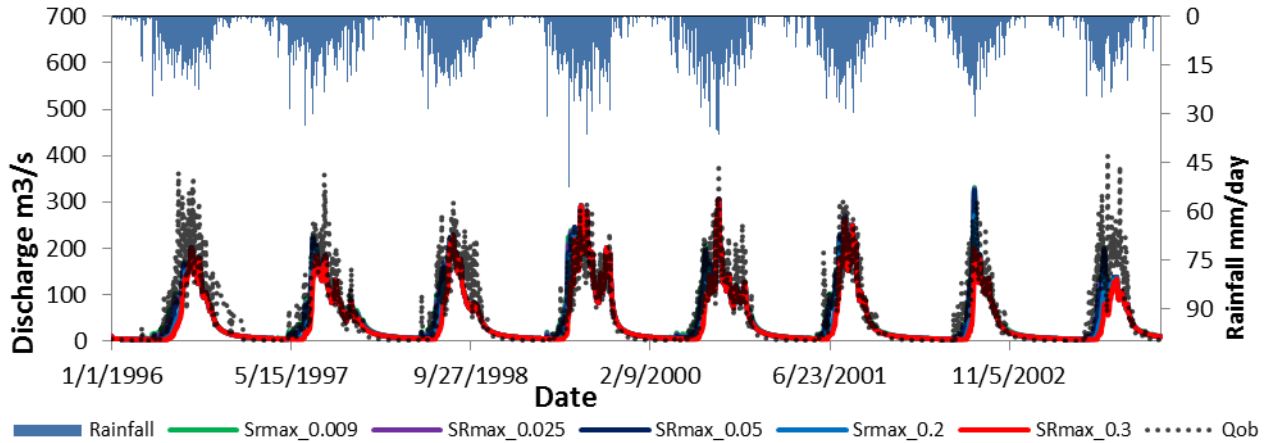


Figure 5-12: Sensitivity of the model to the changes in SRmax parameter

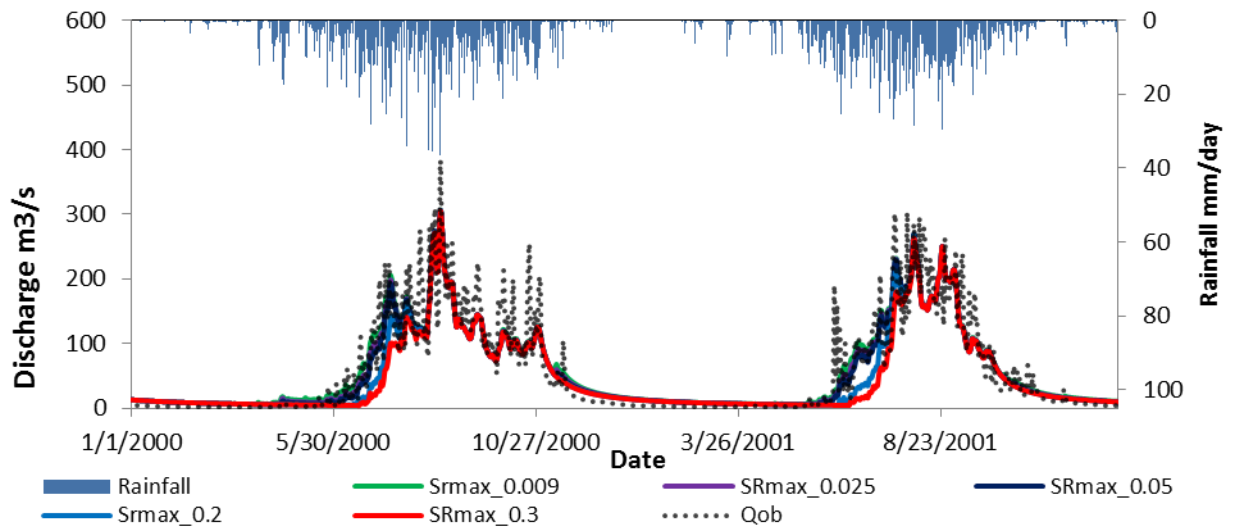


Figure 5-13: Sensitivity of the model to the changes in SRmax parameter (2000-2001)

5.3.2. Model calibration and validation

Model calibration

To improve simulation results many trial and errors have been done by changing only the sensitive parameters m , T_0 and SR_{max} . The parameter values with better model performance are shown in Table 5-5. Figure 5-14 and Figure 5-15 also shows the streamflow hydrograph with good performance of the model. Only little improvement has been done as compared to the first set of parameters in Table 5-1. Both the model efficiencies show little improvement from the first set of parameters. The overall efficiencies in general is good and shows the better performance of the model except for the year 1996 and 2003 in which the peak flows did not much well.

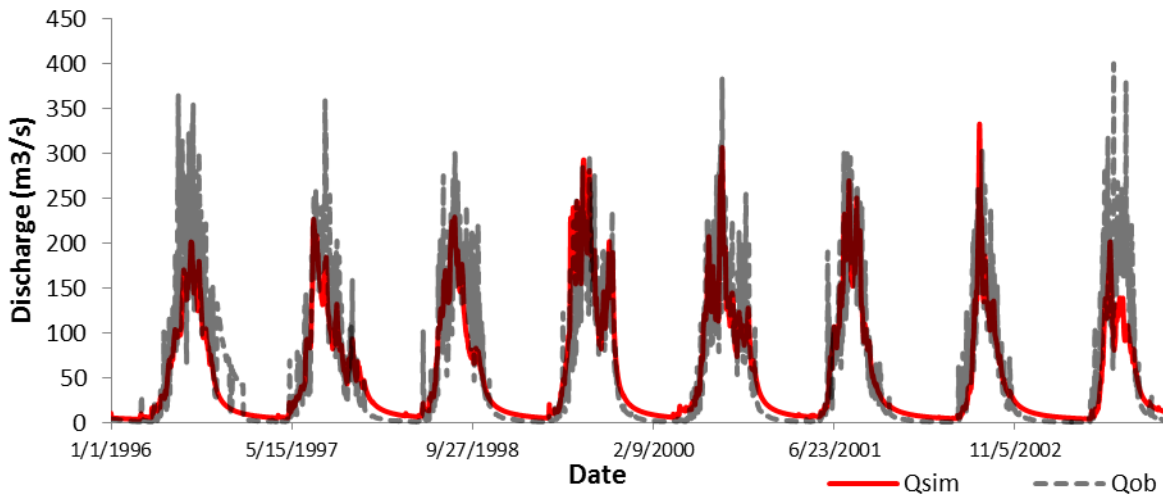


Figure 5-14: Calibration results for the catchment (1996 – 2003)

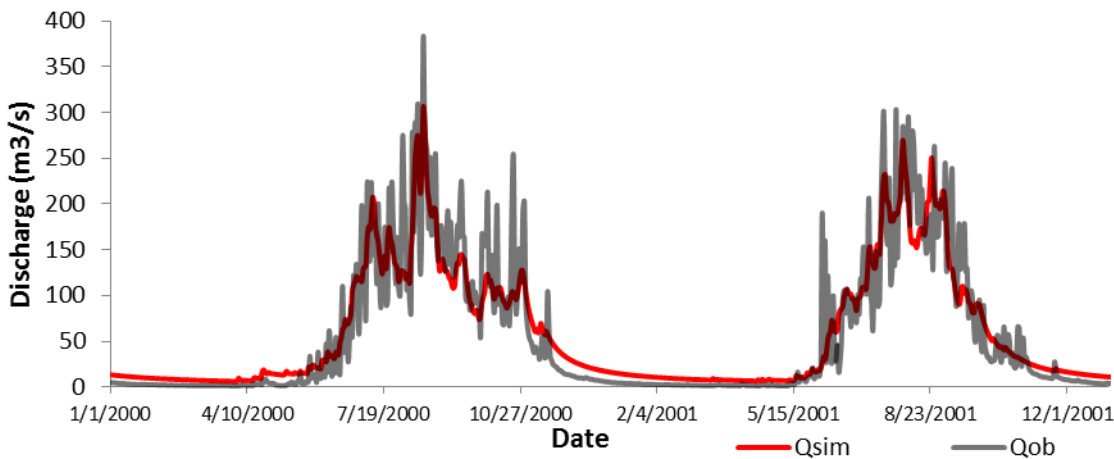


Figure 5-15: Calibrated result of the catchment (2000-2001)

Table 5-5: Optimum parameter values and model efficiencies after calibration

| m | To | SRmax | Nash-Sutcliffe | Relative Volume Error (RV_E) (%) |
|-------|----|--------|----------------|--------------------------------------|
| 0.055 | 5 | 0.0063 | 0.774 | -6.35 |

Model validation

The optimum set of parameters used for calibration is applied for simulation of the 2004 data set to validate the calibrated model performance. Figure 5-16 shows the validation results. Here for the first five months (from January to May) the simulated and observed discharge fit very well even for the next months until the end of August, the result looks reasonable except there is no sharp raise or drop in the simulated hydrograph like the observed hydrograph. However, the general trend shows the model has good capability to simulate the baseflow as well as the recession and falling limbs of the hydrograph. The Nash-Sutcliffe and Relative Volume Error indicate that the model performed well for the validation year. Nash-Sutcliffe is improved from 0.774 to 0.801. The Relative volume Error changed from -6.35% to 9.98% that has also very significant changes to the overall simulation.

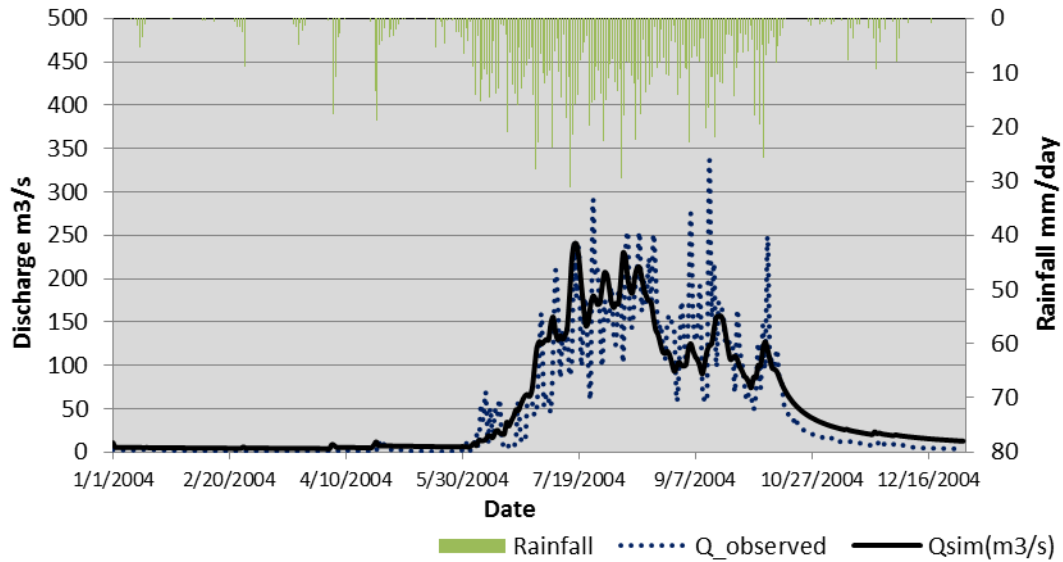


Figure 5-16: Validation result (2004)

5.4. Streamflow simulation using ETa from SEBS

The streamflow simulation using ETa estimated from SEBS on TOPMODEL were done for the data sets of 2004. The optimized parameter set from the calibration procedure for simulation by use of potential evapotranspiration was used for this simulation. The simulation result has similar pattern as the simulation result by potential evapotranspiration. However, the model efficiency is changed. The Nash-Sutcliffe (NS) efficiency is reduced from 0.80 to 0.78 while the Relative volume Error (RV_E) has been improved from 9.98% to 0.596% which suggests very good performance. Figure 5-17 shows the stream flow simulation applying ETa from SEBS and the observed discharge.

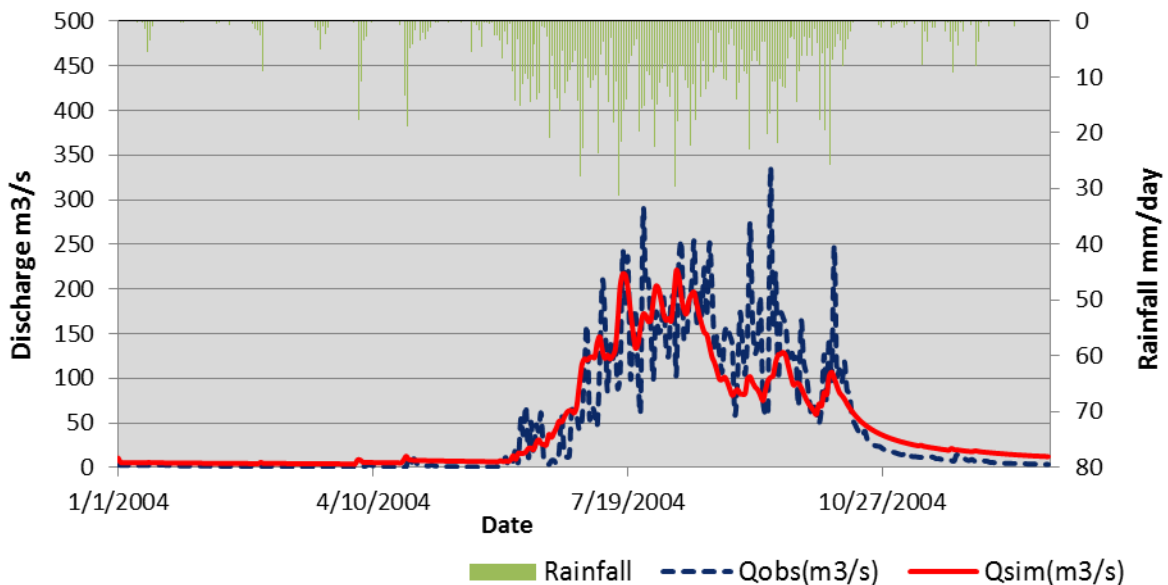


Figure 5-17: Simulated hydrograph using ETa from SEBS

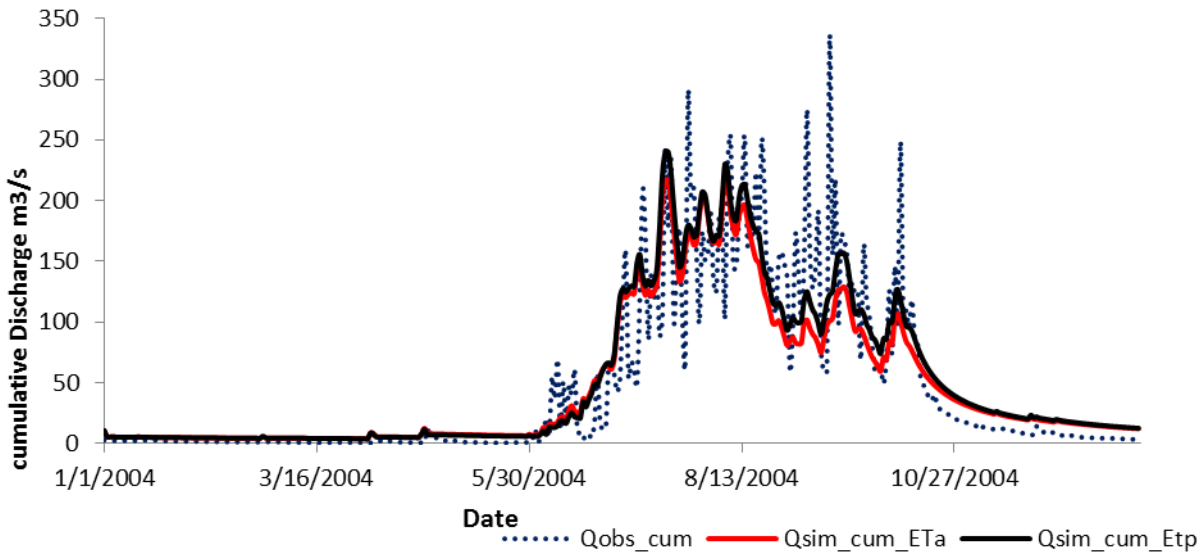


Figure 5-18: Simulated hydrograph when using ETa and ETP

Figure 1-18 shows the simulation hydrograph when using ETa from SEBS and ETP from Penman-Monteith. Almost in the whole season, the simulation from ETP is higher than the simulation from ETa. This implies that the total simulation volume by ETP is higher than the simulation volume by ETa.

Figure 5-19 shows the cumulative discharges of the observed, simulated by ETa from SEBS and ETP from Penman-Monteith. The total volume of water in each hydrograph is calculated by multiplying the discharge with the number of seconds in a day (Daily volume= $Q \text{ (m}^3\text{/s)} \times 24 \times 60 \times 60\text{s}$). The total cumulative Volume of water simulated by potential evapotranspiration is 1,623.65 Mm³, from SEBS is 1485.06 Mm³ and the observed volume of water for the catchment is 1,476.26 Mm³ for the whole year of 2004. The change in total volume of discharge simulated using ETP is higher by 10% than the observed discharge whereas the simulated discharge from SEBS is only 0.6% higher.

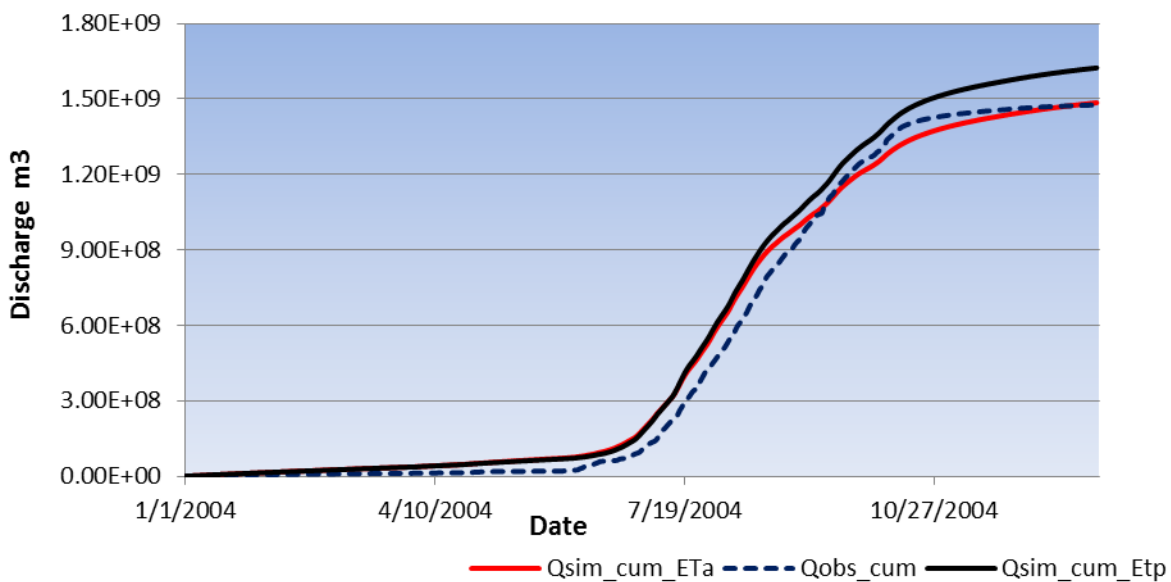


Figure 5-19: Cumulative discharge using ETa from SEBS and ETP in TOPMODEL simulation

5.4.1. ETa simulation by SEBS and TOPMODEL

In TOPMODEL, actual evapotranspiration is estimated from potential evapotranspiration, actual root zone storage deficit and maximum root zone storage deficit applying the formula as described in Equation.3.8 of chapter 3. Figure 5-20 shows the daily ETa from the TOPMODEL and SEBS and the daily rainfall of the Gilgel Abay. Here it can be observed that actual ETa from the TOPMODEL seems only governed by the presence and absence of rainfall. For instance in the dry season when there is no rainfall, ETa approaches zero whereas when there is some rainfall the ETa raise up and becomes even higher than the ETa from SEBS. But during the rainy season the ETa calculated from ETp by the TOPMODEL is lower than ETa by the SEBS. In real situation nearly zero value of ETa during the dry season (when no rain event) for the entire catchment is not realistic because the area consists of different land cover like forest and shrubs and wetlands and some irrigation agriculture lands so that evapotranspiration is expected to occur. This is actually reflected in the ETa estimated by SEBS which shows fair distribution of ETa estimation with the seasonal atmospheric variations. In this sense, the actual ETa calculated in TOPMODEL is underestimated.

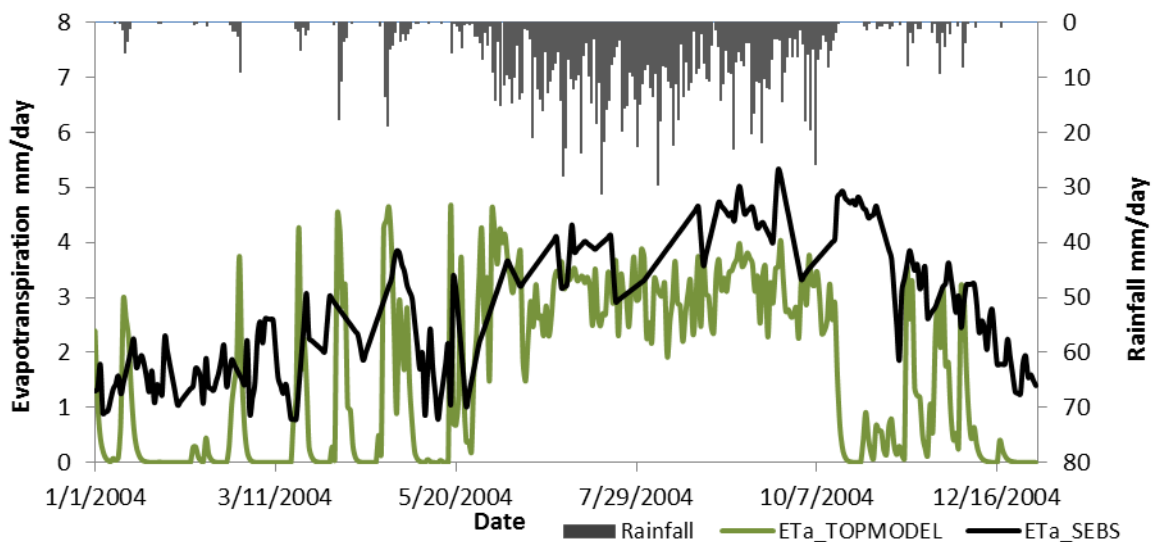


Figure 5-20: Daily evapotranspiration from SEBS and TOPMODEL and Rainfall distribution for 2004

Figure 5-21 shows the cumulative ETa from both TOPMODEL and SEBS. The total actual ETa estimated from SEBS for the whole year is found to be 1068 mm and the total ETa calculated from TOPMODEL using ETp is 594.3 mm. this show the total ETa from SEBS is twice that of the TOPMODEL.

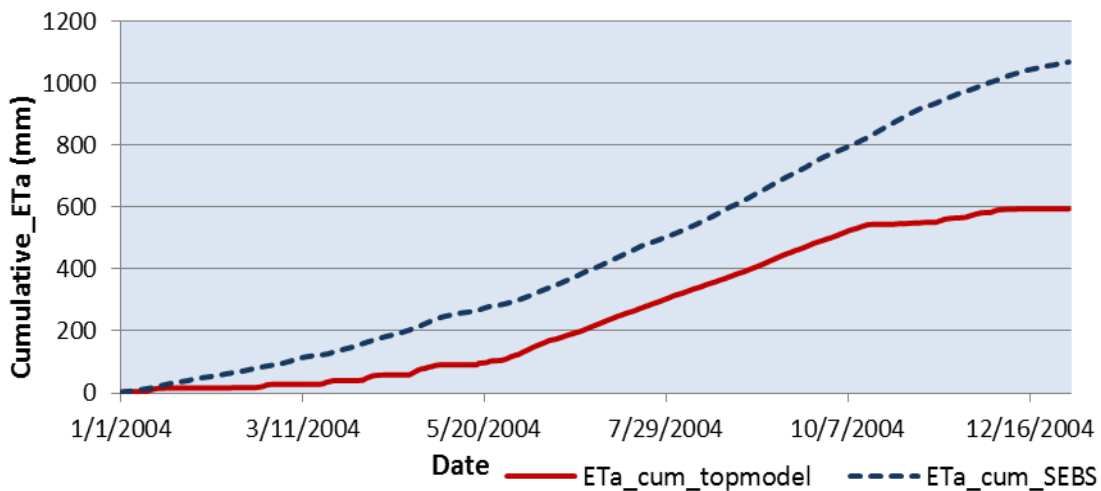


Figure 5-21: Cumulative ETa from TOPMODEL and SEBS

5.4.2. Streamflow Simulation for specific land covers using ETa from SEBS

In TOPMODEL, it was also possible to simulate the streamflow hydrograph of each land cover classes using actual evapotranspiration estimated from respective land cover class. After simulation for each land cover classes, the daily discharge resulted from simulation was multiplied by the areal ratio each land cover class from the total catchment area. Here each land cover class was treated as a sub-catchment and topographic index and Area distance routing were produced for each land cover based on the location in the catchment. In this case, the sets of parameters values were not changed. From the simulation result (see Figure 5-22), it has been shown that the simulation streamflow contribution by the grassland is highly sensitive for the rainfall events. This is because in this land cover most portion of the area have high topographic index values for instance 21.2% of the grass land area has TI of 23 and 19.07% and 17.21% of the area have TI value of 24 and 22 respectively the area with high TI value have high soil moisture storage so that the area responses fast to the rainfall event. The streamflow hydrograph from agricultural land is high throughout the year. This is because about 63% of the area is covered by the agricultural area. From agricultural area about 60% volume of water discharge from the catchment and the rest 19%, 12%, 8% from forest ,shrubs and grassland respectively. Less than 1% volume of water is contributed from both wetland and marshy area.

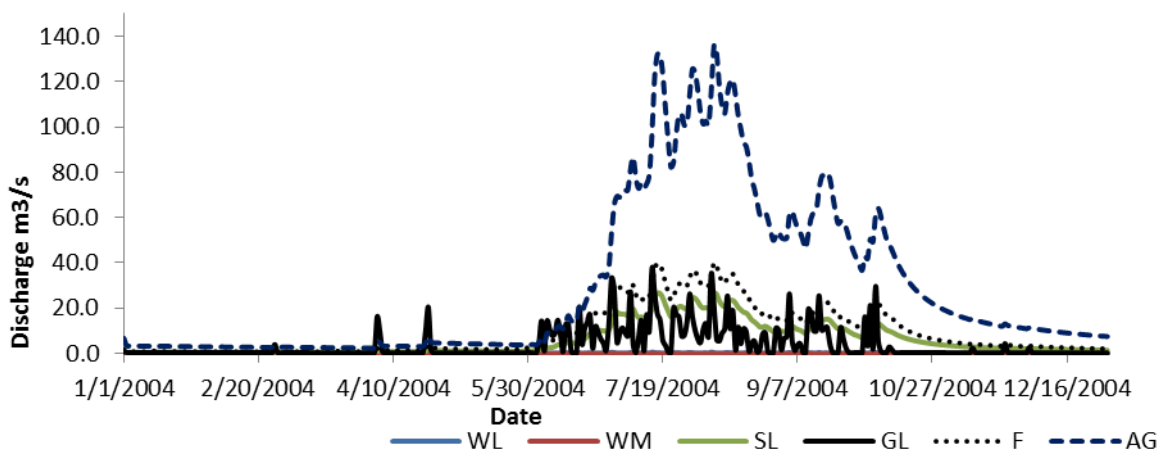


Figure 5-22: Simulated hydrograph from each land cover class using average daily ETa from SEBS

The TOPMODEL simulation was also performed to observe the effect of changes in ETa on the streamflow simulation of the model. The daily average ETa estimated from SEBS for each land cover class was considered for the whole catchment and simulation is performed by changing ETa from respective land cover. Table 5-6 shows the model performance efficiencies when simulation is done by taking the satellite based ETa from each land cover class. The lowest model performance is observed for the forest land cover and followed by shrubs land. Figure 5-23 shows the simulated hydrograph from each land cover class ETa value. In the beginning of rainy season (i.e. from June, 10 to July, 8) the simulated discharge for forest and shrubs land is higher than the observed discharge. The simulation from forest and shrubs is also higher than the other the land cover classes throughout the year. This is actually observed during the estimation of ETa from SEBS that for the forest and Shrubs land cover classes ETa was underestimated (i.e. lower than other land cover classes in the catchment) so that the total simulated discharge is higher than the observed. This is also shown in the model efficiency performance the Nash-Sutcliffe is lower than other land cover classes and the RV_E also shows positive value and higher (i.e. for forest $RV_E=21\%$ and for Shrubs $RV_E=9\%$)

Table 5-6: Model efficiencies when applied to ETa from different land cover classes

| Objective functions | Land cover class | | | | | |
|---------------------|------------------|--------|--------|-------|--------|---------|
| | AG | F | GL | SL | WL | WM |
| Nash-Sutcliffe (NS) | 0.769 | 0.685 | 0.774 | 0.733 | 0.773 | 0.764 |
| RV_E | -1.750 | 21.010 | -8.228 | 9.048 | -2.417 | -11.106 |

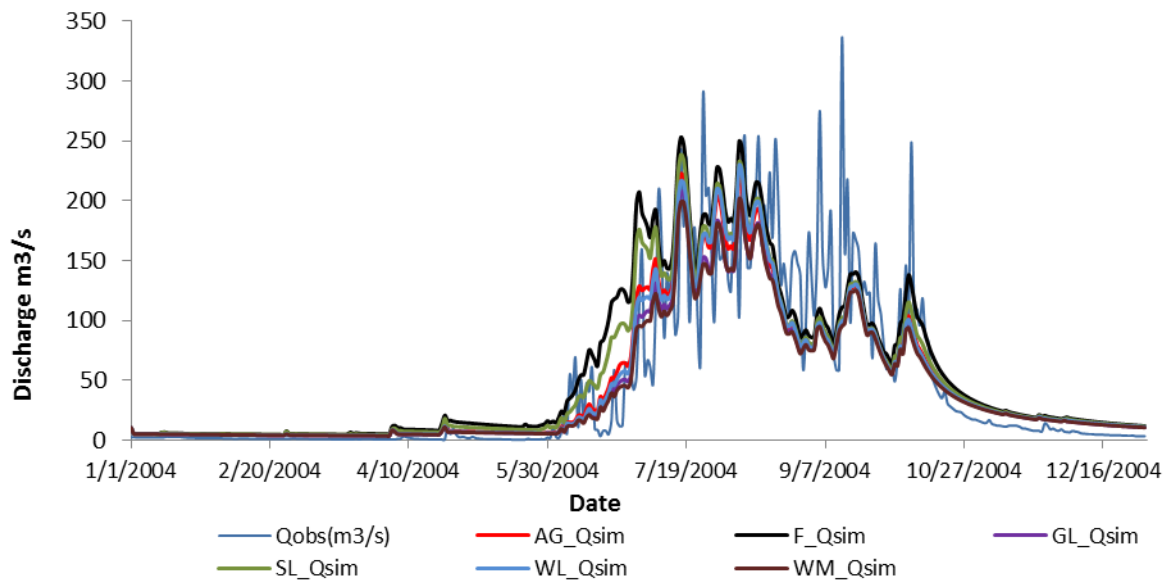


Figure 5-23: Simulated hydrograph applying ETa from land cover classes treating as the whole catchment.

6. CONCLUSION AND RECOMMENDATION

6.1. Conclusion

- The main objective to this study was to simulate the streamflow hydrograph of the Gilgel Abay catchment using a semi-distributed rainfall-runoff model (TOPMODEL) by using the spatially distributed actual evapotranspiration as its input estimated from satellite remote sensing and to observe the change in streamflow simulation results when applying satellite based ET_a and ET_p estimated from point station data.
- Daily ET_a was estimated for both dry and wet season of the area from surface energy balance system (SEBS) algorithm using satellite data from MODIS products and meteorological station data. Because some of the MODIS products were affected by the cloud, at first ET_a was estimated for only 152 days and ET_a estimates for missing days were filled using simple linear interpolation technique. It was possible to calculate ET_a for each land cover class and was assessed the seasonal variation of ET_a for each land cover class. The ET_a estimated from SEBS seems realistic and reflected the seasonal variability of the study area. The highest ET_a was in September 22, (5.3 mm/day) which is the wet season and the lowest ET_a was in March 19, (0.78 mm/day) in dry season.
- Besides this, the potential evapotranspiration for the study area was calculated using FAO Penman-Monteith method from 1996 to 2004. ET_p was estimated from three meteorological stations data of which two are located outside the catchment. Average ET_p from these stations were taken for the sensitivity analysis, calibration and validation of the TOPMODEL simulation for the years 1996 to 2004. The ET_p used for the simulation could not fully represent the catchment because most stations are located outside of the catchment boundary.
- Since there is no ground based measurement of ET_a for validation of SEBS ET_a and due to time constraints to compare with other ET estimation technique, the SEBS ET_a was simply taken for the TOPMODEL streamflow simulation and to calculate the water balance of the catchment. The satellite based ET_a estimation was found relevant for area like Gilgel Abay and is a feasible means for projection of ET_a over the large area.
- Inside TOPMODEL IDL code, there is an empirical formula used to calculate ET_a using ET_p , the actual root zone soil moisture deficit and the maximum soil moisture deficit. Comparison was made between ET_a calculated from the TOPMODEL and the ET_a from SEBS. It was found that The ET_a calculated in TOPMODEL is highly dynamic and depends to the change in rainfall amount. When there is no rainfall ET_a approaches zero. Hence, ET_a calculated from TOPMODEL for the simulation of streamflow hydrograph is underestimated so that affect the water balance of the catchment. The total gross amount of ET_a for the whole year 2004 from SEBS was about 1068 mm per year whereas from TOPMODEL was almost half of it 594.3 mm per year. This effect has also shown on the total water budget of the catchment.
- The model sensitivity analysis for more sensitive parameters m , T_o and SR_{max} was performed to observe how the model is sensitive the change in the parameter for some value ranges. In addition to that the model was calibrated using the set of data from 1996 to 2003 by changing the parameter values manually (Trial and error). Here ET_p from station data were used. Results of the calibration process showed a satisfactory Nash-Sutcliffe model efficiency (NS) of 0.773 and a Relative Volume Error (RV_E) of -6.3%. This indicates that the TOPMODEL performs well for the simulation of streamflow. The TOPMODEL was validated using a 2004 datasets and the result was good with $NS=0.80$. The $RV_E=9.98\%$ indicates a satisfactory model performance.

- The second research question that should be answered was how the TOPMODEL streamflow simulation is affected when satellite based ETa is applied. In this study ETa from remote sensing was estimated for only one year (2004) and the model was calibrated for 1996 to 2003 using Penman-Monteith ETp. However, when these calibrated parameter values are applied while using the SEBS based ETa estimates, the model still has shown good performance both in Nash-Sutcliffe efficiency of (0.78) and Relative Volume Error (0.59%). Especially the Relative Volume Error RV_E suggests a very good performance of the model.
- The model also has been used to simulate streamflow hydrograph from different land cover classes by treating each land cover as a sub-catchment. For each land cover classes the topographic index distribution and area distance distribution values were calculated and then the model was run using average ETa value of each land cover class. The result shows that 60% of the annual discharge by volume was contributed from agricultural area and the rest 19%, 12%, 8% from forest, shrubs and grassland respectively. Less than 1% volume of water is contributed from both wetland and marshy area. Finally the effect of changes in ETa on the streamflow simulation of the model has been done for the catchment as a whole by selecting the average ETa value from each land cover class and tried to observe how the TOPMODEL simulation responses. The simulation results from ETa of each land cover was compared and good model performance were observed when ETa was used from Agricultural ($NS= 0.769$, $RV_E = -1.75\%$) and wetland ($NS=0.773$, $RV_E=-2.417\%$) respectively. The lower model performance were obtained while using ETa from forest ($NS=0.685$ and $RV_E=21\%$). This indicates how the TOPMODEL is sensitive to the changes in ETa so that accurate estimation of ETa from each land cover could be given to emphasis for the better estimation of the water balance.

6.2. Recommendation

The surface energy balance system (SEBS) applied for the estimation of ETa has not been validated with other products of ETa for the area. Other ground based technique at least to measures the heat flux like (eddy flux tower) to measure the latent heat flux and other variable is good for the comparison and better understanding of the surface energy fluxes of the area. Most of the meteorological data for the SEBS like wind speed; sunshine hours, Temperature and humidity were taken simply from three stations which are sparsely located in the study area. Therefore, additional meteorological stations with more measuring instruments are necessary to have better representative station data for the Gilgel Abay catchment.

The land cover class used for the SEBS for the estimation of aerodynamic roughness height is from the work of Kebede (2009) for the 2001. Some significant change on the land cover of the study area might happen between the 2001 and 2004. Therefore, land covers classification and accuracy assessment by collecting more ground control points may represent the accurately and will have better representation of the area and will give good results of the surface parameter especially in the estimation of aerodynamic roughness height in the surface energy balance system (SEBS) algorithm.

Besides the satellite based ETa, one of the meteorological forcing elements used as input for TOPMODEL is rainfall. Further researches could focus on the application of satellite based rainfall data like from TRMM (Tropical Rainfall Measuring Mission) satellite and from MSG satellite Multi-Sensor Precipitation Estimate (MPE) products that could provide areal rainfall estimation and could compare the station rainfall data for more accuracy and better estimation of water balance of the catchment on TOPMODEL.

The spatial variation in soil hydraulic and physical properties of the catchment play an important role in movement of soil moisture from the land surface to the water table through the unsaturated zone and

affects the response the catchment to certain rainfall intensity by the occurrence of surface overland flow. This affects both the groundwater recharge process and the surface runoff response. Hence field measurements on the surface and subsurface soil layers properties are important and valuable for modelling of unsaturated flow and to develop catchment based rainfall runoff relationships.

The calibration process applied in this study is by trial and error which is time taking and tedious. Other technique like the application of Generalized Likelihood Uncertainty Estimation (GLUE) for set of parameters may give better simulation result.

LIST OF REFERENCES

- Abdo, K. S. Fiseha, B. M. Rientjes, T. H. M. Gieske, A. S. M. Haile, A. T. (2009). Assessment of climate change impacts on the hydrology of gilgel abay catchment in lake tana basin, ethiopia. *Journal Hydrological processes : an international journal*, 23(6), 3661-3669.
- Allen, R. G..... (1998). *Crop evapotranspiration : Guidelines for computing crop water requirements* (Vol. 56). Rome: FAO.
- Badola, A. (2009). *Validation of surface balance systems sebs over forest land cover and sensitivity analysis of the model*. ITC, Enschede.
- Beven. (2001). *Rainfall runoff modelling : The primer*. Chichester etc.: Wiley & Sons.
- Beven and Kirkby. (1979a). A physically based, variable contributing area model of basin hydrology. *Hydrological Sciences-Bulletin-des Sciences Hydrologiques*, 24(1), 43-69.
- Beven and Wood. (1983). Catchment geomorphology and the dynamics of runoff contributing areas. *Journal of Hydrology*, 65(1-3), 139-158.
- Beven, K. (1997). "Topmodel: A critique.". *Hydrological Processes*, 11, 1069-1085.
- Beven, K. Lamb, R. Quinn, P. Romanowicz, R. Freer, J. (1995). Topmodel. *Computer models of watershed hydrology*, 627-668.
- Beven , K. J. and Kirkby , M. J. (1979). ' A physically-based variable contributing area model of basin hydrology'. *Hydrol.Sci.Bull.*, 24, 43-69.
- Beven, K. J. and Kirkby, M. J. (1979b). A physically based, variable contributing area model of basin hydrology. *Hydrological Sciences-Bulletin-des Sciences Hydrologiques*, 24(1), 43-69.
- Brutsaert, W. (2005). *Hydrology : An introduction*. Cambridge: Cambridge University Press.
- Deginet, M. D. (2008). *Land surface representation for regional rainfall - modelling, upper blue Nile basin, ethiopia*. ITC, Enschede.
- Garbrecht, J. and Martz, L. W. (1999). *Digital elevation model issues in water resources modeling*. In: *Proceedings from invited water resources sessions*. Paper presented at the ESRI international user conference.
- Gash. (1979). Analytical model of rainfall interception by forests. In: *Quarterly journal of the royal meteorological society*, 105(1979)443, pp. 43-55.
- Gash Lloyd, C. R. Lachaud, G. (1995). Estimating sparse forest rainfall interception with an analytical model. *Journal of Hydrology*, 170(1-4), 79-86.
- Glenn, E. P. Huete, A. R. Nagler, P. L. Hirschboeck, K. K. Brown, P.. (2007). Integrating remote sensing and ground methods to estimate evapotranspiration. *Critical Reviews in Plant Sciences*, 26(3), 139-168.
- Gumindoga, W. (2010). *Hydrologic impacts of landuse change in the upper gilgel abay river basin, ethiopia : Topmodel application*. University of Twente Faculty of Geo-Information and Earth Observation ITC, Enschede.
- Houser, P. R. Shuttleworth, W. J. Famiglietti, J. S. Gupta, H. V. Syed, K. H. Goodrich, D. C. (1998). Integration of soil moisture remote sensing and hydrologic modeling using data assimilation. *Journal Water resources research*, 34(12), 3405-3420.
- Iguchi , T. Toshiki, K. Robert, M. Jun, A. Ken'ichi, O.... (2000). Rain - profiling algorithm for the trmm precipitation radar. In: *Journal of applied meteorology*, 39(2000), pp. 2038-2052.
- Jacob, F. Petitcolin, F. o. Schugge, T. Vermote, É. French, A. Ogawa, K. (2004). Comparison of land surface emissivity and radiometric temperature derived from modis and aster sensors. *Remote Sensing of Environment*, 90(2), 137-152.
- Kebede, E. W. (2009). *Hydrological responses to land cover changes in gilgel abay catchment, ethiopia*. ITC, Enschede.
- KIRKBY, M. J. (1997). Topmodel: A personal view. *HYDROLOGICAL PROCESSES*, 11, 1087±1097.
- Kustas, W. P. and Daughtry, S. T. (1989). Estimation of the soil heat flux - net radiation ratio from spectral data. In: *Agricultural and Forest Meteorology*, 49(1990), pp. 205-223.
- Maathuis, B. H. P. (2007). Dem based hydro-processing: Introduction to the tools developed, tutorial with exercises version 1. Department of Water Resources, ITC.
- Myneni, R. B. Hoffman, S. Knyazikhin, Y. Privette, J. L. Glassy, J. Tian, Y. Wang, Y. Song, X. Zhang, Y. Smith, G. R. Lotsch, A. Friedl, M. Morisette, J. T. Votava, P. Nemani, R. R. Running, S. W. (2002). Global products of vegetation leaf area and fraction absorbed par from year one of modis data. *Remote Sensing of Environment*, 83(1-2), 214-231.
- Nash, J. E. and Sutcliffe, J. V. (1970). River flow forecasting through conceptual models, part i : A discussion of principles. *Journal of hydrology*, 10(3), 282-290.

- Quinn, P. F. and Beven, K. J. (1993). Spatial and temporal predictions of soil moisture dynamics, runoff, variable source areas and evapotranspiration for plynlimon, mid - wales. *In: Hydrological processes*, 7(1993), pp. 425-448.
- Rientjes, T. H. M. (2010). Modeling in hydrology. Lecture notes. Enschede, the netherlands.
- Román, M. O. Schaaf, C. B. Woodcock, C. E. Strahler, A. H. Yang, X. Braswell, R. H. Curtis, P. S. Davis, K. J. Dragoni, D. Goulden, M. L. Gu, L. Hollinger, D. Y. Kolb, T. E. Meyers, T. P. Munger, J. W. Privette, J. L. Richardson, A. D. Wilson, T. B. Wofsy, S. C. (2009). The modis (collection v005) brdf/albedo product: Assessment of spatial representativeness over forested landscapes. *Remote Sensing of Environment*, 113(11), 2476-2498.
- Shaka, A. K. (2008). *Assessment of climate change impacts on the hydrology of gilgel abbay catchment in lake tana basin, ethiopia*. ITC, Enschede.
- SMEC, I. P. (2007). "Hydrological study of the tana-beles sub-basins." *part 1*.
- Su, Z. (2002). Surface energy balance system sebs for estimation of turbulent heat fluxes. *Journal Hydrology and earth system sciences (HESS)*, 6(1), 85-99.
- Su, Z. Schmugge, T. Kustas, W. P. Massman, W. J. (2001). An evaluation of two models for estimation of the roughness height for heat transfer between the land surface and the atmosphere. *J. Appl. Meteorol.*, 40, , 1933–1951.
- van Dam, J. C. (2000). *Field - scale water flow and solute transport : Swap model concepts, parameter estimation and case studies*. Wageningen: Wageningen Agricultural University.
- Yanbo , H.Z, S.L, J.Yuanyuan , Z.G, R.Shili, W.Jun, W.Yingyu, H. (2005). Estimation of daily evapotranspiration in northern china plain by using modis - terra images. *In: Remote sensing for agriculture, ecosystems and hydrology VII : proceedings of the conference, Bruges, Belgium, 20-22 September 2005. / ed. by. M. Owe and G. D'Urso. Bellingham: SPIE, 2005. (Proceedings of SPIE ; 5976) paper 59761M-1. pp. 413-424.*

APPENDICES

List of Acronyms

| | |
|-----------------|---|
| DEM | Digital Elevation Model |
| DF | Diffusion Factor |
| ECMWF | European Center for Medium-Range Weather Forecast |
| EOS | Earth Observation System |
| EOSDIS | Earth Observation System Data and Information System |
| ET | Evapotranspiration |
| ET _a | Actual evapotranspiration |
| ET _p | Potential evapotranspiration |
| ETM+ | Enhanced Thematic Mapper |
| FAO | Food and Agricultural Organization of United Nations |
| FC | Fraction Cover |
| GPS | Global Positioning System |
| HDF-EOS | Hierarchical Data Format- Earth Observation System |
| ILWIS | Integrated Land and Water Information System |
| IDL | Iterative Data Language |
| LAADS | Level 1 and Atmospheric Archive and Distribution System |
| LAI | Leaf Area Index |
| LANDSAT | LAND Remote Sensing Satellite |
| LP DAAC | Land Processes Distributed Active Archive Center. |
| LST | Land Surface Temperature |
| MODIS | Moderate Resolution Imaging Spectroradiometer |
| MRT | MODIS Reprojection Tool |
| NASA | National Aeronautic and Space Administration |
| NDVI | Normalized Difference Vegetation Index |
| RH | Relative Humidity |
| SEBS | Surface Energy Balance Systems |
| SRTM | Shuttle Radar Topography Mission |
| UTM | Universal Transverse Mercator |
| WGS | World Geodetic System |

Appendix A: MODIS Technical specification

| | |
|---------------------|--|
| Orbit: | 705 km, 10:30 a.m. descending node (Terra) or 1:30 p.m. ascending node (Aqua), sun-synchronous, near-polar, circular |
| Scan Rate: | 20.3 rpm, cross track |
| Swath Dimensions: | 2330 km (cross track) by 10 km (along track at nadir) |
| Telescope: | 17.78 cm diam. off-axis, a focal (collimated), with intermediate field stop |
| Size: | 1.0 x 1.6 x 1.0 m |
| Weight: | 228.7 kg |
| Power: | 162.5 W (single orbit average) |
| Data Rate: | 10.6 Mbps (peak daytime); 6.1 Mbps (orbital average) |
| Quantization: | 12 bits |
| Spatial Resolution: | 250 m (bands 1-2), 500 m (bands 3-7) and 1000 m (bands 8-36) |
| Design Life: | 6 years |

(<http://modis.gsfc.nasa.gov/about/specifications.php>)

Appendix B: Average surface downward shortwave radiation

| Julian Day | Radiation W/m ² |
|------------|----------------------------|------------|----------------------------|------------|----------------------------|------------|----------------------------|------------|----------------------------|------------|----------------------------|------------|----------------------------|
| 1 | 845.93 | 41 | 919.77 | 76 | 685.47 | 141 | 866.43 | 251 | 696.63 | 300 | 856.90 | 338 | 806.40 |
| 2 | 825.12 | 42 | 872.84 | 77 | 844.36 | 145 | 588.67 | 253 | 711.67 | 301 | 832.99 | 339 | 792.22 |
| 3 | 825.12 | 43 | 892.46 | 79 | 763.38 | 150 | 730.69 | 255 | 596.78 | 303 | 877.32 | 342 | 798.97 |
| 4 | 794.37 | 44 | 885.84 | 81 | 976.50 | 161 | 653.20 | 256 | 702.64 | 304 | 827.78 | 343 | 749.18 |
| 6 | 795.48 | 45 | 796.77 | 83 | 907.15 | 166 | 574.82 | 258 | 484.33 | 310 | 821.45 | 344 | 754.52 |
| 8 | 775.88 | 47 | 950.87 | 84 | 911.78 | 180 | 665.30 | 260 | 633.41 | 313 | 737.80 | 345 | 810.30 |
| 9 | 845.91 | 49 | 937.64 | 90 | 1022.05 | 182 | 445.05 | 264 | 720.83 | 314 | 660.43 | 346 | 769.82 |
| 10 | 825.13 | 51 | 952.80 | 92 | 966.66 | 184 | 500.33 | 265 | 520.13 | 315 | 797.48 | 347 | 783.90 |
| 11 | 762.39 | 52 | 955.47 | 103 | 1019.21 | 116 | 660.41 | 266 | 836.61 | 317 | 815.54 | 348 | 775.70 |
| 16 | 813.17 | 54 | 870.94 | 105 | 895.90 | 187 | 652.44 | 267 | 616.50 | 319 | 779.49 | 349 | 733.48 |
| 17 | 802.91 | 59 | 890.36 | 118 | 926.29 | 191 | 518.81 | 275 | 668.17 | 320 | 730.47 | 351 | 749.63 |
| 19 | 825.40 | 60 | 819.58 | 119 | 795.76 | 195 | 411.14 | 278 | 650.36 | 321 | 759.63 | 354 | 814.40 |
| 20 | 777.99 | 61 | 799.87 | 124 | 683.55 | 201 | 529.38 | 288 | 840.61 | 323 | 784.27 | 355 | 804.06 |
| 22 | 824.77 | 63 | 889.76 | 127 | 911.59 | 203 | 354.54 | 289 | 861.54 | 324 | 743.42 | 358 | 736.84 |
| 23 | 824.47 | 64 | 926.92 | 128 | 918.69 | 214 | 450.50 | 291 | 849.38 | 327 | 708.87 | 360 | 735.85 |
| 24 | 848.42 | 65 | 933.60 | 129 | 784.55 | 235 | 713.99 | 292 | 903.84 | 330 | 719.66 | 361 | 803.23 |
| 25 | 838.42 | 66 | 933.40 | 131 | 882.89 | 237 | 504.80 | 294 | 925.31 | 331 | 770.99 | 362 | 829.04 |
| 27 | 860.35 | 67 | 885.93 | 132 | 922.06 | 243 | 702.38 | 295 | 910.11 | 332 | 782.41 | 363 | 781.16 |
| 28 | 841.42 | 70 | 983.55 | 134 | 844.13 | 247 | 600.62 | 296 | 859.10 | 333 | 829.18 | 364 | 635.85 |
| 33 | 793.25 | 72 | 834.59 | 138 | 877.31 | 248 | 687.95 | 297 | 875.77 | 335 | 797.41 | 365 | 748.97 |
| 39 | 817.97 | 74 | 767.98 | 139 | 921.05 | 249 | 481.97 | 298 | 843.62 | 336 | 812.03 | | |
| 40 | 889.2568 | 75 | 678.62 | 140 | 966.96 | 250 | 757.45 | 299 | 894.53 | 337 | 806.40 | | |

Appendix C: TOPMODEL equations

The unsaturated zone thickness in the TOPMODEL is given by

$$Z = D(1 - W) \quad (C-1)$$

Introducing the exponential K assumption that describes the saturated hydraulic conductivity then transmissivity reduces exponentially in the subsurface.

$$aR = T_o \tan \beta e^{-fz_i} \quad (C-2)$$

Therefore, the soil moisture deficit can be expressed by

$$z_i = -\frac{1}{f} \ln \left(\frac{Ra}{T \tan \beta} \right) = \bar{Z} - \frac{1}{f} \left(\ln \frac{a}{\tan \beta} - \lambda \right) \quad (C-3)$$

By integrating the local deficit over the entire catchment, we can get the mean depth \bar{Z} to the water table.

$$\bar{Z} = \frac{1}{A} \int_A Z_i dA = \frac{1}{fA} \int_A \left\{ -\ln \left(\frac{a}{T_o \tan \beta} \right) - \ln R \right\} dA \quad (C-4)$$

This equation assumes for water tables rising above the soil surface. When rewriting Eq. [C-2] above by substituting this for R in Eq. [C-4] then an expression is found with eliminating R and \bar{Z} becomes the function of topographic and physiographic properties only and give by

$$\bar{Z} = \frac{1}{f} \left\{ -\frac{1}{A} \int_A \ln \left(\frac{a}{T_o \tan \beta} \right) dA + f \bar{Z} + \ln \left(\frac{a}{T_o \tan \beta} \right) \right\} \quad (C-2)$$

Or

$$f(\bar{Z} - Z_i) = \left\{ \ln \left(\frac{a}{\tan \beta} \right) - \lambda \right\} - \{ \ln T_o - \ln T_A \}$$

where

$$\lambda = \frac{1}{A} \int_A \ln \left(\frac{a}{\tan \beta} \right) dA$$

$$\ln T_A = \frac{1}{A} \int_A \ln T_o dA$$

For more description of the equation see (Beven and Kirkby, 1979a; Beven and Wood, 1983)

Appendix D: Some equation used in surface energy balance system (SEBS)

In the atmospheric surface layer, the similarity relationships for the profiles of the mean wind speed, u , and the mean temperature, $\theta_0 - \theta_a$, are usually written in integral form as

$$u = \frac{u_*}{k} \left[\ln \left(\frac{z-d}{z_{om}} \right) - \Psi_m \left(\frac{z-d}{L} \right) + \Psi_m \left(\frac{z_{om}}{L} \right) \right] \quad (D-1)$$

$$\theta_0 - \theta_a = \frac{H}{ku_*\rho C_p} \left[\ln \left(\frac{z-d}{z_{oh}} \right) - \Psi_h \left(\frac{z-d}{L} \right) + \Psi_h \left(\frac{z_{oh}}{L} \right) \right] \quad (D-2)$$

where z is the height above the surface, $u_* = (\tau_o / \rho)^{1/2}$ is the friction velocity, τ_o is the surface shear stress, ρ is the density of air, $k = 0.4$ is von Karman's constant, d is the zero plane displacement height, z_{om} is the roughness height for momentum transfer, θ_o and θ_a are the potential temperature and potential air temperature at the surface, and at height z respectively. z_{oh} is the scalar roughness height for heat transfer, Ψ_m and Ψ_h are the stability correction functions for momentum and sensible heat transfer respectively, L is the Obukhov length defined as

$$L = \frac{u_*^3 \cdot c_p \cdot \rho \cdot \theta_v}{k \cdot g \cdot H} \quad (D-3)$$

Where g is the acceleration due to gravity and θ_v is the potential virtual temperature near the surface.

The roughness length of heat transfer can be calculated using the momentum transfer value by the following equation.

$$z_{oh} = z_{om} / \exp(kB^{-1}) \quad (D-4)$$

Where B^{-1} is the inverse Stanton number, which is a dimensionless heat transfer coefficient and its value is estimated as proposed by Su et al (2001) using the following formula

$$kB^{-1} = \frac{kC_d}{4C_{t,u(h)} \frac{u_*}{u(h)} (1 - e^{-n_{ec}/2})} f_c^2 + 2f_c f_s \frac{k \cdot u_* / u(h) \cdot \frac{z_{om}}{h}}{C_t^*} + kB_s^{-1} f_s^2 \quad (D-5)$$

Where f_c and f_s are the fractional canopy coverage and its complement respectively. C_t is the heat transfer coefficient of the leaf and is bounded as $0.005N \leq C_t \leq 0.075N$ (N is number of sides of a leaf to participate in heat exchange).

The heat transfer coefficient of the soil is given by

$$C_t^* = Pr^{-2/3} Re_*^{-1/2} \quad (D-6)$$

Where Pr is the Prandtl number and Re_* is the roughness Reynolds number.

The wind speed extinction coefficient (n_{ec}) can be calculated using leaf area index (LAI) and drag coefficient as

$$n_{ec} = \frac{C_d \cdot LAI}{2u_*^2 / u(h)^2} \quad (D-7)$$

Where $C_d = 0.2$ and $u(h)$ is the horizontal wind speed at the top of canopy.

Evaporative fraction

The evaporative fraction in SEBS is determined by considering the two limiting conditions known as the dry-limit and the wet-limit. In dry-limit, soil moisture is limited and the sensible heat flux is at its maximum value so that evaporation becomes zero. The energy balance equation becomes

$$\lambda E_{\text{dry}} = R_n - G - H_{\text{dry}} = 0 \text{ Or } H_{\text{dry}} = R_n - G \quad (\text{D-8})$$

Under the wet-limit, the evaporation takes place with its potential and only limited by the available energy in the atmosphere. The energy balance equation becomes

$$\lambda E_{\text{wet}} = R_n - G - H_{\text{wet}} \text{ Or } H_{\text{wet}} = R_n - G - \lambda E_{\text{wet}} \quad (\text{D-9})$$

The relative evaporation is then can be estimated dividing the actual evaporation by the potential one, and is given by

$$\Lambda_r = \frac{\lambda E}{\lambda E_{\text{wet}}} = 1 - \frac{\lambda E_{\text{wet}} - \lambda E}{\lambda E_{\text{wet}}} \quad (\text{D-10})$$

By substitution and rearranging, we get the following

$$\Lambda_r = 1 - \frac{H - H_{\text{wet}}}{H_{\text{dry}} - H_{\text{wet}}} \quad (\text{D-11})$$

By Combination of equations above, a similar to the Penman-Monteith combination equation is derived when the resistance terms are grouped into the bulk internal (or surface, or stomata) and external (aerodynamic) resistances, and can be written in the following form.

$$\lambda E = \frac{\Delta r_e (R_n - G_0) + \rho C_p (e_{\text{sat}} - e)}{r_e (\gamma + \Delta) + \gamma r_i} \quad (\text{D-12})$$

Assuming that the internal resistance equal to zero under the wet-limit condition, an equation similar to Penman-Monteith combination equation can obtain for the sensible heat flux and given below

$$H_{\text{wet}} = \left((R_n - G_0) - \frac{\rho C_p}{r_{\text{ew}}} \frac{e_s - e}{\gamma} \right) / \left(1 + \frac{\Delta}{\gamma} \right) \quad (\text{D-13})$$

The external resistance for the wet-limit is given by

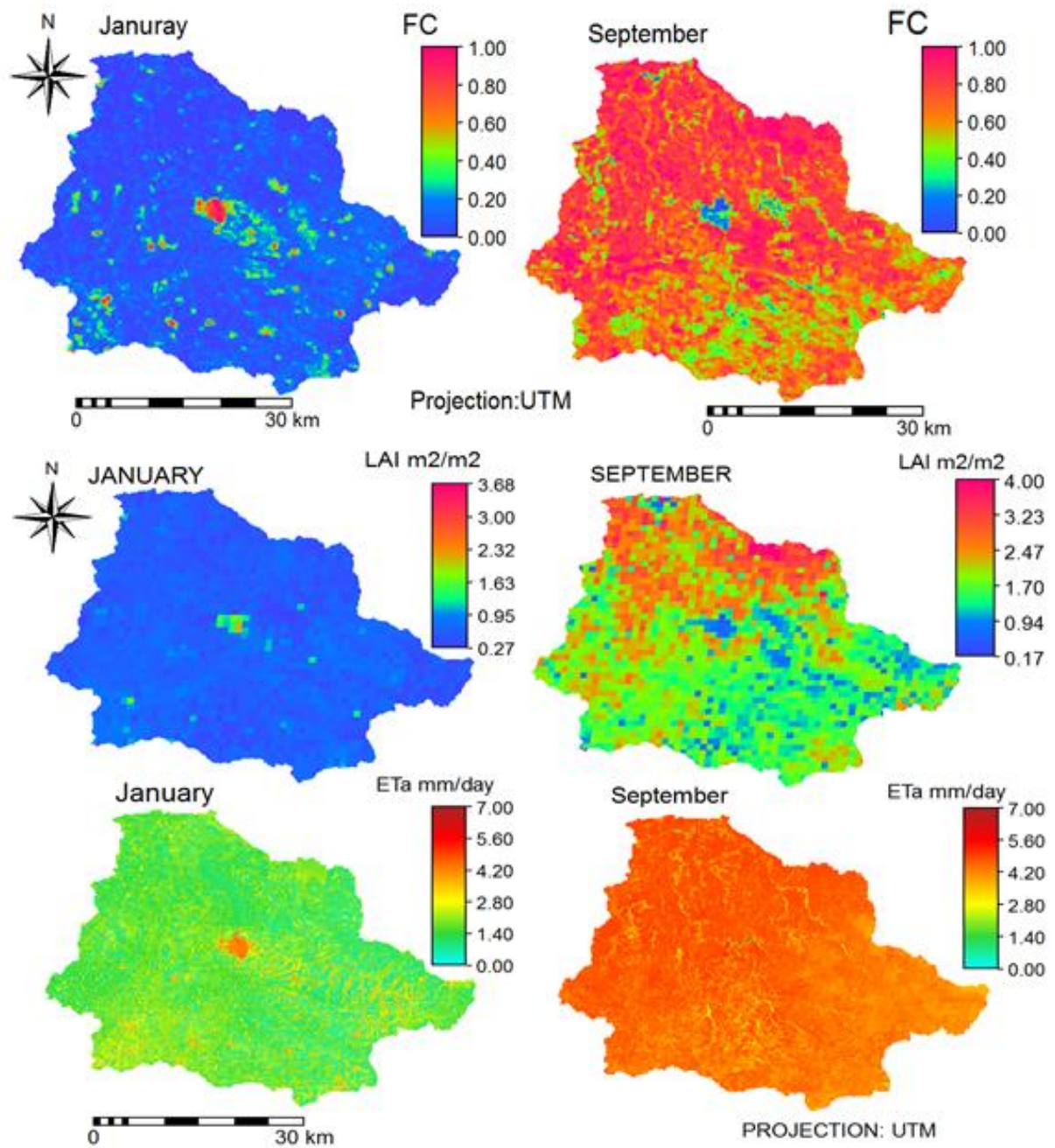
$$r_{\text{ew}} = \frac{1}{k u_*} \left[\ln \left(\frac{z-d}{z_{\text{oh}}} \right) - \Psi_h \left(\frac{z-d}{L_w} \right) + \Psi_h \left(\frac{z_{\text{oh}}}{L_w} \right) \right] \quad (\text{D-14})$$

In addition, the wet limit stability length can be determined as

$$L_w = - \frac{\rho u_*^3}{\text{kg} * 0.61 * (R_n - G_0) / \lambda} \quad (\text{D-15})$$

For more descriptions about the surface energy balance equation see (Su, 2002)

Appendix E: Inter-comparison of fc, LAI and ETa for dry and wet season



Appendix F: The parameters used for the estimation of interception and intercepted rainfall estimated from land covers

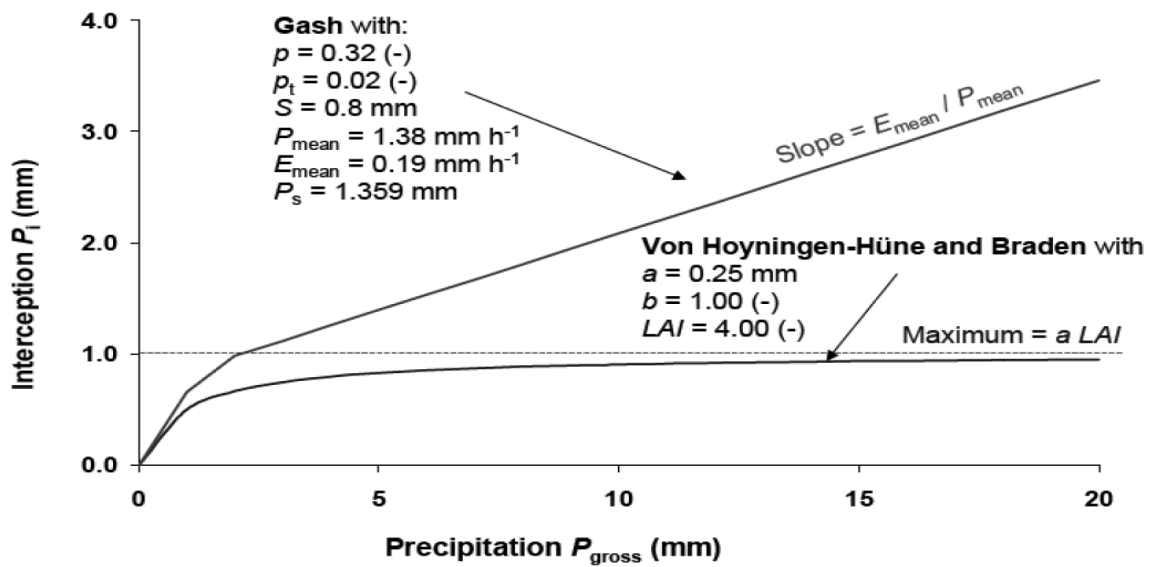


Figure F-1: Interception for agricultural crops (Von Hoyningen-Hüne, 1983; Braden, 1985) and forests (Gash, 1979; Gash, et al., 1995) (After Gumindoga (2010))